*H*igh res*o*luti*o*n past climate and pale*o*envir*o*nmental rec*o*nstructi*o*n during the *H*ol*o*cene : a stalagmite-based rec*o*rds study fr*o*m Caum*o*nt cave, *o*rmandy (France)

Ingrid Bejarano Arias

Normandie Université

UNIVERSITÉ DE ROUEN NORMANDIE

THÈSE

Pour obtenir le diplôme de doctorat

Spécialité **GEOGRAPHIE**

Préparée au sein de l'**Université de Rouen Normandie**

High resolution past climate and paleoenvironmental reconstruction during the Holocene: a stalagmite-based records study from Caumont cave, Normandy (France)

Présentée et soutenue par

INGRID BEJARANO ARIAS

Thèse soutenue le 15/11/2024

devant le jury composé de :

M. DAMASE MOURALIS	Professeur des Universités - Université de Rouen Normandie (URN)	Directeur de thèse
M. PHILIPPE NEGREL	Directeur de Recherche - Bureau de Recherches Geologiques et Minieres	Président du jury
M. SEBASTIEN BREITENBACH	Professeur des Universités - Université de Newcastle (R-U)	Membre du jury
MME CAROLE NEHME	Maître de Conférences - Université de Rouen Normandie (URN)	Membre du jury
MME SOPHIE VERHEYDEN	Chercheur - Royal Belgian Institute of Natural Sciences, Geological Survey	Membre du jury
M. LAURENT LESPEZ	Professeur des Universités - UNIVERSITE PARIS 12 VAL DE MARNE	Rapporteur du jury
MME ANA MORENO	Directeur de Recherche - Université de Zaragoza (ESPAGNE)	Rapporteur du jury

Thèse dirigée par **DAMASE MOURALIS** (Identité et Différenciation des Espaces de l'Environnement et des Sociétés)

ÉCOLE DOCTORALE 556 HSRT

Normandie Université

idees UMR 6266 / IDEES-Rouen

THÈSE

Pour obtenir le diplôme de doctorat

Spécialité GÉOGRAPHIE

Préparée au sein de l'Université de Rouen Normandie

High resolution past climate and paleoenvironmental reconstruction during the Holocene : a stalagmite-based records study from Caumont cave, Normandy (France).

Présentée et soutenue par

Ingrid BEJARANO ARIAS

Thèse soutenue publiquement le 15/11/2024

devant le jury composé de:

M. DAMASE MOURALIS	Professeur des Universités - Université de Rouen Normandie	Directeur de thèse
M. SEBASTIAN BREITENBACH	Professeur des Universités - Northumbria University (R-U)	Co-Directeur de thèse
Mme CAROLE NEHME	Maître de Conférences - Université de Rouen Normandie	Co-Encadrante de thèse
Mme ANA MORENO	Directrice de Rcherche - Université de Zaragosa (ESPAGNE)	Rapportrice
M. LAURENT LESPEZ	Professeur des universités - Université Paris 12	Rapporteur
Mme SOPHIE VERHEYDEN	Chercheuse - Royal Belgian Institute of Natural Sciences (BELGIQUE)	Examinatrice
M. PHILIPPE NEGREL	Chargé de Recherche - Bureau de Recherches Geologiques et Minieres	Examinateur

Thèse dirigée par DAMASE MOURALIS, UMR IDEES 6266 (ROUEN)

High resolution past climate and paleoenvironmental reconstruction during the Holocene: a stalagmite-based records study from Caumont cave, Normandy (France).

Ingrid Bejarano Arias

Supervisors: **Damase Mouralis (Director)**
Sebastian Breitenbach (Co-director)
Carole Nehme (Co-supervisor)

Université de Rouen Normandie, Geography department
IDEES UMR 6266 CNRS
Mont St-Aignan, France

Abstract

Speleothem-based studies are globally very significant for paleoclimate reconstructions given the abundance of information that can be extracted from the geochemical proxies recorded during calcite precipitation. The proxies (stable isotope and trace elements), provide information on precipitation, temperature and vegetation conditions that, along with the Uranium/Thorium (U/Th) dating method, allow to reconstruct the climate back in time. This thesis presents the first stalagmite-based studies in the north-western France, from the chalk cave of Caumont. Whilst research on paleoenvironmental reconstruction of the Holocene in Normandy has been published, such studies present lower resolution and need better age constraints. This information gap highlights the importance of Caumont stalagmites to complement the regional studies.

The aim of this thesis is to investigate the potential of the Caumont cave and quarry stalagmites as recorders of climate and environmental conditions, at high resolution, during the past 10 ka. To achieve this we did cave monitoring, U-series dating, stable isotopes ($\delta^{13}C$ and $\delta^{18}O$) and trace elements analysis. The 18-month monitoring results provide an understanding of the cave dynamics and the factors influencing the proxy signal during calcite precipitation. The stalagmite $\delta^{13}C$ signal reflects summer effective infiltration dynamics, influencing (longer-term) prior carbonate precipitation. The $\delta^{18}O$ signal likely reveals changes in the composition of precipitation above the cave, from annual to multi-annual scale. The recent stalagmite (CCB-1), yield a high-resolution record that covers the 20th century, allowing direct comparison with meteorological data. Such study helped to identify the historical drought events of the 20th and 21st centuries. Further evaluation of geochemical records with the precipitation-evapotranspiration index (SPEI) shows a shift in drought dynamics for the past two decades. During most of the 20th century, droughts appear driven by a pluvial (deficit) regime, but from the late 1990s, drought was driven by higher evapotranspiration due to increased temperature.

The Holocene stalagmites from the natural conduits of Caumont site show enough sensitivity to record the climate variability of the last 10 ka. The comparison of the geochemical proxies with the regional records provides insight of the paleoclimate evolution in Normandy, complements the paleoenvironmental reconstruction of previous studies and agrees with the onset of the human impact on the landscape. The multi-centennial climate trends from Caumont stalagmites are found generally in agreement with the Holocene climate variability for north-western Europe. This is demonstrated by comparing Caumont Holocene records with nearby speleothem records, continental archives (lake, mire) and North Atlantic marine proxy records.

Key words: chalk cave**,** climate monitoring**,** geochemistry, drought, paleoclimate, Holocene

Résumé

Les recherches sur les spéléothèmes sont de plus en plus demandées pour les reconstructions du climat passé, grâce à la richesse des informations extraites des *proxies* géochimiques enregistrés pendant la précipitation du calcaire dissous sous sa forme minérale, la calcite. Parmi ces proxies, les isotopes stables et les éléments traces fournissent des informations sur les variations climatiques (précipitations et température) et la couverture végétale. En outre, les datations absolues calculées gràçe à la méthode Uranium/Thorium (U/Th) permettent de contraindre d'une manière assez précises la chronologie de ces variations climatiques dans le temps. Cette thèse présente la toute première étude paléoclimatique basée sur l'analyse géochimiques des stalagmites du nord-ouest de la France, issues de la grotte crayeuse de Caumont. Bien que plusieurs recherches sur la reconstruction paléoenvironnementale de l'Holocène en Normandie aient été publiées, ces études présentent une résolution plus faible et nécessitent des datations plus précises pour mieux contraindre les variations climatiques du passé. Ces lacunes justifient notre recherche sur les stalagmites de Caumont, permettant ainsi de compléter les études paléoclimatiques et paléoenvironnementales régionales.

L'objectif de cette thèse est d'étudier le potentiel des stalagmites de la grotte et carrière de Caumont en tant qu'enregistreurs du climat et des conditions environnementales, à haute résolution, au cours des derniers 10.000 ans. Pour réaliser cet objectif principal, nous avons effectué un suivi climatique de la grotte, des datations U/Th sur les échantillons prélevés ainsi que des analyses d'isotopes stables ($\delta^{13}C$ et $\delta^{18}O$) et d'éléments traces. Les résultats de ce suivi climatique sur 18 mois ont permis d'identifier les conditions environnementales et les facteurs qui influencent le signal isotopique au moment de la précipitation de la calcite. Le signal du $\delta^{13}C$ reflète la dynamique de l'infiltration effective (ou efficiente) durant les saisons plus sèches (l'été), influençant, sur le long terme, la précipitation primaire de la calcite au sein même de l'épikarst (PCP). Le signal du $\delta^{18}O$ révèle plus des changements dans la quantité des précipitations, et serait liée plus précisément à l'infiltration après déduction de l'évapotranspiration au sein de l'epikarst. La stalagmite récente (CCB-1) qui couvre le 20^{e} siècle fournit un enregistrement paléoclimatique à haute résolution, permettant une comparaison directe avec les données météorologiques du 20^{e} siècle. Cette étude a permis d'identifier les épisodes de sécheresse historiques du 20^{e} et le début du 21^{e} siècle. Une évaluation plus poussée des enregistrements géochimiques avec l'indice précipitation - évapotranspiration (SPEI) montre un changement dans la dynamique de la sécheresse au cours des deux dernières décennies. Nos résultats montrent que si, pendant la majeure partie du 20^{e} siècle, les sécheresses semblent avoir été liée plus au déficit de la quantité de précipitations, la dynamique aurait changé à la fin des années 1990 avec une évapotranspiration plus élevée, associée à l'augmentation de la température.

Les stalagmites holocènes prélevées des conduits naturels à Caumont sont suffisamment sensibles pour enregistrer la variabilité climatique des derniers 10.000 ans. La comparaison des proxies géochimiques issues des stalagmites étudiées avec les enregistrements régionaux disponibles donne un aperçu de l'évolution du paléoclimat en Normandie, complète la reconstruction paléoenvironnementale des études précédentes et montre les débuts de l'impact anthropique sur le paysage. Les tendances climatiques pluri-centennales des stalagmites de Caumont sont généralement comparables à celles d'autres sites du Nord-Ouest Européen. Ceci est démontré en comparant les enregistrements Holocène des stalagmites de Caumont avec ceux des spéléothèmes de sites proches, ceux d'autres archives continentales (lac, tourbière) et marines de l'Atlantique Nord.

Mots clés : grotte crayeuse, suivi climatique, géochimie, sécheresse, paléoclimat, Holocène

Acknowledgements

I want to express my gratitude to all the people who one way or another encouraged and helped me through these four years of working on my PhD thesis. I would like to thank the Region Normandy for funding my PhD project, the RIN-PALECONOR (2019-2022) project that funded the analysis and fieldwork, and Paul Rabel from the French Federation of speleology and canyoning for providing access to Caumont cave and quarry.

Firstly, I am very thankful to my supervisors, Damase Mouralis and Carole Nehme for giving me the opportunity to discover the world of speleothems in Normandy. They made me feel welcomed since the beginning and supported me through the process of changing countries. Thank you for all your guidance and encouragement throughout these four years. A huge thanks also to Sebastian Breitenbach, who was my third supervisor and provided extra guidance and encouragement during my thesis.

Gracias infinitas a mis papás y a mi hermana que desde la distancia siempre me respaldan e impulsan a seguir cumpliendo mis metas. Gracias a ellos y el resto de la familia por el gran apoyo moral que me mandan desde Colombia.

To all my friends, since childhood, from back home and the others that came along the way during my time in Lund and in France, I thank you greatly for your company and encouragement. I am also extremely grateful to be able to share the experience and challenges of doing a PhD with friends going through the same journey.

I am deeply grateful to all the colleagues from our Laboratory IDEES for welcoming me into the team. Thank you especially to the PhDs, post-docs, engineers, interns and former colleagues from the open space, for the good atmosphere and company. Special thanks to Igor, Kim, Clement and Daniel who helped me a lot in the first years of my thesis and for their company during fieldwork. Likewise, I want to thank Dominique and Stoil, for their guidance, and to Zoe, France, Victor, Florent and Olivier who always offered me a hand. I am especially grateful to Lea for all her generous help and support in many occasions. Thank you all greatly for the shared moments during these four years and for the guidance into the French way of life.

A special thanks to the team at Northumbria University, Sevi, Stuart, Jade and Ola who along with Seb welcomed me warmly to their Lab. I'm very grateful for your assistance with the lab work, the company and all the coffee/hot chocolate breaks that made my various stays in Newcastle so enjoyable.

I also want to thank Isabelle Couchoud (EDYTEM, Univeristé de Savoie), for the supervision with the sampling and Edwige Pons-Branchu (LSCE, Univeristé Paris-Saclay) for the guidance with the chemical analysis, of the U/Th ages. To James Baldini, (Durham University) for the assistance and supervision of the trace elements measurements as well as the analysis of the data. To Monica Ionita (AWI) for the support with the climatic data and guidance with its interpretation.

Lastly, I want to thank the members of the jury for accepting being a part of my defence panel and for their dedication to my thesis.

Table of contents

General introduction

Motivation

The current climate situation, with global warming and drastic changes impacting modern society such as heat waves, more stormy weather and drought events, is leading to issues such as flooding (Blöschl et al., 2020), water shortages (Bakke et al., 2020), economic losses (WMO, 2021) and affecting natural systems (Smith and Matthews, 2015). The climate prediction for Europe is for an increasing trend of droughts events (GIEC, 2023), which calls for having a better understanding of how climate fluctuations occur, what are the drivers, and how it can impact the hydrological cycle. Studying instrumental records describing temperature and precipitations can provide an insight of the past climate changes. The climate data and drought events are well documented in European historical records (Le Roy Ladurie, 1967; Chuine et al., 2004; Camenisch and Salvisberg, 2020; Cook et al., 2022), however the historical data and instrumental records are restricted and therefore there is a need for records that can go further back in time. The continental natural archives that can record paleoclimate data include tree rings (Büntgen et al., 2011), lake and mires sediments (Kühl and Litt, 2003), and secondary caves deposits, speleothems (Wong and Breecker, 2015) .

The study of the past rapid climate fluctuations during the Holocene can help understand the patterns of climate systems and environmental changes on centennial time scales, and also evaluate the past impact of human activities (Kalis et al., 2003) and our potential impact on the future climate (IPCC, 2007). Different climate fluctuations or cold events were identified based on temperature and precipitation proxies (e.g. ice cores, sea, lake and peat bog sediments, and speleothems), as well as glacier reconstruction analysis (Bond et al., 2001; Wanner et al., 2011). In recent decades, numerous studies have focused on the analysis of speleothem-based proxy records (stable isotopes and trace elements) to further disentangle the Holocene climate. These studies have also shown how the cold events were not evenly recorded in all the stalagmites around Europe, proving the complexity of past climate reconstructions (Mayewski et al., 2004). Even though western Europe has the most stalagmite-based paleoclimate studies globally, there are still certain areas with gaps of information such as France (Lechleitner et al., 2018). Several authors have concluded that there is still a need for more paleoclimate studies, particularly stalagmite-based records, that can help provide a more

robust knowledge about the Holocene paleoclimate (Verheyden et al., 2014; Breitenbach et al., 2019).

One of the areas that lacks stalagmite-based paleoclimate data is the Normandy region in northern France. Our study on Caumont Cave aims to fit this spatial gap and to provide robust paleoclimatic data. The cave monitoring and sampled stalagmites, provide information regarding the capacity of Caumont cave to record paleoclimate data. The stalagmite-based proxy records allow to disentangle the potential drivers of climate dynamics during the Holocene and its significance in north-western Europe.

Aims and structure of the thesis

This thesis aims at investigating the potential of the speleothems from the Caumont cave and quarry system, to serve as high-resolution archives for past climate and environmental conditions. The specific research questions relate to: 1) the present-day conditions of the cave, 2) understanding how it records the climatic signal in the calcite and its significance, then to 3) be able to interpret the recorded paleoclimate signal further back in time:

1. How do the present cave internal settings (e.g., temperature, drip rate) affect the paleoenvironmental signals recorded in stalagmites? What are the major drivers influencing the geochemical proxies ($\delta^{18}O$, $\delta^{13}C$ and trace elements)?

2. Does a well dated and highly-resolved recent stalagmite (CCB-1) have the capacity to record drought events? What are the mechanisms behind drought events during the last century? How do the recorded climatic proxies ($\delta^{18}O$, $\delta^{13}C$ and trace elements) of the last century compare to the historical and instrumental records? Have drought dynamics remained the same for the last 120 years or has there been a change?

3. How do the Holocene stalagmites record the environmental and climatic evolution of the last 10.000 years before present? What were the main forcings driving hydrological, climate and environmental change? How do the geochemical proxy records ($\delta^{18}O$, $\delta^{13}C$ and trace elements) compare in a regional scale in Normandy and in the north-west European scale during the Holocene?

In order to address the aims and research questions, the thesis contains 5 chapters, with a common reference list at the end. Chapter 1 provides an introduction to the topic presenting the general description of the Holocene epoch, the state of the art for Holocene paleoclimate studies in Europe, and how speleothems are used as archives of paleoclimate. There is no individual methods chapter as each chapter describes the methodology used and Chapter 1 presents a general description of the used methods.

Chapter 2 to 4 are the thematic chapters where the main results and discussions of the thesis are presented. Chapter 2 is a published article in the *International Journal of Speleology* (IJS), Chapter 3 has been submitted, and is under review, as a scientific article to the journal *Scientific Reports* and Chapter 4 is developed with the structure of scientific article, with the aim of submitting for publication soon.

Chapter 2 shows the results of the monitoring study of Caumont, done on three different sites from both natural cave and quarry. This study describes how the geochemical signals are recorded in recent calcite and in the water, under current cave climate conditions. The results show how do the factors influencing calcite deposition (e.g. precipitation and temperature), relate in Caumont cave. The collected water and recent calcite stable isotope data are compared to records from other close by monitoring station in France and to global records (global meteoric water line).

Chapter 3 focuses on the recent stalagmite (CCB-1), sampled from a quarried gallery, and the comparison of the obtained highly resolved geochemical proxy record with temperature, precipitation and drought index climatic data. The evaluation of these records provides information about drought events, corroborated with historical data. Moreover, the comparison allows to disentangle the drought dynamics and asses for fluctuations during the last 120 years.

Chapter 4 concerns the climate and environmental changes registered in stalagmites from the natural conduits, Rivière de Robots and La Jacqueline, during the Holocene epoch. The obtained multi-proxy record is the only stalagmite-based record in north-western France. The high resolution and evaluation with regional studies allows to improve the understanding of the Holocene climate variability in Normandy. The comparison with north-west European records gives an insight into the forcings driving climate change and how the changes are recorded in Caumont cave.

Chapter 5 presents the general conclusions, where the main findings of the thesis are summarised, and the recommendations for future research.

CHAPTER 1: Research context and state of the art

1.1 The Holocene epoch

The uppermost period of the geological record is the Quaternary Period (last 2.6 Ma), and is subdivided into the Pleistocene and Holocene epochs (Gibbard and Head, 2020). The Pleistocene climate was characterized by repeated cycles of glacier expansion, which were interrupted by rapid climate warming (glacial/interglacial cycles) and fast melting events (Palacios et al., 2023). These fluctuations were caused by changes in the Earth's orbital configuration, defined by precession, eccentricity and axial tilt, producing solar radiation cycles as described by Milankovitch, (1941). The onset of the ultimate deglaciation (glacial termination) began when the large continental ice sheets of the Northern Hemisphere started retreating after reaching their last maximum expansion, induced by an increase in northern hemisphere summer insolation (Palacios et al., 2023). The last glacial maximum period (26.5 – 19 ka), exhibited the lowest sea levels (Clark et al., 2009), and global average temperatures of ca. 5 °C, lower than in the Holocene (Burke et al., 2018).

The onset of the Holocene is defined at 11.7 ka, and was identified in the Greenland NorthGRIP2 (NGRIP2) ice cores, by the abrupt increase/decrease in deuterium excess values and in dust loads, amongst other parameters (Walker et al., 2018). The Holocene refers to the warm period, occurring after the last glacial period until today, with the term meaning the "entirely recent", as proposed by Paul Gervais in the late 1860's (Davis and Oldroyd, 2011). The Holocene was generally considered to have relatively stable climatic conditions, especially in comparison to the Pleistocene period. Some of the first subdivisions of the Postglacial period, made in the 19th century in Scandinavia, were based on vegetation dynamics reflecting climate changes (Steenstrup, 1841). Later, Sernander, (1908) used the terms Boreal, Atlantic, Subboreal and Subatlantic, introduced by Blytt (1876), as a stratigraphic succession of periods for the Holocene. This classification was done based on the correlation of Swedish peatlands reflecting climate variations. In the 20th century von Post (1916), presented the potential of studying pollen records and developed palynology as a dating method. To reconstruct vegetation dynamics and past climate the pollen zones were determined by correlating them to the development of different forest species along with climate changes.

In past decades, new studies have focused on studying other proxy records, at a centennial to decadal time scale (Boch et al., 2011). A better constraint of the proxy records revealed significant climate fluctuations that were classified in the tripartite subdivision of the Holocene (Wanner et al., 2008; Walker et al., 2018). The early Holocene, starting at 11.7 ka, and the onset of the middle Holocene at 8.2 ka, were both defined in the NGRIP $\delta^{18}O$ ice record. The start of the Holocene, represents the first signs of the fundamental shift towards warmer climate, meanwhile the onset of the middle Holocene shows a clear signal of cooling conditions (Walker et al., 2008). The onset of the late Holocene is identified by a marked shift to lower speleothem $\delta^{18}O$ values, from Mawmluh cave, in north-eastern India, at ca. 4.2 ka (Fig. 1.1), indicating an abrupt decrease in precipitation due to weakening of the Monsoon in India (Berkelhammer et al., 2012). On a wider scale, this event reflects the reorganisation of atmospheric and ocean circulation patterns (Paasche and Bakke, 2009). The Holocene climate variability has been further developed in recent decades with studies that have identified distinct climate changes (Mayewski et al., 2004; Boch et al., 2009; Rehfeld et al., 2018), and studies by Wanner et al. (2008) and Walker et al. (2018) defining the tripartite subdivision.

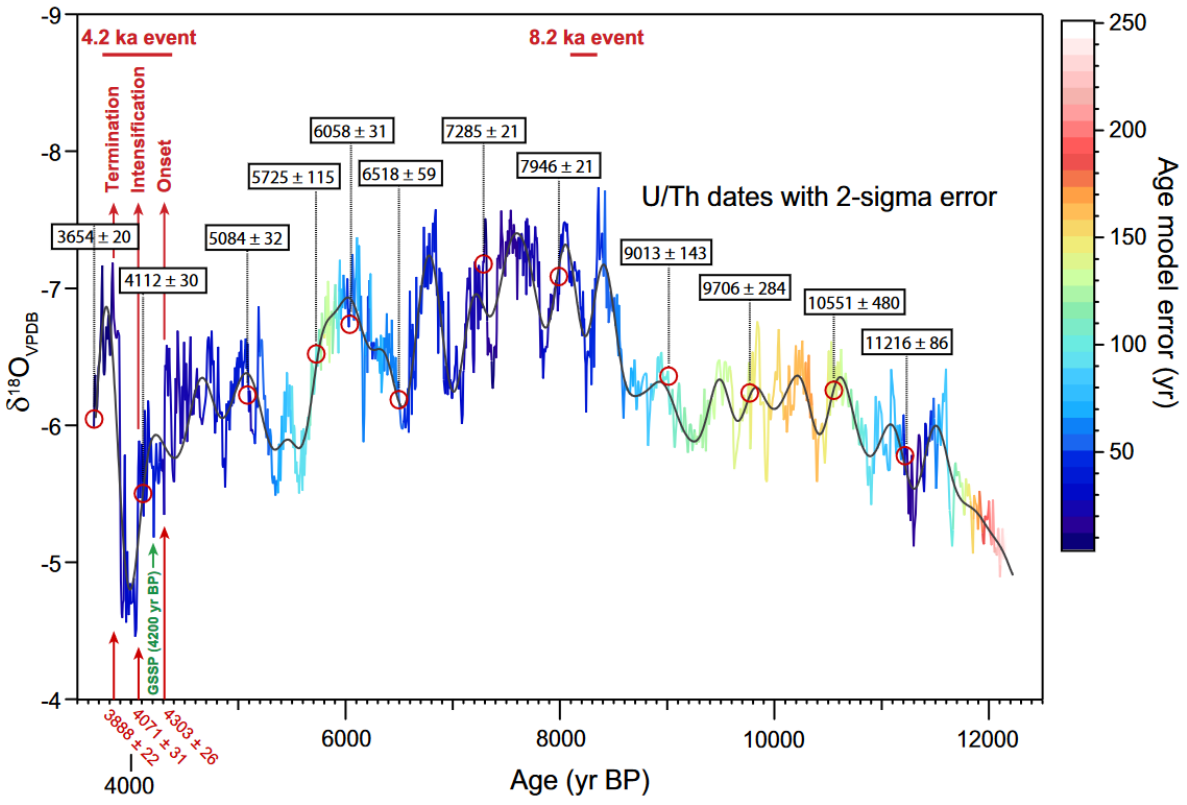

Figure 1. 1. The Mawmluh Cave $\delta^{18}O$ record for speleothem KM-A, shows the position of the 4.2 ka event on the stable isotope trace (after Berkelhammer et al., 2012). Red circles mark the Uranium - Thorium (U/Th) dates, given with their 2σ analytical uncertainty (black boxes). Age uncertainty (95%

confidence interval) was assessed using a Monte Carlo fitting procedure through the U-Th dates, shown by variations in colour along the trace. The onset and termination of the event are shown by the arrowed red lines, and the beginning of the most intensive phase of weakened monsoon is shown by a third arrowed red line: their dates (in red) are given with uncertainty, also assessed using the Monte Carlo fitting procedure. The position of the GSSP, with a modelled age of 4200 yr BP (4250 b2k) is indicated by the green arrow. Figure and caption from (Walker et al., 2018).

1.2 Holocene studies in Europe

The most commonly used archives for studying the Holocene paleoclimate in Europe have been sediments from lakes and mires. Proxy records such as pollen, extracted from these sediments are used for providing information about temperatures, vegetation composition and climatic conditions in the past (Grafenstein et al., 1999; Kalis et al., 2003; Roberts, 2013). Climatic fluctuations identified during the Holocene reflect the relationship between temperature and vegetation. At the onset of the Holocene, the landscape evolution documented in the pollen records typically shows the development of forest as temperatures increased, changing from pine dominated to more deciduous taxa. Likewise, the onset of human impacts on vegetation is identified firstly by the landscape clearings and then by the appearance of cereal species and progressive agriculture (Litt et al., 2009). Pollen-based temperature reconstructions for Europe show how the North, central and South of the continent showed slightly different vegetation responses, with the North being more sensitive to the traditional mid-Holocene thermal maximum (Davis et al., 2003).

Speleothems (secondary cave carbonates) have been increasingly used over recent decades for Holocene paleoclimate reconstructions (Wong and Breecker, 2015), since they can precipitate under various climates and are fairly preserved in confined environments, such as caves. One of the major assets of speleothems as continental archives is the possibility of using U-series dating with a precision better than 0.5 % (Cheng et al., 2009). This method can be used for samples from 150 years (Zhao et al., 2009), to ~600 ka and the U-Pb technique for much older ones (Woodhead et al., 2006). Speleothem studies can also allow us to reconstruct climate variability through the stable isotope records of $\delta^{18}O$, strongly linked to rainfall, and $\delta^{13}C$, linked to vegetation bio-activity. The climate can be reconstructed from a seasonal scale to older time scales as the Glacial-Interglacial periods. The reconstruction of trace elements in speleothems allow us to link their variability with local or regional drivers such as vegetation

dynamics, epikarst processes and even human impact through the study of S, Pb, Yt, and Rare Earth elements (Fairchild and Treble, 2009; Pons-Branchu et al., 2014).

The potential use of speleothem records is concentrated mostly in carbonate rock areas and the European geology contains extensive carbonate deposits (Chen et al., 2017) (Fig. 1.2.). The compilation of stalagmite records (Speleothem Isotopes Synthesis and AnaLysis - SISAL), by Lechleitner et al., (2018) showed that on a global scale, the majority of the stalagmite-based studies are in located western Europe. However, it is not a homogeneous distribution, with extensive areas of carbonate rocks in countries like Spain, Germany and France underrepresented by studies (Fig. 1.2). The analysis of the compiled stalagmite $\delta^{18}O$ records does not show a coherent regional trend for the Holocene climate variability for western Europe. The 8.2 ka event was used as a benchmark to subdivide the Holocene given its significance in North Atlantic temperature variations, yet it has not been identified in all records, highlighting issues of low temporal resolution and age modelling uncertainties of some records (Lechleitner et al., 2018).

Another study by Mayewski et al., (2004) compiled and examined ~50 globally distributed paleoclimate records, with high resolution, dating quality and that preferably fully cover the Holocene. The study classified 6 significant rapid climate changes (RCCs), based on the glacier fluctuation record (Denton and Karlén, 1973), for the periods of 9-8, 6-5, 4.2-3.8, 3.5-2.5, 1.2-1 and 0.6-0.15 cal ka BP. Mayewski et al. (2004) described the first RCC, 9-8 cal ka BP, as the only event that is related partly to volcanic forcing, and during which a significant short lived cooling was registered at 8.2 cal ka BP (Alley et al., 1997). The rest of the RCCs, except for the most recent, were characterized by bipolar cooling with the intensification of the atmospheric circulation at high latitudes. The most recent RCC (>0.6 cal ka BP) is described as more complex than the other RCCS, with high levels of volcanic aerosols related to its onset. The general climate forcing was attributed to solar variability and long-term insolation changes. The authors conclude that despite the apparent global significance of the RCCs, not all sites respond synchronously, which highlights the complexity of the Holocene climate variability.

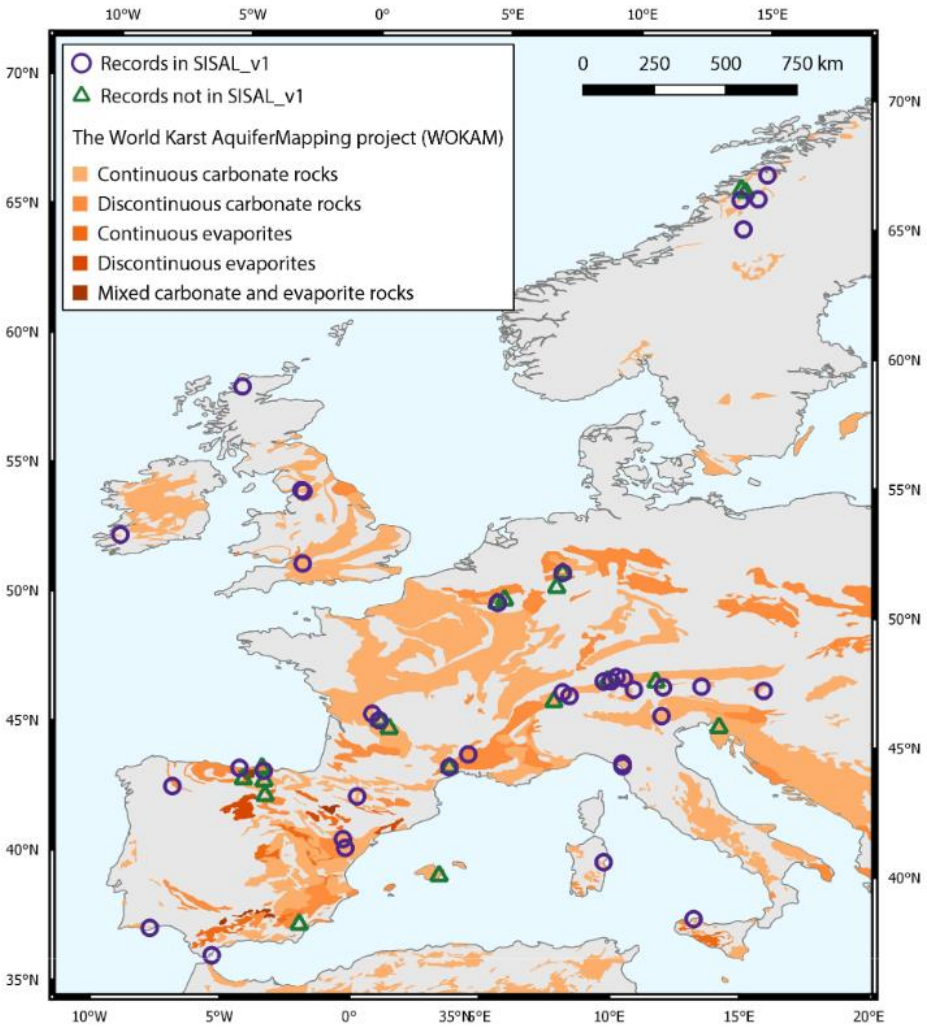

Figure 1. 2. Distribution map showing the carbonate and evaporative rocks from the World Karst Aquifer Mapping project (Chen et al., 2017). Purple circles show the sites included in SISAL_v1, while green triangles indicate study sites identified by the SISAL working group, but not yet included in SISAL_v1 database.

Amongst western European countries with speleothem-based Holocene climate studies are Belgium, France, Italy, Ireland, Germany, Spain and United Kingdom. In order to have a better understanding of a studied cave and its stalagmite records, several authors emphasize the importance of preliminary cave monitoring, including regular sampling of seepage water, modern calcite, cave air temperature, humidity measurements, among others (Verheyden et al., 2008; Riechelmann et al., 2011; Treble et al., 2013; Surić et al., 2018). This is considered a prerequisite for later interpreting the speleothem data regarding climate variability.

A monitoring campaign was carried out in Père Noël Cave in southern Belgium, between 1991 and 1998 (Verheyden et al., 2008). The results revealed that the drip rate signal

is highly influenced by season as well as being controlled by water excess and rainfall. The modern calcite analysis showed that the stable isotope and trace elements signal are also closely linked to the water recharge and hence drip rate. The understanding of the recent cave deposition gave way to later study a multi-proxy stalagmite-based record, covering 12.9 to 18 ka BP (Verheyden et al., 2014). The fluctuations of the $\delta^{18}O$, $\delta^{13}C$ and trace elements records, growth rate, stalagmite diameter were interpreted in relation to climatic variations. Verheyden et al. (2014) interpreted the early Holocene as generally wet, with a rapid wet/dry episode at ca. 8.5 ka BP. Wetter and warmer conditions were identified between 7.9 and 6.6 ka BP, followed by a dry and/or colder climate after 6.6 ka BP. The dry conditions were reflected by the increase in the geochemical data, until the final "drying out" of the stalagmite from 5.3 to 1.8 ka. The authors concluded that to have a more robust regional climatic reconstruction, the results should be compared to other stalagmite records from Père Noël Cave as well as other caves, also to identify possible local effects.

The study from McDermott et al. (1999) analysed stalagmite records from Crag Cave, in south-western Ireland, Grotta di Ernesto (GDE), in north-western Italy, and Grotte de Clamouse (GDC), in south-eastern France. The climate variations during the Holocene of the three cave records presented some differences, associated with temperature and rainfall variations of each cave. During the early Holocene, the Crag Cave record showed low $\delta^{18}O$ values indicating cooler climate as the $\delta^{18}O$ record is related to temperature and the proximity to the Laurentide icesheet deglaciation. Unlike Crag, the $\delta^{18}O$ record from GDE presented high values reflecting warm and/or dry conditions; the GDC record showed relatively lower values, related to wetter conditions. For the last 3 ka BP, the $\delta^{18}O$ records from Crag showed higher values, indicating warmer conditions on the Atlantic, whereas the GDE and GDC records presented lower $\delta^{18}O$ values, reflecting cooler conditions. McDermott et al. (1999) conclude that there seem to be a decoupling of the Atlantic (Crag) and Mediterranean (GDE and GDC) records and highlights the need for more studies in the regions to better constrain the climate variability.

Stalagmite records from two caves in Germany, Bleßberg (E) and Bunker (NW) (Breitenbach et al., 2019), were used to reconstruct the local and regional environmental conditions during the Holocene. The stalagmite study from Bleßberg cave showed that the $\delta^{13}C$ and Sr/Ca inform about the local environmental changes above the cave, such as vegetation and soil variations, as well as effective infiltration during the Holocene. Whereas the $\delta^{18}O$

record shows a more regional signal and is related to moisture source dynamics and temperature. Moreover, Breitenbach et al. (2019) compared the stalagmite multi-proxy record ($\delta^{18}O$, $\delta^{13}C$ and trace elements) from the two caves in Germany to lake records in SW Greenland. The analysis showed the complexity of the boundary, between oceanic and continental climate, that frequently fluctuated east to west over the last 4 ka BP. The shifts were identified based on Bleβberg and Bunker $\delta^{18}O$ records' response to the North Atlantic Oscillation (NAO) dynamics and Siberian High strength, which both influence temperature, and the soil development and precipitation during winter across Europe. The authors also conclude that the estimated climate boundary dynamics is limited due to the reduced amount of well dated and high resolved reconstructions in Europe.

In northern Spain, a stalagmite high resolution $\delta^{18}O$ record from Kaite Cave spans the past 4 ka. In this study Domínguez-Villar et al. (2008), focused on analysing the causes and variability of the $\delta^{18}O$ record on millennial, centennial and decadal time scales. On the decadal time scale, the main driver of the $\delta^{18}O$ record was ascribed to the rainfall amount effect, which refers to the rainfall isotopic depletion as a result of a higher rainfall amount. This effect is described as producing a variability ranging from between 1 and 2 ‰ in Kaite Cave. On the long-term, millennial and centennial time scales, the main drivers of $\delta^{18}O$ record variability were related to a combination of rainfall amount and fluctuations in the oceanic source isotopic composition or storm tracks.

The study of speleothem trace element records from Uamh an Tartair cave in northern Scotland, showed high frequency fluctuations and long-term trend in Mg/Ca, Sr/Ca and Ba/Ca during the Holocene. Roberts et al. (1998), defined that the elemental variations reflected hydrochemical processes in the unsaturated zone above the cave. The variations of the Mg/Ca record on a short-term scale resulted from seasonal temperature changes. For the long-term trends, the authors attribute the oscillations to variations in water residence time, which are controlled by effective precipitation. This study highlights the potential of speleothems to provide high resolution insight for paleoclimate variability and encourages the comparison with other stalagmites from the same period.

The stalagmite-based records from different study sites in north-western Europe, show how the parameters influencing stalagmite deposition, and consequently the proxy records, may vary depending on the cave. Overall, during wet and warm conditions, the continental

records reflected low isotopic values, except in Ireland where high values reflected warm conditions. On the contrary, the periods of dry and cold conditions showed high isotopic values, in the continent, and lower isotopic values in Ireland. The spatial variations evidence the complexity of paleoclimate variability and how the reconstructed fluctuations as well as the drivers influencing the geochemical signal may also differ between locations.

The studies of recent speleothems, deposited in the last centuries, and the relevance of monitoring studies (Chapter 2), have also increased in the past decade. Since recent speleothem studies can be directly compared to instrumental data and historical records, this allows to disentangle recent climate parameters like rainfall variability (Treble et al., 2013) and drought events (Büntgen et al., 2021; Cook et al., 2022, Chapter 3). Likewise, recent stalagmite studies can provide a better assessment of the human impact on factors like pollution of water resources (Pons-Branchu et al., 2014; Garagnon et al., 2023) and in cave environnements (Verheyden et al., 2006).

In the north of Paris recent stalagmites deposited in the aqueduct of Belleville, provide evaluations of the human impact during the past three centuries, from stalagmite studies. The analysis of trace elements like Pb, Mn, Cu, Al, showed higher values since the 1900s, giving insight to the increase in water pollution, triggered by urbanization (Pons-Branchu et al., 2015). Likewise, in Garagnon et al. (2023), the stalagmites from Belleville were used to do further water resource pollution studies based on the organic pollutant, polycyclic aromatic hydrocarbons (PAHs), used as an anthropogenic proxy. The PAHs end up in the stalagmites after being emitted into the atmosphere, then deposited in the surface and, similarly to cave speleothems, transported by infiltrating waters into the aquatic setting. Their analysis showed that these organic pollutants have been present since the last 300 years and the quantity have increased by 7 times in the last few decades.

Moreover, at Han-sur-Lesse cave, in Belgium, Verheyden et al. (2006), studied recent speleothems and gave insight on the anthropogenic perturbation of the cave environment, in Salle du Dôme. Traces of straw found on top of the stalagmite were dated and evidenced the presence touristic visits of the cave between 1760 and 1810 CE. Additionally, the pollution of soot on the calcite proves the visits of humans with torches in the cave, which were dated until 2001 CE. The whiter calcite deposited at ca. 1917 and between 1940 and 1945 CE, indicates the period when the cave was closed to visitors during WWI and WWII. These examples of

recent stalagmite studies highlight the abundant information that can be extracted along with a wide range of applications that can be given to stalagmite studies.

1.3 Speleothems, archives of Holocene paleoclimate

Speleothems are defined as mineral deposits that grow with in caves or secondary cave deposits (Moore, 1952), which have been classified as stalagmites, stalactites, flowstones, among others (Hill and Forti, 1997). In the last decades speleothems have been categorised as one of the most significant resources that help understand past conditions on Earth' surface, since the Pleistocene until present day (Fairchild and Baker, 2012). Speleothems are good archives of paleoclimate due to their formation process, which can be sensitive to temperature patterns, precipitation composition and other climate parameters. The climatic conditions above the cave can be recorded in the chemical composition of the calcite laminae, at the moment of deposition. The geochemical analysis of the calcite, which can be done in high resolution, then allows to unravel the stored information, as explained in the following sections.

Almost all speleothems used for paleoclimate research are largely composed of calcium carbonate and form within carbonate rocks, which can be limestone or dolomite. These rocks can have the capacity to store, transmit and transfer water making them aquifers. Carbonate aquifers are found in karstic regions where the water drains into the bedrock (Ford and Williams, 2007). The karstic areas are characterized by presenting sinking streams, caves, enclosed depressions and large springs (Ford and Williams, 2007). These features can occur in the limestone bedrock when it develops cavities which vary in size from tiny pores, to enlarged fissures and then conduits, that result from past or present-day active ground streams. The further development of the drainage system in the karst generally produces the phreatic and vadose zones divided by the water table. In the overlying vadose zone, the cave formation results in downwards vertical cuts or passages and in the abandoned passages is where speleothem formation occurs (Fairchild and Baker, 2012).

Calcareous speleothems form in almost all continental regions, on a global scale, but are limited by the presence of karstic host rock and dripping water into the cave. In France there are different karst deposits divided by region into Mountainous (Alpine and Pyrenees), Mediterranean, Plateaus and Plaines (sedimentary basins) karst. Most of the mountainous and

Mediterranean karst is exposed, while the plateaus and plains karst are covered (Fig. 1.3). Amongst the plateaus and plains karst there is the Aquitaine and Paris basins (Nicod, 1995), from which the latter is composed by Cretaceous chalk with an important level of fracturing that allows the development of karstic networks (Rodet, 1992). The karst in the Paris basin, specifically in Normandy, is covered by tertiary sand and loess deposits with clay and flint (Nicod, 1995). The cave formation in the Normandy karst, has been studied in the last decade (Ballesteros et al., 2020, 2021; Nehme et al., 2020; Farrant et al., 2023). The specificity of speleothem formation in the Normandy chalk bedrock, at Caumont, is further explained in the separate sections of site setting in Chapters 3, focused in a recent stalagmite, and Chapter 4 focused on Holocene stalagmites.

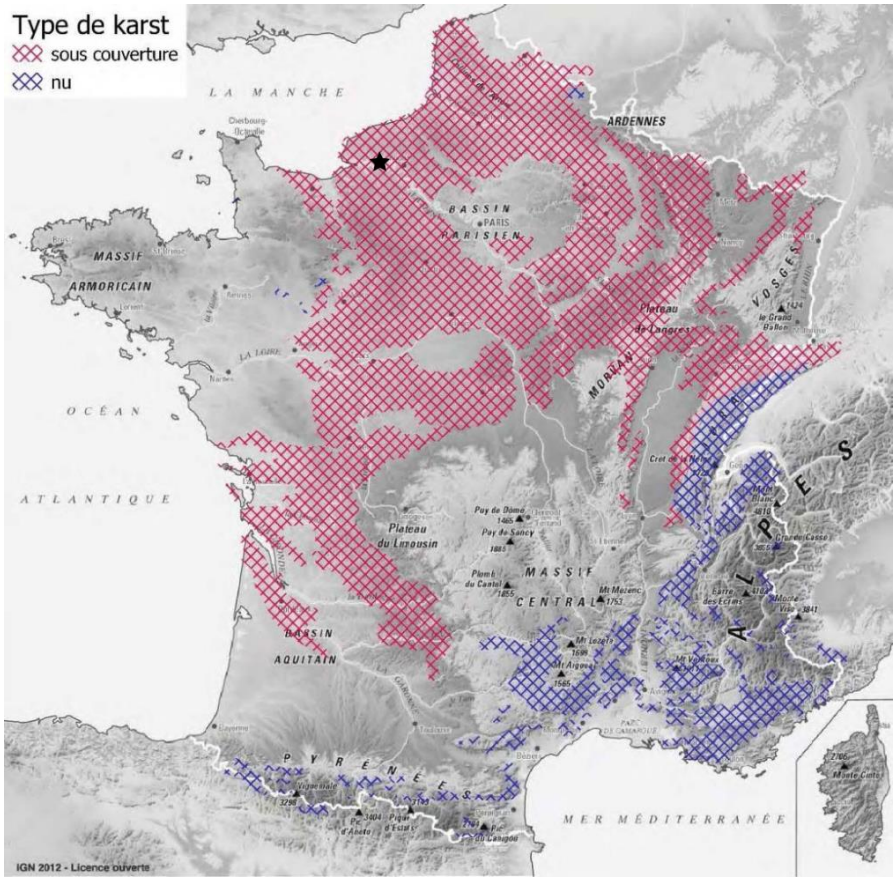

Figure 1.3. Simplified map of France, depicting the exposed (blue) and the covered (pink) karst, with the location of Caumont cave (black star) in the north. Map from the BRGM, based on Nicod et al., 2010.

The formation of speleothems in caves, considered as a confined environment, allows them to be protected from surface weathering and erosion (Demény et al., 2021). Additionally, with the right internal conditions for carbonate deposition and preservation, the speleothems can be preserved for millions of years. Given the chemical properties of speleothems they can

be precisely dated, with U-series methods, and register a wealth of climatic and environmental information (Demény et al., 2021; Verheyden et al., 2022). This information can be extracted through proxy records (eg. $\delta^{18}O$, $\delta^{13}C$ and trace elements), making speleothems widespread and excellent archives of paleoclimate and environmental data (Fairchild and Baker, 2012; Walker et al., 2018).

1.3.1 Speleothem formation

The formation or deposition of speleothems inside a cave is a process controlled by factors that occur both above and inside the cave. The bedrock, geomorphology, vegetation and climate conditions above the cave influence the water distribution, quantity and chemistry that percolates through the karstic aquifer. The geometry and aquifer properties also influence the cave microclimate, which can be specific to each cave (Fairchild et al., 2007).

There is a variety of speleothems that form in caves, such as stalagmites, stalactites and flowstones. Stalagmites are better adapted to produce records of interest for paleoclimate studies due to their successive deposition of convex laminae that can record chronologically along their axe (White, 2004). The laminae, growing upwards from the floor, can be used as a coherent chronological axe. Stalactites, growing from the ceiling downwards, present a laminated structure yet the water that percolates goes through a central canal and it flows as a water film on the outer walls, making it difficult to define the chronological sequence (Couchoud, 2008). Flowstones, speleothem sheets formed in the walls and floors from thin water flow, grow relatively parallel to the host surface. They can grow over thousands of years but the abundant impurities can compromise the dating accuracy (Fairchild et al., 2007)

A series of chemical exchanges occur in the deposition process of stalagmites, starting with the rain on the surface to the resulting concretion inside the cave (Holland et al., 1964). Precipitation infiltrates into the soil where it becomes recharged with CO_2 (cf. equation I) which is then released by root respiration, micro-organisms and decomposition of organic matter (Fig. 1.4) into the soil (Couchoud, 2008).

The soil can reach a 10 % of CO_2 concentration and the rest is released back in to the atmosphere. The presence of dissolved CO_2 makes the water acidic and aggressive for the limestone, which then infiltrates the soil until it comes in contact with the bedrock (Fairchild

and Baker, 2012). The limestone is dissolved until the water is close to equilibrium (cf. equation II). If there is enough water residence time in contact with the bedrock, the percolating water through the limestones fissures is saturated with dissolved carbonates (Couchoud, 2008).

As the water reaches the roof of the cave it is no longer in equilibrium with the local environment. The CO_2 partial pressure (pCO_2) in the soil is very high compared to the atmosphere, and hence the water CO_2 pressure is also high. In the cave, the pCO_2 is generally higher than in the atmosphere but lower than that of the infiltrating water (Ford and Williams, 2007). In the cave, the water dripping from the ceiling into the ground then releases CO_2 becoming supersaturated in carbonates and after the rebalancing occurs, the calcite precipitates (II) (Couchoud, 2008).

$$CO_2 + H_2O \leftrightarrow H^+ + HCO_3\text{-} \quad \text{(I)}$$

$$CaCO_3 + CO_2 + H_2O \leftrightarrow Ca^{2+} + 2HCO_3\text{-} \quad \text{(II)}$$

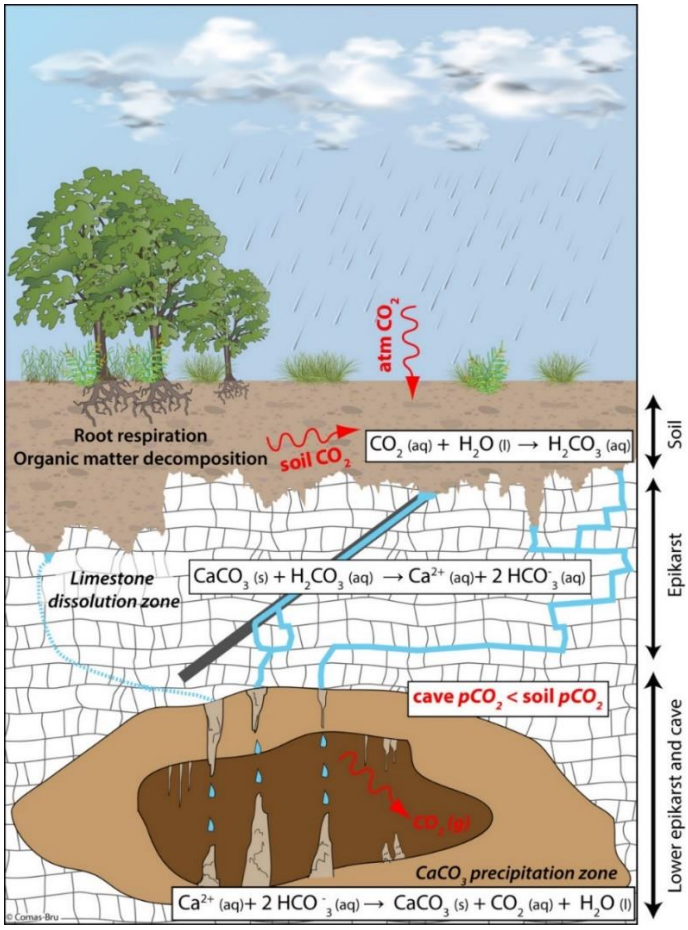

Figure 1.4 Schematic of the general speleothem formation. Depicting the chemical reactions from precipitation to the depositions of stalactites and stalagmites. Illustration from Paleoclimate Data Syntheses EGU blog, by Laia Comas-Bru.

The upward extension rate of stalagmites, defined as growth rate, depends in part to the regional climate. In warm and humid regions, the growth rate could be of one millimetre per year and in the cool temperate regions is normally of the order of less than 100 µm per year (Fairchild and Baker, 2012). Dreybrodt, (1981) stated that the growth rate of speleothems is primordially influenced by the degree of mineralization (Ca^{2+}) which is directly linked to the water capacity of dissolving calcium carbonate, and depends on pCO_2 in soil water. Meaning that the activity above the cave of soil microorganisms and plants determine the biogenic CO_2 production and influences the speleothem growth rate.

1.3.2 Speleothem dating by U-series dating

The U/Th or ^{230}Th dating is the preferred method to use in speleothems (Hellstrom, 2003), given the high level of precision achieved with the thermal ionization mass spectrometry (TIMS), during the 1990's. Later improved by multi-collector inductively coupled plasma mass spectrometry (MC-ICPMS) which also decreased even more the needed sample size. Likewise, it is possible to date speleothems from ~500,000 years in age, until present with an analytical precision of 100 years or less (Cheng et al., 2013).

For this dating method the principle is based on the incorporation of uranium during speleothem growth, transported in aqueous solution from the surface and into the cave. The U is naturally soluble at the surface under normal conditions of temperature, pressure and bedrock pH. The percolating water is enriched in U as it leaches through the soil above the cave and bedrock (Columbu, 2016). It is normally assumed that there is no incorporation of thorium because it is insoluble and usually results in detrital particles (Bourdon et al., 2003). After a speleothem growth layer deposits, the ^{230}Th nuclide accumulates over time, by the radioactive decay from ^{234}U (Fairchild and Baker, 2012). The deposition of the calcite layer closes the system and sets the "time" to zero after which the U decays eventually reaching secular equilibrium, defined as the necessary time to reach equilibrium between "parent" (U) and "daughters" (^{234}U and ^{230}Th) nuclides (Honiat, 2022).

In order to generate accurate ages, the radioactive system must occur in a closed geochemical system and the initial ^{230}Th concentrations should be well constrained. The measurement quality also depends on the U purity and quantity, there should be enough (~ tens of U ppb), in the sample (Cheng et al., 2013). Pollution of the sample may include initial ^{230Th}

which could result in artificially older ages but this could be corrected with the isochron method (Couchoud, 2008).

1.3.3 Stable isotope analysis

The chemical elements that present the same atomic number, meaning the same number of protons and electrons, but with different mass number (neutrons), are defined as isotopes (Fairchild and Baker, 2012). The difference in mass of the isotopes results in different physical properties, making them useful recorders of environmental processes. Stable isotopes are not radioactive, meaning they do not decay in time, and their composition offers an insight on the fractionation conditions. Isotopic ratios abundances are small, not given in absolute values, generally expressed in per mil (‰) difference from a standard and in the deviation form with δ notation (Coplen, 1994). The oxygen isotopic composition, is denoted with the equation (III):

$$\delta^{18}\mathrm{O}\ (\text{in } ‰) = \left(\frac{\left(\frac{^{18}O}{^{16}O}\right)}{\left(\frac{^{18}O}{^{16}O}\right)} - 1 \right) \text{x } 1000 \qquad \text{(III)}$$

The established standard for calcite stable isotopes is Vienna Pee Dee Belemnite (VPDB) and for oxygen water isotope is Vienna Standard Mean Ocean Water (VSMOW) (Lin et al., 2010). The comparison of the ‰ variation through time between the standard and the sample (water or rock), allows for climate interpretations. Samples with higher or more positive isotopic values are enriched regarding the standards, which is traditionally defined as heavier. On the contrary, for the lower or more negative isotopic values they are called lighter (Fairchild and Baker, 2012).

The fractionation of the stable isotope, that occurs during a phase change, can be determined by the mass difference between higher (heavy) and lower values (lighter), for example ^{18}O (heavier) and ^{16}O (lighter) for oxygen (Lachniet, 2009). Isotope ratios fluctuate in nature due to physical or chemical environmental processes (Kim and O'Neil, 1997; Coplen, 2007). The fractionation behaviour can be quantified and it is expressed as fractionation factors, α (cf. equation IV):

$$\propto_{A-B} = \frac{R_A}{R_B} \quad \text{(IV)}$$

It describes the fractionation from state R_A to state R_B (Sharp, 2017). Fractionation may occur under equilibrium or disequilibrium (kinetic) conditions, where kinetics can make the original climatic signal unclear (Lachniet, 2009). However, if the isotopic equilibrium is maintained the resulting calcite precipitation will therefore be in equilibrium with the infiltrating water, and where the $^{18}O/^{16}O$ variations depend and $^{13}C/^{12}C$ could be independent of climate (Hendy, 1971). One way of testing the isotopic equilibrium is by replicating the $\delta^{18}O$ records in two or more coeval stalagmites from adjacent locations or in the same cave (Dorale and Liu, 2009).

1.3.3.1 Calcite $\delta^{18}O$ and $\delta^{13}C$

The stable isotope analysis in speleothems is usually done with oxygen ($\delta^{18}O$) and carbon ($\delta^{13}C$) elements. The $\delta^{18}O$ record generally provides large scale information while $\delta^{13}C$ is more sensitive to changes in a local scale (Cheng et al., 2016). The factors influencing calcite $\delta^{18}O$ have a complex interplay of atmospheric circulation (Breitenbach et al., 2010), moisture source, amount of precipitation and drip water residence time in the epikarst (Lachniet, 2009).

The calcite $\delta^{18}O$ of speleothems depends on cave air temperature and precipitation $\delta^{18}O$ values, which subsequently relies on regional hydrological cycle and evaporation pathways. The drip water isotopic signature is recorded in speleothems, as they precipitate, and therefore they may also record the rainwater that infiltrates from the soil, through the bedrock and into the cave.

The soil-karsts system creates a filtering effect in the calcite $\delta^{18}O$ signal which can result in a temporally attenuated signal, compared to the original precipitation $\delta^{18}O$ (McDermott et al., 2011). The calcite deposition rate may change seasonally due to the soil pCO_2 and dripwater calcium content seasonal fluctuations, resulting in a possible seasonal bias of the stalagmite $\delta^{18}O$ and $\delta^{13}C$. In order to detect this, detailed monitoring of drip sites is recommended to better understand the controlling factors of the growth rate seasonal variability (McDermott, 2004). Therefore, with the careful analysis of factors influencing the $\delta^{18}O$ record, it can be used as a hydroclimate record.

For the $\delta^{13}C$ stalagmite record one of the main controlling factors is the biogenic CO_2 and how the vegetations fractionates this gas during photosynthesis, which subsequently depends the type of vegetation C_3 or C_4. C_3 vegetation is dominant in temperate regions and produces a lighter CO_2 resulting in $\delta^{13}C$ values between -14 and -6 ‰ in the stalagmite. C_4 vegetation, such as dry grasslands, emit CO_2 values that result in higher calcite $\delta^{13}C$ values between -6 and 2 ‰ (McDermott, 2004). The recorded $\delta^{13}C$ values in the stalagmite can then be used as a proxy for vegetation changes and evolution driven by climate, and this could be verified by comparing with other proxies such as pollen records (Dorale et al., 1998; Columbu, 2016).

Another factor that influenced the $\delta^{13}C$ records is the infiltrating water pathway, which may experience a degassing phase, occurring in bedrock pockets filled with low pCO_2 air or low humidity (Oster et al., 2010). In this instance evaporation may occur triggering prior calcite precipitation (PCP) and increasing the $\delta^{13}C$ values. Moreover, a longer water residence time can also result in evaporation and hence result in higher $\delta^{13}C$ values (Fairchild and McMillan, 2007). The relative reduction in precipitation decreases the vegetation activity at the surface and then causes a hydrological flow slowdown, enhancing the evaporation possibilities with the end result of speleothem $\delta^{13}C$ enrichment. In contrast, an increase in precipitation yields lower $\delta^{13}C$ values (Fairchild and Baker, 2012).

1.3.4 Trace elements

Trace elements are defined as the chemical species that present much lower concentrations than calcium, oxygen and carbon in speleothems, representing less than 0.1 % or <1000 ppm of the bedrock composition (Faure, 1998). The most common trace elements present in speleothems are Mg, Sr, Ba, P, Cu, Mn, Th, among others. The abundance of trace elements in speleothems depends on different geochemical and hydrological factors, related to climatic and environmental conditions present at the time of calcite deposition (Fairchild and Treble, 2009). Individual elemental variability and incorporation into the speleothem derive from the interaction between the atmosphere deposition, soil and vegetation processes, bedrock, epikarst and dripping water into the cave (Verheyden, 2004).

For some elements, there is a fast response to water infiltration, while others are leached by a slower seepage water flow. High flow result in faster and an elevated flux of soil-derived

colloids which contain the trace elements. Contrarily, drier conditions cause degassing of CO_2, which result in PCP and the enrichment of the water feeding the speleothems with elements such as Mg, Sr and Ba (Fairchild and Treble, 2009). Given that PCP has a seasonal occurrence, it may change from periods of low Mg and Sr content to periods of elevated values, with a positive correlation, reflecting seasonality for long-term records (Johnson et al., 2006). The seasonal variations make Mg, Sr and in less extent Ba, to be considered the most suitable trace elements for paleohydrological studies. Moreover, the speleothem Mg record can be used as paleo-aridity proxy, along with other supporting studies such as modern monitoring or covariations with other proxies as stable isotope records (Fairchild and Treble, 2009). Hellstrom and McCulloch, (2000), emphasise the value and efficacy of combining trace elements with stable isotope records for paleoclimatic studies.

1.4 Study sites and sampling

The selection of the monitoring sites and the stalagmites sampling was based on previous work and exploratory sampling campaigns done in Caumont by the UMR IDEES 6266 CNRS in 2019, as a result of the RIN-Archeomateraux Territoire Patrimoine (ATP) (2017-2019) and Paleo-Ecosystemes Normandie (PALECONOR) (2019-2022) projects. The three monitoring sites were chosen based on the possibility of having dripping or running water as well as rapid calcite precipitation. Another important criterion was that the locations were not easily accessed by caving groups, allowing the use of temperature loggers that could continuously record data, for further details see Chapter 2.

A total of 20 recent stalagmites were collected from 10 different sites within the quarried (man-made) galleries of Caumont, which were later cut in half and polished to assess the quality and quantity of their laminae. From these stalagmites sample CCB-1 was chosen because it presented the highest number of laminae with a preserved internal structure and was located at the end of Salle des Rois, with reduced ventilation and re-dissolution processes.

Another sampling campaign targeted stalagmites from the natural cave conduits of Caumont site. The Rivière de Robots, yielded two stalagmites, CAU-1 and CAU-2 (Fig. 1.5A), which covered the Holocene epoch. In 2021, a second sampling campaign took place in the natural conduit of La Jacqueline, with the objective of sampling other stalagmites that were also Holocene age (Fig. 1.5 B and C). This campaign yielded four stalagmites, from which three

were selected (JAC-1, JAC-3 and JAC-4), based on the preservation quality of the laminae, minimum dissolution and longer age range.

Figure 1.5 Sampling campaigns at the natural conduits of Caumont, Rivière de Robots (A) and La Jaqueline (C) where samples were taken with hammer, chisel and mechanic drill, for samples deposited on top of flowstones (B).

CHAPTER 2: Climate monitoring in the Caumont cave and quarry system (Northern France) reveal near oxygen isotopic equilibrium conditions for carbonate deposition

Dripping stalactites at monitoring station CAU-3, Rivière de Robots.

This chapter has been published in *International Journal of Speleology* as:
Bejarano-Arias, I., Nehme, C., Breitenbach, S.F.M., Meyer, H., Modestou, S., Mouralis, D., 2024. Climate monitoring in the Caumont cave and quarry system (northern France) reveal near oxygen isotopic equilibrium conditions for carbonate deposition. International Journal of Speleology, 53(1), 13-23. https://doi.org/10.5038/1827-806X.53.1.2482

Author contributions: CN and DM designed and directed the study. IB did the fieldwork under the supervision of CN. The measurements and analysis of modern carbonate was done by IB with the supervision and assistance of CN, SB, and SM. Water sample analysis was done by HM. IB prepared the manuscript with contributions from CN, SB, and DM.

2.1 Abstract

The study of modern cave deposits forming under near isotopic equilibrium conditions can potentially help disentangle the processes influencing the oxygen isotope system and suitability of stalagmites as archives of past hydrological or thermal changes. We used cave monitoring to evaluate the impact of kinetic isotope fractionation and assess the conditions under which modern cave carbonates form in the Caumont cave and quarry system, located in Normandy, northwest France. Over 20 months, we collected climatological data, dripwater, and modern carbonate samples at 2–4-week intervals at three different stations inside the Caumont cave and quarry system. We find highly stable (10.4 ± 0.3 – 11.3 ± 0.1°C) temperature in the deeper sections of the Caumont cave and quarry system. The temporal dynamics of $\delta^{18}O_{drip}$ indicates that the drip water composition in Caumont reflects the original (though subdued) signal of precipitation, rather than the impact the seasonal to interannual cave air temperature has on isotopic fractionation. The monitoring reveals that $\delta^{13}C$ of modern carbonate is influenced by prior carbonate precipitation that occurs during the summer season when evapotranspiration can minimize effective infiltration. Comparison of $\delta^{18}O$ from dripwater and modern calcite, precipitated on glass plates and collected every two to four weeks, reveals that modern calcite forms near oxygen isotope equilibrium. A Hendy test on modern carbonate deposited on a stalagmite-shaped glass flask over 20 months confirms this finding because neither does $\delta^{13}C$ increase with distance from the apex, nor are $\delta^{13}C$ and $\delta^{18}O$ positively correlated. We conclude that the $\delta^{13}C$ signal in speleothems reflect summer (and longer-term) prior carbonate precipitation in response to effective infiltration dynamics, and that the $\delta^{18}O$ signal likely reflects annual to multi-annual changes in the composition of precipitation above the cave.

Keywords: Water isotopes, modern cave calcite, PCP, climate monitoring, chalk cave, Normandy

2.2 Introduction

In recent years, paleoclimate studies based on speleothems have benefited greatly from the information gleaned from cave monitoring. Many studies emphasize the importance of monitoring cave environments to support interpretations on speleothem-based paleoclimate reconstructions and focus on cave climate dynamics and the local processes and conditions that

make each cave a distinctive system (Verheyden et al., 2008; Mattey et al., 2010; Riechelmann et al., 2011, 2019; Tremaine et al., 2011; Van Rampelbergh et al., 2014; Breitenbach et al., 2015; Czuppon et al., 2017; Surić et al., 2018). Although monitoring is a powerful strategy to understand the processes that influence the environmental proxies that are recorded in stalagmites, it must be considered with caution. The implied uniformitarianism can be disrupted by random factors like earthquakes or sudden opening of new entrances, or human activities.

The formation of speleothems is influenced by numerous factors, both external and internal to the karst system. Processes linked to local surface environment, bedrock lithology, soil type, local vegetation and seasonal setting to karst hydrology, morphology and cave climate all affect the way in which environmental signals are transferred from the surface into the speleothem archive (Mattey et al., 2010; Breitenbach et al., 2015). Conducting extended monitoring of selected internal parameters (e.g., air temperature, drip rates) helps to understand the sensitivity that a site has (i.e., the speed and magnitude of its response) to external environmental processes, like rainfall and temperature changes at different timescales. It helps to assess whether and to what extent, environmental parameters are reflected in drip rates and dripwater chemistry. Thus, environmental monitoring in caves guides the interpretation of speleothem proxy records regarding past climate and environmental variability (Spötl et al., 2005; Fairchild et al., 2007; Riechelmann et al., 2011).

Although numerous monitoring studies have been reported from Central Europe (Dreybrodt and Scholz, 2011; Genty et al., 2014; Labuhn, 2014; Baker et al., 2018), some regions remain understudied, such as Normandy, north-western France. Here, we find the cave and quarry system of Caumont that hosts actively growing stalagmites, one of which is currently the subject of detailed investigation. The results of that study will be published in a separate publication. Here, we present the results from an 18-month monitoring campaign and discuss the implications for future speleothem proxy records from Caumont. We analyse how surface precipitation and temperature dynamics are reflected in the dripwater stable isotope composition and evaluate how these key parameters are archived in cave carbonate deposits. We aim to characterize the present condition of the cave and how the internal settings (e.g., temperature, drip rate, etc.) influence the paleoclimate environmental signals recorded in stalagmites.

2.3 Site settings

Normandy's chalk plateau in northwester France hosts many caves along the valley of the Seine River, which cuts deep meanders into the chalk (Nehme et al., 2020). Caumont study site (N 49°22'41"; E 0°54'47"; 15 m above sea level) is the largest cave and quarry system in Normandy (Fig. 2.1A), located on the left bank of the Seine, ca. 25 km southwest of Rouen.

Excavated for building stone since medieval times until the early 20th century, the Caumont cave and quarry system has numerous entrances that are located ca. 200 m from the Seine River (Fronteau et al., 2010). The underground quarry system comprises a ca. 12 km long network of with ca. 20 m wide and ca. 50 m long galleries (Fig. 1B) (Ballesteros et al., 2022). The quarry galleries intersect natural cave passages which total ca. 4 km (Rodet & Lautridou, 2003). During WWII, the Caumont quarry was occupied in 1943 by German soldiers who began to build an underground factory for liquid oxygen. In 1944, the factory was abandoned leaving behind a ~250 m long bunker made of concrete (Fig. 2.1B) (Sibout, 2011).

The thickness of the epikarst is ca. 120 m (Ballesteros et al., 2021) and the overlying vegetation is composed of hardwoods and conifers forest (C3 type). For the last two centuries, successive survey maps of the area show no evidence of a drastic change of the vegetation cover over the study area (Geoportail.gouv.fr).

The cave is developed in dedolomitized chalk with flint layers from the upper Cretaceous chalk group, specifically the Soteville Formation (Fm) (Coniacian, 86.3-89.8 Ma) (Fig. 2.1B). The chalk group is covered by Quaternary deposits, mostly sand and clay residue weathered from the overlying Paleogene sediments. The chalk bedrock presents subhorizontal bedding (Ballesteros et al., 2021) and is moderately deformed, with low amplitude anticlines and local faulting (Nehme et al., 2020). The soils above the cave are predominantly classified as poorly developed rendzina rich in calcium and magnesium. Towards the West, some brown leached soils are found which correspond to slightly clayey aeolian silts (SIGES, 1974). The cave has an underground stream, "*Rivière de Robots*", which flows in a NE direction and drains into the Seine River (Fig. 2.1B).

The nearest meteorological station is Rouen-Boos, located 20 km east of Rouen. Normandy's climate is classed as temperate maritime (Cantat, 2004) where the wettest months are October to January and the driest March to July. Monthly rainfall varies from 25 to 163

mm and the average annual air temperature is 11.3°C, with a range from 7°C to 15.5°C (Cantat, 2004). Recent research suggests that the potential evapotranspiration (PET) in the region since 1959 is higher in the spring and summer months (Diomard and Chéron, 2020).

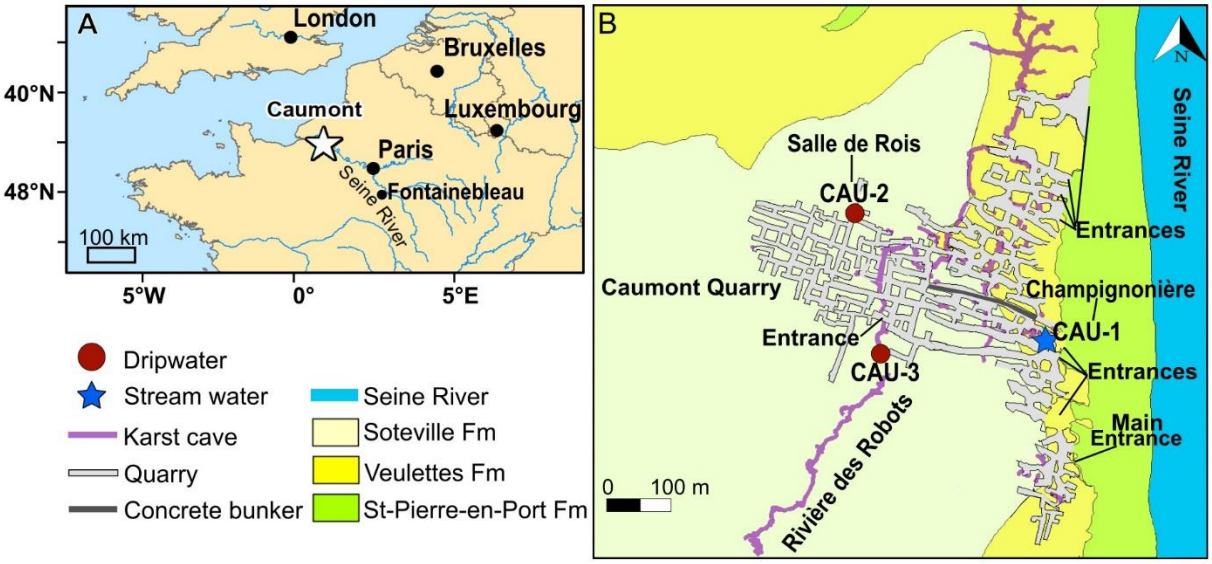

Figure 2. 1. A) Location of the Caumont cave system in northwest France relative to the Seine River. B) Geological map of Caumont displaying the quarry, natural cave, and concrete bunker contours, along with the location of the three monitoring stations and the different cave entrances. Map modified from Ballesteros et al. (2020).

2.4 Methods

2.4.1 Collection of regional climatic data

Regional climate data from the nearest meteorological station Rouen-Boos, located ca. 20 km from the cave, is used for direct comparison with monitoring results from the cave. We selected monthly temperature and precipitation (P) for the monitoring period (November 2019 to July 2021). Effective infiltration was obtained by calculating the potential evapotranspiration (PET) with the online Thornwaite method (https://ponce.sdsu.edu/onlinethornthwaite.php, Palmer & Havens, 1958) and then, subtracting precipitation (P) with evapotranspiration (P-PET). Precipitation isotope data were acquired from the nearest available global network of isotopes in precipitation (GNIP) station Fontainebleau, located at ca. 169 km south-east of Caumont, which provides a local meteoric water line (LMWL).

2.4.2 Collection of monitoring data in the cave and quarry system of Caumont

The monitoring campaign was carried out in both underground quarry and cave. Two galleries in the quarry were studied, 'La Champignonière' and 'Salle des Rois', which host the monitoring stations CAU-1 and CAU-2, respectively (Fig. 2.1B). The third station (CAU-3) is located in the 'Rivière des Robots', a natural karst conduit with variable dimensions along the Robots stream (Ballesteros et al., 2022). The stream opened a passage of ~1.60 m wide, and as it intercepts larger chambers it widens up to ca. 3-5 m. The 'Rivière des Robots' flows in a north-east direction towards the Seine River (Fig. 2.1B).

We collected calcite grown on glass plates and water (drip and stream), and measured cave parameters every 2-4 weeks between November 2019 and July 2021, with a few gaps in 2020, due to Covid lockdown. Both cave air and water temperatures were measured using the same instruments. For sites CAU-2 and CAU-3, Niphargus temperature loggers (Burlet et al., 2015) were left from January 2020 to July 2021 and recorded air temperature every 20 minutes. CO_2 concentrations were measured twice (December 2022 and February 2023) at the three monitoring sites using a handheld Vaisala CARBOCAP with a GM70 CO_2 probe. Several CO_2 measurements were performed along the Rivière de Robots up to the monitoring site CAU-3.

2.4.3 Stable isotope measurements in water and calcite

During the whole monitoring period, 74 stream and dripwater samples were collected in 50 ml and 12 ml plastic vials respectively. At station CAU-1 only stream water from the Rivière des Robots was collected (Fig. 2.2A) and at stations CAU-2 and CAU-3 dripwater samples were collected. The water sampling for the three stations was done every 2-4 weeks. At station CAU-2, the dripwater from two drip spots runs through fractures and falls ca. 4.7 m from the ceiling to plastic collection bags with funnels. At station CAU-3, the dripwater was collected directly from stalactites (Fig. 2.2C) at two adjacent spots. During the monitoring period from November 2019 to July 2021, drip rates (drip counts per minute) were measured during each field visit at station CAU-2.

All water samples were measured at the Alfred Wegener Institute Helmholtz Centre for Polar and Marine Research (AWI), Potsdam (Germany). Of each sample, 12 µl of water were

processed using a PICARRO L2130i Isotopic Water Liquid Analyzer. The results are given in $\delta^{18}O$ and $\delta^{2}H$ permil (‰) relative to the Vienna Standard Mean Ocean Water (VSMOW) standard (Meyer et al., 2000; Juhls et al., 2020). We collected dripwater samples and modern calcite on glass plates at station CAU-2 (Fig. 2.2B). The glass plate was exchanged during each field visit (every 2-4 weeks). A glass flask was left for 20 months upside-down 50 cm from the monitored site of CAU-2 and collected in July 2021 for calcite sampling and analysis. The calcite harvested from the glass plates was collected using a cleaned scalpel and analysed for stable oxygen and carbon isotopes. Calcite deposited on the glass flask was sampled with a scalpel from different ~3 x 3 mm areas from side to side, mimicking sampling along a stalagmite growth axis for a Hendy test (Hendy, 1971). The glass flask left on site was cut vertically and scanning electron microscope (SEM) images were taken of the exposed crystal fabrics at the Department of Geography and Environmental Sciences, Northumbria University, Newcastle upon Tyne (England).

Calcite powders were measured for $\delta^{18}O$ and $\delta^{13}C$ using an isotope ratio mass spectrometer (IRMS) at the Department of Geography and Environmental Sciences, Northumbria University. 95-125 µg of calcite powder were weighed using a Mettler Toledo MT5 FACT microbalance and placed into 12 ml borosilicate glass vials. Sample vials were flushed with Helium using a Sercon autosampler. The samples were acid digested at 72°C using orthophosphoric acid (H_3PO_4) and analysed using a Gasbench II coupled with a ConFloIV and a ThermoFisher Scientific Delta V Advantage IRMS following the methodology of (Spötl, 2004; Breitenbach and Bernasconi, 2011). The raw isotope values were corrected using the in-house carbonate standard, Plessen and the international standards NBS18, NBS19, and IAEA603. In-house standard Pol-2 was measured in each run as control for long-term accuracy. Isotope results are reported in delta notation against the international Vienna Peedee Belemnite (VPDB) standard. The long-term external precision of both, $\delta^{18}O$ and $\delta^{13}C$, is 0.1‰ (1 standard deviation) or better.

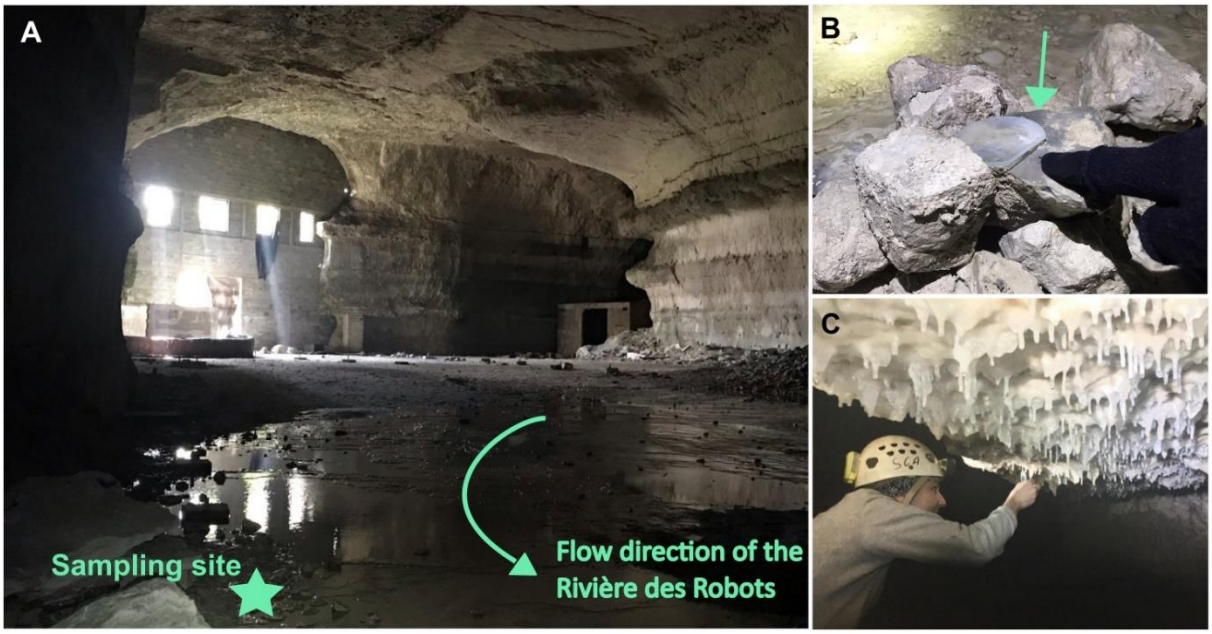

Figure 2. 2. A) Station CAU-1 in La Champignonière with the stream flowing in NE direction. B) Station CAU-2 in Salle de Rois, showing the glass plate where calcite was harvested approximately bi-weekly through the study. C) Station CAU-3 at the Robots stream, where dripwater was collected directly from soda straws.

2.5 Results

2.5.1 Regional climatic parameters

Over the monitoring period the air temperature recorded in Rouen-Boos meteorological station shows an average of ca. 11°C, with a maximum of 20.4°C in August 2020 and minimum of 3.8°C in January 2021 (Fig. 2.3). The rainfall distribution between November 2019 and June 2021 reveals a clear seasonal pattern, with overall higher rainfall during the winter seasons and drier conditions during summer. Precipitation was higher in November and December 2019 and rains persisted until March 2020. The following rainy season was slightly less pronounced at the end of 2020. The driest month in both 2020 and 2021 was April with an average of 0.8 mm and 0.5 mm, respectively. The average $\delta^{18}O$ of precipitation ($\delta^{18}O_{prec}$) observed at Fontainebleau between –10.7 and –2.2‰ (Fig. 2.3) and the precipitation $\delta^{2}H$ over the sample period ranges between –74.5 and –38.7‰. The lowest $\delta^{18}O_{prec}$ values are recorded in November 2019 (–10.5‰) and December 2020 (–10.7‰) and the highest values in March (–2.6‰) and July 2020 (–2.2‰). The $\delta^{18}O$ of the dripwater ($\delta^{18}O_{dw}$) in the Caumont quarry (station CAU-2) is very stable with a mean value of –7.34 ± 0.1‰ VSMOW, this $\delta^{18}O_{dw}$ value is ca 1.6‰

lower compared to the average value in annual precipitation. The effective recharge results show the highest infiltration in November 2019 (143 mm) and December 2020 (130 mm). Negative infiltration was recorded from April until September 2020 plus February and April 2021, with the lowest point being July 2020.

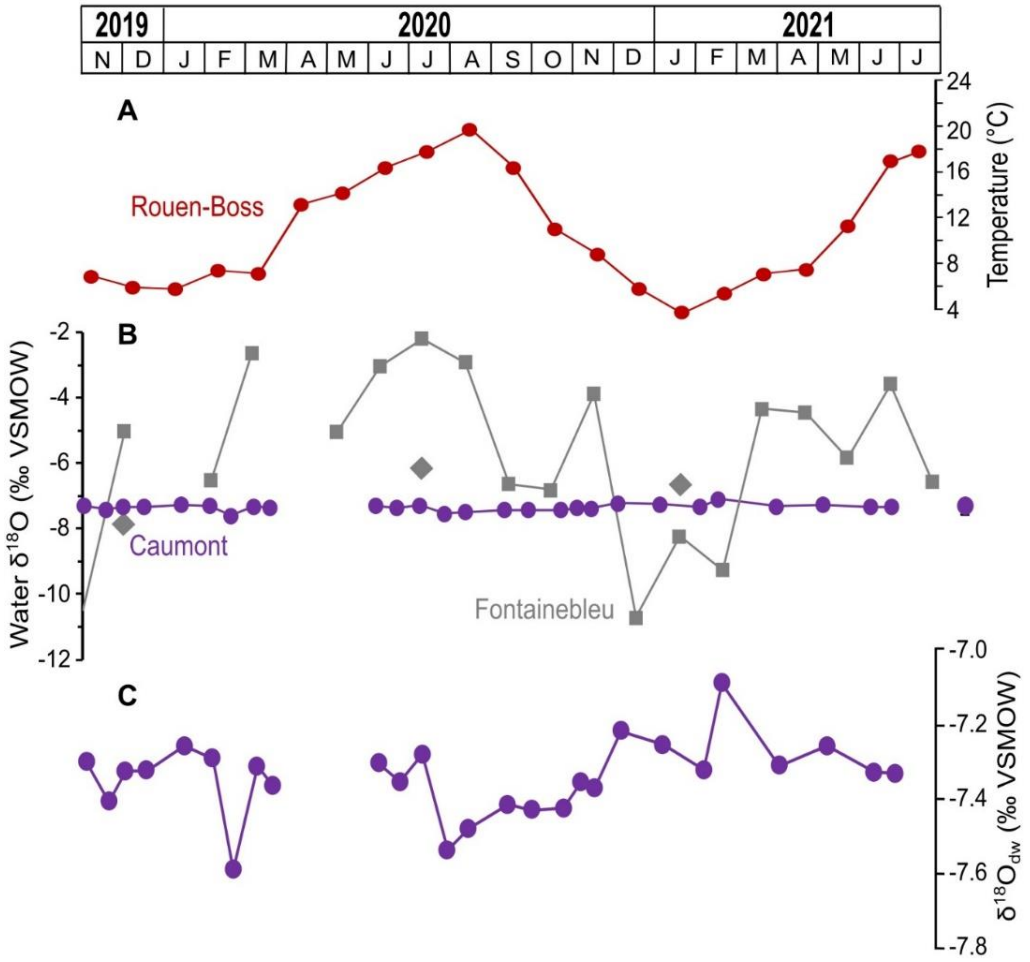

Figure 2. 3. A) shows mean monthly temperature recorded at the meteorological station of Rouen-Boos. B) shows $\delta^{18}O_{prec}$ at the GNIP station of Fontainebleau, with the weighted annual mean of 2019, 2020, and 2021 (diamonds), and $\delta^{18}O_{dw}$ values observed at station CAU-2 in Caumont. On the right CAU-2 average, purple circle, which covers the small error of ±0.1‰. C) shows the expanded version of $\delta^{18}O_{dw}$ record from station CAU-2. CAU-2 $\delta^{18}O_{dw}$ data falls between the three values of annual weighted mean of precipitation.

2.5.2 Cave microclimate and monitoring data

Cave air temperatures are 10.4 ± 0.3°C at station CAU-2 and 11.3 ± 0.1°C deeper in the cave and quarry system at CAU-3 (Fig. 2.4). A wider temperature range was observed at

site CAU-1 near the entrance to the Champignonière. Here a minimum temperature of 4°C and a maximum of 12.5°C was observed. The stream water temperature at CAU-1 is similar to the air temperature, with a range of 6.5 to 11°C over the monitoring period.

CO_2 concentrations at stations CAU-1 range from 490-560 ppm and at CAU-2 from 480-570 ppm, only slightly higher than atmospheric values. In the Rivière des Robots, CO_2 values were measured along the natural conduit towards the monitoring station CAU-3. The values increased drastically from 510-550 ppm at the entrance of the conduit to 2580-4940 ppm at CAU-3 inside the gallery (Appendix 1).

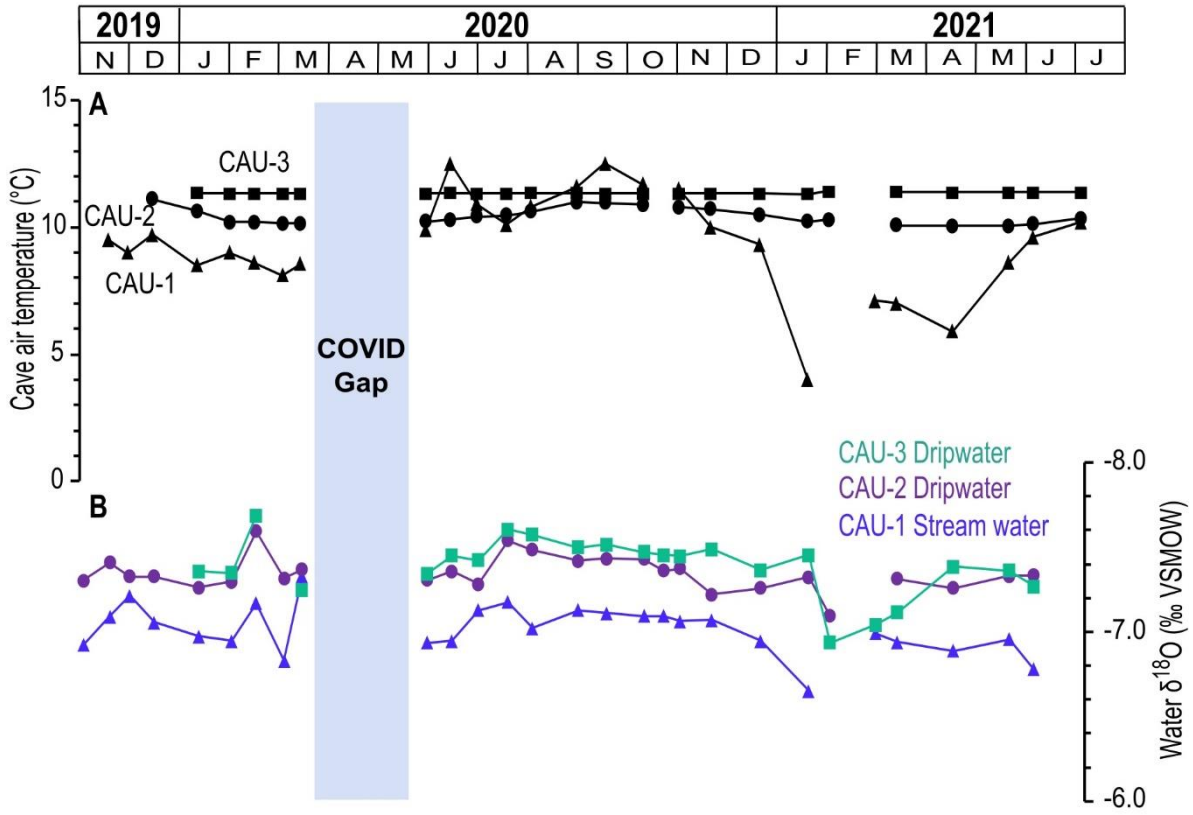

Figure 2. 4. Comparison of (A) monitored cave air temperature and water $\delta^{18}O$ (B). At CAU-1, samples were taken from stream water and at sites CAU-2 and CAU-3 from dripwater.

2.5.3 Isotopic composition of stream and drip water

Twenty-eight stream water (sw) samples collected at CAU-1 yielded $\delta^{18}O_{sw}$ values from –7.3 to –6.7‰. These are slightly higher than the dripwater samples collected at CAU-2 and CAU-3 (Fig. 5). The dripwaters collected at stations CAU-2 and CAU-3 show a range of –7.7 and –6.9‰ for $\delta^{18}O_{dw}$ and –36.2 and –49.6‰ for $\delta^{2}H_{dw}$ (Fig. 2.5). The results for $\delta^{18}O_{dw}$,

$\delta^{18}O_{sw}$, and $\delta^{2}H$ show that all samples fall close to the global meteoric water line (GMWL) and Fontainebleau local meteoric water line (LMWL) (Fig. 5).

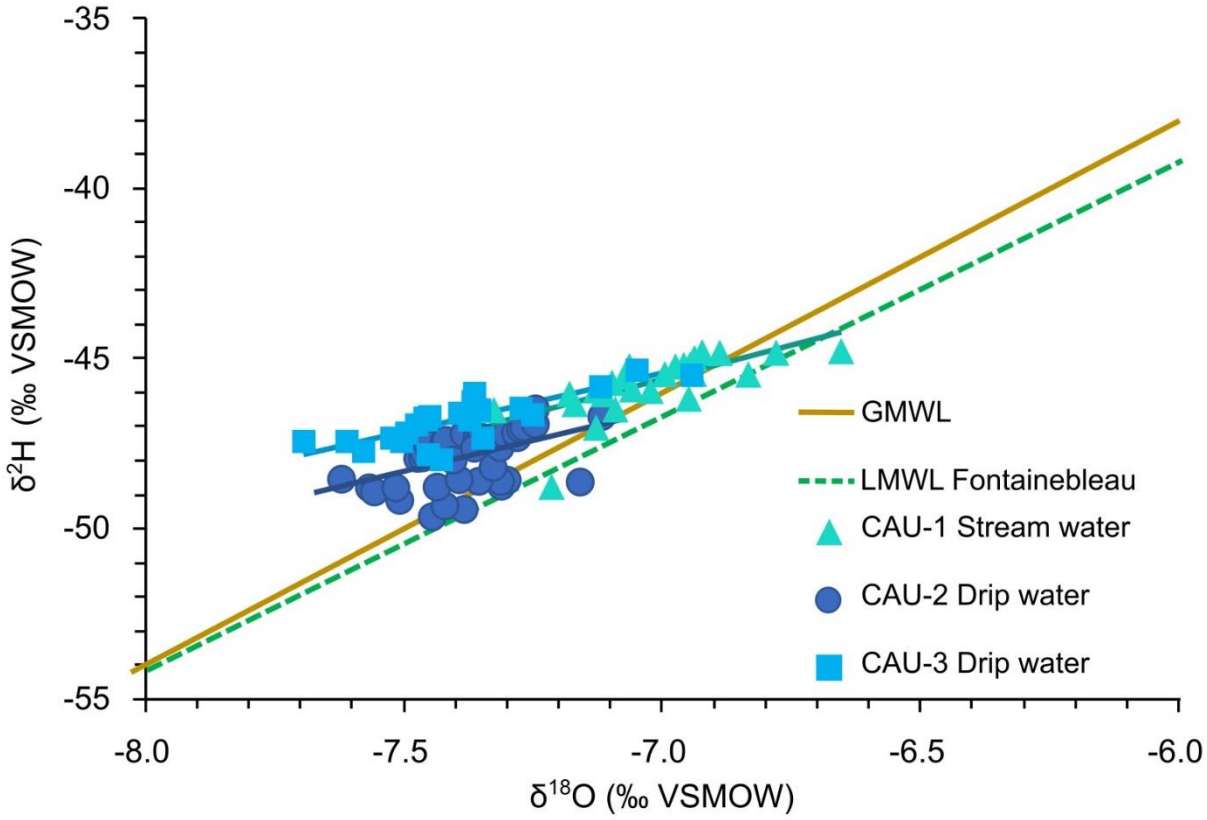

Figure 2. 5. The $\delta^{18}O$ and $\delta^{2}H$ values of the 83 samples collected at stations CAU-1 (triangles), CAU-2 (circles), and CAU-3 (squares) for both stream and dripwater in relation to the GMWL and LMWL at Fontainebleau.

2.5.4 Isotopic composition of modern calcite

The 22 modern calcite samples collected from glass plates placed at station CAU-2 yielded a carbon isotope ($\delta^{13}C_{calc}$) signal between –11.1 and –5.7‰. The lowest $\delta^{13}C_{calc}$ value is observed in December 2020 and the highest in September 2020. For the carbonate oxygen isotope ($\delta^{18}O_{calc}$) the average value is –5.2 ± 0.3‰ over the monitoring period (every 2-4 weeks) (Fig. 2.6). The $\delta^{18}O_{calc}$ varies only ~0.6‰ from –4.3‰ in October 2020 to –5.6‰ in March 2021. Both, $\delta^{13}C_{calc}$ and $\delta^{18}O_{calc}$ seem to covary, albeit with minimal variance in $\delta^{18}O_{calc}$ (Fig. 2.6C, D). The samples obtained from the glass flask, collected at the end of the monitoring period, also show stable $\delta^{18}O_{calc}$ values with a range of –5.04 and –5.5‰. The $\delta^{13}C_{calc}$ values range from –11.3 to –10.9‰.

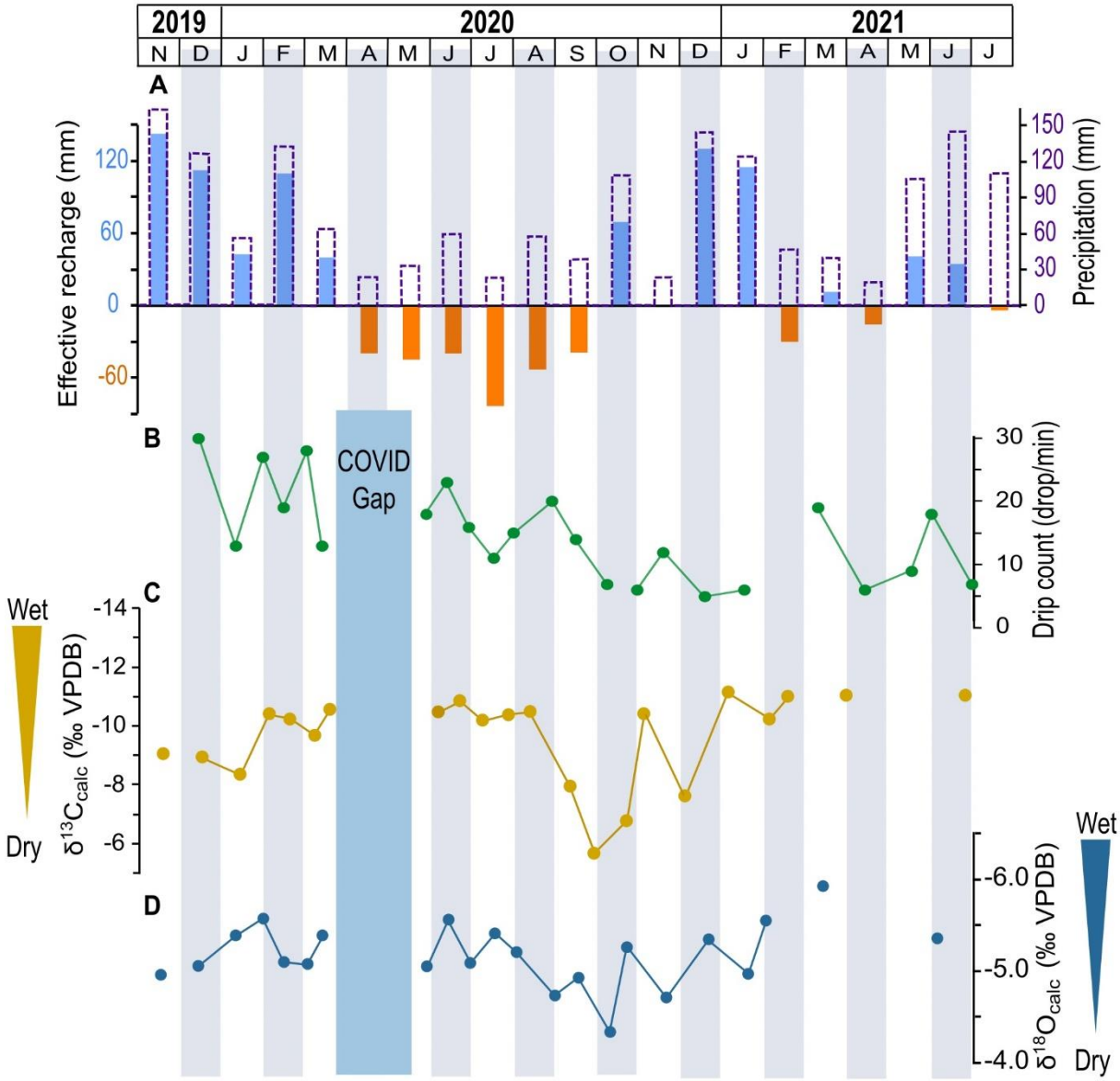

Figure 2. 6. Monthly precipitation and effective recharge at station Rouen-Boss (data source: Meteo France) A), compared to CAU-2 drip rate B), modern carbonate $\delta^{13}C$ C) and modern $\delta^{18}O$ D). Effective recharge is calculated using the Thornwaite equation *(*Palmer and Havens, 1958*)*. The significant increase in $\delta^{13}C$ values between September and December 2020 might reflect the hydrological (increased PCP) response to the prolonged lack of infiltration over the spring and summer of 2020 (shown in A).

2.6 Discussion

2.6.1 Cave atmospheric dynamics and internal parameters

2.6.1.1 Cave air temperature and CO_2 concentrations

Temperature and CO_2 variations in the cave affect calcite precipitation rates and $\delta^{13}C$ and $\delta^{18}O$ signatures (Deininger et al., 2012; Fohlmeister et al., 2020). Since cave air temperature and CO_2 concentration depend on ventilation dynamics the latter indirectly affects calcite precipitation (Verheyden et al., 2008; Riechelmann et al., 2011). Temperature gradients between surface and cave can enhance or subdue cave ventilation, which in turn can affect CO_2 level and relative humidity in the cave air. Cave ventilation could lower the relative humidity sufficiently to induce evaporation from the water film on stalagmites and enhance CO_2 degassing from incoming dripwater (Fairchild et al., 2007). Both processes can alter the isotopic signature in speleothem carbonate (Verheyden et al., 2008; Mattey et al., 2010; Fairchild and Baker, 2012). The temperature gradient between cave and surface can vary at diurnal to seasonal timescales (e.g., (Breitenbach et al., 2015; Giesche et al., 2023). The ventilation of a cave also depends on the geometry of the cave, the number of entrances, the dimensions of passages, and orientation of entrances towards main wind direction(s) (e.g., (Riechelmann et al., 2019). Assessing the temperature variability and amplitude at different sites is essential to characterize the environmental controls on calcite precipitation.

Air temperature measurements at each of the three stations provide information on cave atmosphere and ventilation. Temperature inside the cave and quarry system of Caumont differs between monitoring stations CAU-1, CAU-2, and CAU-3 (Figs. 2.1B; 2.3). At station CAU-1 near the Champignonière entrance, air temperature varies between ca. 4°C in January and 12.5°C in September. Located 50 m from this entrance CAU-1 (Fig. 2.1B) is more strongly affected by ventilation and direct air exchange with the surface which explains the large air temperature variability (Fig. 2.4). Temperature recorded at station CAU-2 varies <1°C between summer and winter seasons over the monitoring period (Fig. 2.3). At station CAU-3 the temperature range is even more stable, with an amplitude of <0.1°C. The observed reduced temperature range with increase in distance from the entrances reflects the effect of decreasing ventilation at stations CAU-2 and CAU-3 stations.

Our data show that the distal sections, especially station CAU-3, are highly thermally stable and do not respond to surface temperature changes at short timescales (diurnal to seasonal). Such stable conditions make these cave and quarry sections suitable for testing near-equilibrium carbonate deposition.

2.6.1.2 Drip rate

Drip rate is controlled by surface processes (e.g., precipitation, evaporation, soil moisture capacity) and aquifer characteristics including reservoir capacity and bedrock permeability (Treble et al., 2013; Markowska et al., 2015). The local hydrology feeding the stalagmite determines whether a seasonal signal might be preserved or not. (Baldini et al., 2021), divided the bedrock pathways that recharge the drip into diffuse, fracture and conduit flows. Naturally, drip dynamics can also reflect a mix of diffuse and fracture flow. Diffuse flow sites are distinguished by a slow response to precipitation events, while fracture flow sites have a more rapid response. Finally, conduit flow is generally characterized by rather rapid response to individual rainfall events followed by a fast return to baseline flow (Atkinson, 1977; Smart and Friederich, 1986). Very slow drips are also more strongly affected by isotope fractionation, due to prolonged CO_2 degassing and/or evaporation (Mühlinghaus et al., 2007, 2009). Therefore, monitoring drip rates over several seasons helps to characterize the recharge dynamics, lagged response to rainfall, the seasonality signal preserved in the cave hydrology, and isotope fractionation conditions (Atkinson, 1977; Baker and Brunsdon, 2003; Kaufman et al., 2003; Baker et al., 2019; Baldini et al., 2021).

Seasonal drip rate changes depend on rainfall amount and temporal distribution, evapotranspiration, and recharge dynamics throughout the year. Lower dry season rainfall and high surface temperature result in enhanced impact of evapotranspiration on the epikarst, reducing infiltration and lowering drip rates. In contrast, during winter, evapotranspiration is lower and effective precipitation is enhanced resulting in increased infiltration and higher drip rates (Fig. 2.6A)(Van Rampelbergh et al., 2014).

At station CAU-2 dripwater is available throughout the year. While the station does not reveal clear seasonal cycles, we observed lower drip rates at the end of summer and during the autumn in 2020 (Fig. 2.6). Decreasing drip rate reflects the drying in the epikarst after lower infiltration summer periods. Both fractures and chalk matrix of the epikarst were less saturated with meteoric water during dry periods, resulting in reduced head pressure and lower drip rates. After a prolonged dry period, like summer 2020, drip rates are likely to respond more slowly to rainfall events due to a partly emptied epikarst reservoir. Following a longer rainfall and refilling of the epikarst, as it occurred during winter season 2020-2021, drip rate increased and might react more directly to rainfall events.

The classification scheme of Baldini et al. (2021) was used with the limited drip rate data obtained at CAU-2. In the scatter plot, our values map above and parallel to the 1:1 line between monthly maximum vs minimum drip rates. This range has been classified as a "mixture of diffuse and fracture flow" and/or "ideal seasonal flow" by (Baldini et al., 2021). Therefore, increasing recharge after December 2020 could be explained by the high level of fractures present in Caumont quarry (Ballesteros et al., 2020; Chevalier, 2022). This is observed especially at station CAU-2, where stalagmite deposition occurs preferentially below fractures (Fig. 2.7). However, the limited temporal resolution of the drip count at station CAU-2 does not allow us to quantify the lag between rainfall events and drip response, although the available data suggest a response within 4-6 months.

Figure 2. 7. Stalagmite growth near station CAU-2 aligns with fractures in the gallery's ceiling. This growth pattern strongly suggests that fracture flow is a key characteristic for drips in Caumont Quarry.

2.6.2 Rain and drip water isotopic composition

The degree to which cave dripwater $\delta^{18}O_{dw}$ reflects the $\delta^{18}O$ of meteoric precipitation ($\delta^{18}O_{prec}$) is significant for paleoclimate studies and requires detailed monitoring. Numerous

publications investigated the relationship between $\delta^{18}O_{prec}$ and $\delta^{18}O_{dw}$ in order to establish the sensitivity of cave systems to surface hydrology and links between surface environment and speleothem-based $\delta^{18}O$ time series (Riechelmann et al., 2011; Johnston et al., 2013; Surić et al., 2018; Baker et al., 2019; Nehme et al., 2019; Baldini et al., 2021). $\delta^{18}O_{dw}$ values may reflect $\delta^{18}O_{prec}$ on timescales ranging from annual (Baker et al., 2019) to individual (intense) recharge events, depending on the site's hydrological characteristics. Other factors such as overburden thickness, lithology, residence time and mixing of the water within the epikarst, soil depth, and aquifer hydraulics can add further complexity.

The oxygen isotopic composition in rainwater is influenced by changes in air temperature, atmospheric circulation (especially dynamics linked to the North Atlantic), precipitation amount and seasonal distribution. The temperature control on $\delta^{18}O_{prec}$ at the Orleans-La-Source station in north-western France is ca. +0.23‰/°C. The nearest GNIP station (Fontainebleau), shows cooler $\delta^{18}O$ values (–4.5‰) during the summer months, and lower values in winter (January-March; –9.6‰) (Fig. 2.3). The $\delta^{18}O_{dw}$ values in Caumont do not show a clear relationship with monthly precipitation, and the very small variation (± 0.4‰) results most likely from thorough mixing of waters of different age in the epikarst. When the $\delta^{18}O_{dw}$ values are compared to $\delta^{18}O_{prec}$ data from Fontainebleau, where a clear seasonal variation is observed around a mean value of –5.7 ± 2.7‰, the $\delta^{18}O_{dw}$ values tend to be more negative with an average of –7.3 ± 0.1‰ throughout the year (Fig. 2.3). The observed offset between $\delta^{18}O_{prec}$ and $\delta^{18}O_{dw}$ implies that dripwater at Caumont is biased towards the high-infiltration season (e.g., winter).

To detect possible secondary evaporation from infiltrating water either in the overburden or in-cave we evaluate the $\delta^{18}O_{dw}$ and $\delta^{2}H$ values relative to the LMWL (Ayalon et al., 1998; Breitenbach et al., 2015). All dripwater $\delta^{18}O$ and $\delta^{2}H$ values fall close to the GMWL and LMWL (Fig. 2.5). Samples from stations CAU-1, 2, and 3 cluster around an average value of –7.3 ± 0.2 ‰, showing that these waters are well mixed within the epikarst. Furthermore, this indicates that few secondary evaporation occurred and that the dripwater likely retains the (average) precipitation signal (Riechelmann et al., 2011).

The fact that the isotope signatures of all three stations closely overlap at the lower left end of the GMWL suggests that the former reflect wet (winter) season recharge, rather than annual average infiltration (Genty et al., 2014).

2.6.3 Testing modern carbonate for kinetic isotope fractionation

Information on the importance of kinetic processes is of great relevance for the interpretation of speleothem-based isotope time series in terms of past environmental changes (Mühlinghaus et al., 2009). We therefore tested i) whether carbon and oxygen isotope ratios of samples deposited at the same time vary significantly in response to CO_2 degassing and/or evaporation (effectively a Hendy test on modern carbonate; (Hendy, 1971), and ii) whether carbon and oxygen isotope ratios vary over time in response to changes in temperature and humidity.

2.6.3.1 A Hendy test on modern carbonate

To test whether kinetic processes affect $\delta^{13}C$ and/or $\delta^{18}O$ we collected 13 calcite subsamples from the bottom of a reversed glass flask that was left at station CAU-2 for 20 months (Fig. 2.8A-D). This test mimics a Hendy test along a speleothem 'growth layer' (here the glass flask) and allows us to estimate the impact of kinetic isotope fractionation at different distances from the central drip spot. SEM microscopy indicates that ~60 µm of blocky calcite was deposited over 20 months (Fig. 2.8B).

The $\delta^{18}O$ and $\delta^{13}C$ values obtained from the 13 subsamples indicate only minimal variability of 0.4‰, where carbon and oxygen isotope ratios are uncorrelated (R^2 and p-value of 0.03 and 0.57, respectively (Fig. 2.8C). Neither isotope ratio shows a trend towards higher values with distance from the apex (Fig. 2.8D). These observations indicate that kinetic isotope fractionation through CO_2 degassing or evaporation did not affect the studied isotope system because CO_2 degassing from the water film would lead to increasing $\delta^{13}C$ values and evaporation would lead to increasing $\delta^{18}O$ values with distance from the apex (Hendy, 1971). If both processes were active, the $\delta^{13}C$ and $\delta^{18}O$ values should be positively correlated (Hendy, 1971). Our data suggest that the kinetic processes are negligible at this station and that the carbonate contains the original environmental signal of the infiltrating water (i.e., processes in the atmosphere, soil, and epikarst). To evaluate the sensitivity of both isotope systems against

environmental processes, we tested their evolution over time with modern carbonate samples, deposited at different times.

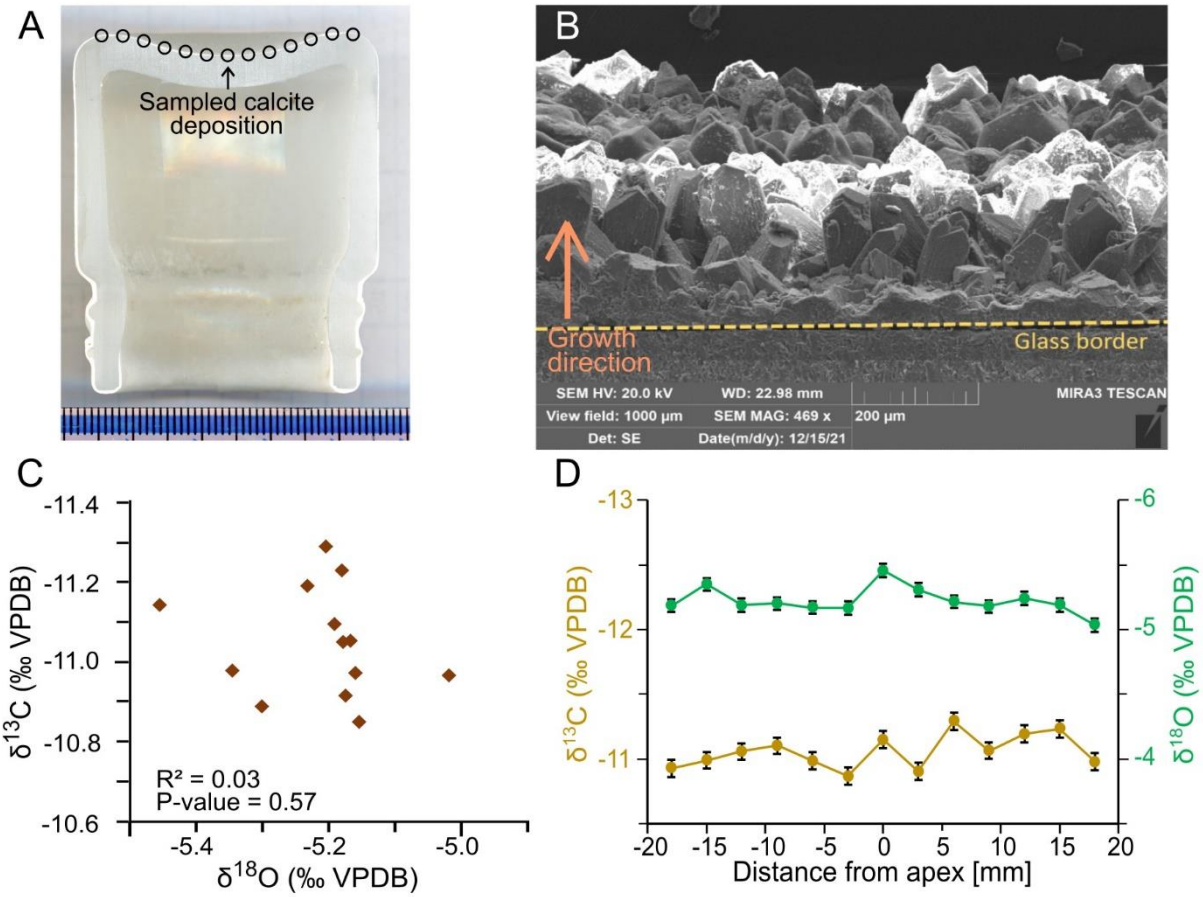

Figure 2. 8. A) Cross section of the cut glass flask with sample location. B) SEM image of a cut piece from the glass flask. It clearly shows calcite crystals precipitation. C) Cross correlation of $\delta^{18}O$ and $\delta^{13}C$ values D) Hendy test done on the modern calcite vs distance

2.6.3.2 Temporal evolution of the isotopic composition of modern calcite

To test the temporal variability of carbon and oxygen isotope ratios we repeated the glass plates calcite growth experiments at station CAU-2 at bi-monthly to monthly intervals (Fig. 2.6C, D). The $\delta^{18}O_{calc}$ of the 22 modern samples ranges from –5.9 to –4.3‰, with the highest values observed in late summer 2020 (Fig. 2.6C). When we combine water and carbonate $\delta^{18}O$ values and cave air temperature to calculate the water-calcite oxygen isotope fractionation factor we find that all samples fall either on or near the regression line proposed by (Coplen, 2007) and above the one by (Tremaine et al., 2011) for (near-)equilibrium conditions (Fig. 2.9). This finding bolsters our notion that kinetic processes are negligible at

station CAU-2 and that $\delta^{18}O$ could reflect changes in precipitation and humidity above the cave.

The observed $\delta^{18}O$ changes of ca. –1.6‰ might be related to changes in air temperature, or changes in the dripwater composition (Van Rampelbergh et al., 2014). The minimal temperature variability of <1°C at station CAU-2 is too small to have a significant influence on the isotopic composition. We conclude that the $\delta^{18}O_{calc}$ variation is linked to dripwater changes and by extension to the isotopic composition of the precipitation and (potentially) PCP in the epikarst. Thus, $\delta^{18}O_{calc}$ is a sensitive proxy for environmental changes above the Caumont cave/quarry system.

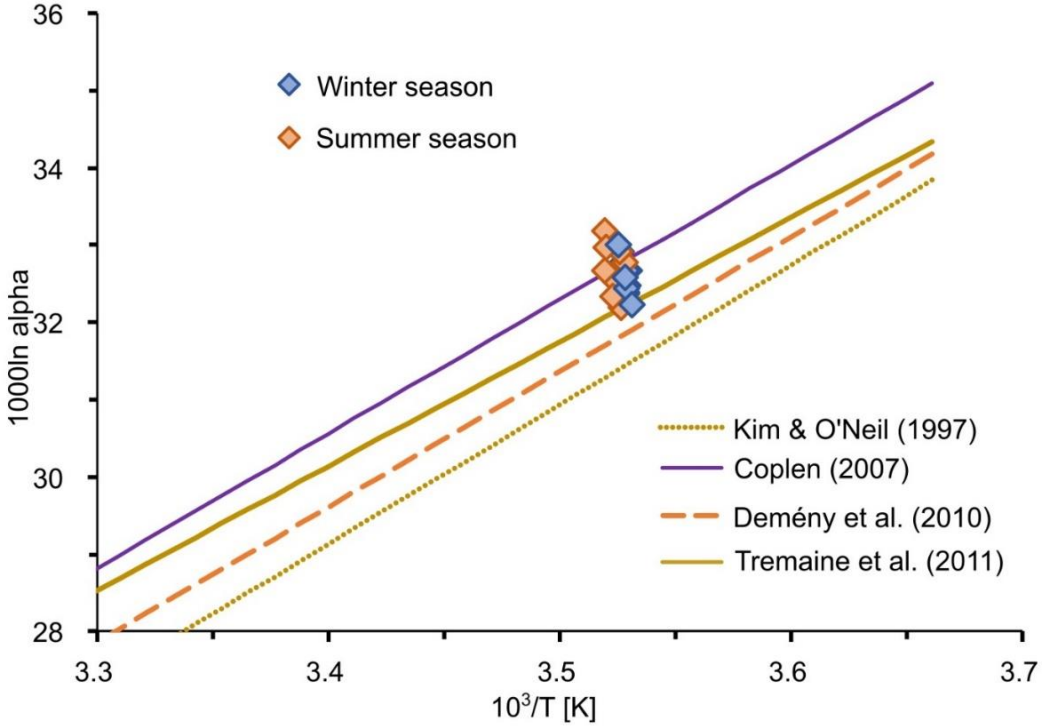

Figure 2. 9. Plot of calculated water-calcite oxygen isotope fractionation factors, based on the isotope values of modern calcite and water and cave air temperature. All our samples fall either on the regression line of Coplen (2007), or that of Tremaine et al. (2011), strongly suggesting (near-)equilibrium conditions. We show the regressions of Demény et al. (2010) and Kim and O'Neil (1997) for reference. The blue diamonds reflect the samples from winter months and orange from summer months.

The carbon isotopes from the modern samples ($\delta^{13}C_{calc}$) vary more significantly around a mean of –9.7 ± 1.5‰. In late summer and autumn 2002, $\delta^{13}C_{calc}$ values increase ca. 2‰,

returning to more negative values around the end of 2020 (Fig. 2.6). With no noticeable kinetic isotope fractionation is occurring in the cave, this suggests that the isotopic signature of the dissolved inorganic carbon (DIC) of the infiltrating water is affected by processes in the epikarst.

Following (Riechelmann et al., 2013), processes that could result in higher $\delta^{13}C_{calc}$ values include i) reduced drip rates and longer water residence time on the stalagmite's surface that allow for CO_2 degassing and isotope fractionation, and ii) variations in pCO_2 of the cave atmosphere caused by ventilation changes. As discussed above, the in-cave conditions at station CAU-2 are very stable, rendering either process unlikely candidates for the observed changes. We also do not find a link between drip rate and $\delta^{13}C$, with a R^2 of < 0.02 and p-value of 0.64. (Fig. 2.6B and C). Therefore, the more plausible explanation for the observed $\delta^{13}C_{calc}$ increase is prior carbonate precipitation (PCP) in the epikarst (Fohlmeister et al., 2020). The fact that $\delta^{13}C$ in the modern carbonate increases during late summer and autumn suggests that higher summertime evapotranspiration above the cave reduced effective infiltration, thereby allowing partial emptying of the epikarst reservoir. Infiltrating water encountering air-filled voids in the epikarst will be subject to PCP, and thus alteration of the $\delta^{13}C$ signal. This mechanism has also been observed at Han-sur-Lesse Cave in Belgium (Van Rampelbergh et al., 2014) where higher $\delta^{13}C_{calc}$ values during the summer months have been associated with intensified PCP.

Thus, the carbon isotope signal in the Caumont cave and quarry is a sensitive proxy for local infiltration changes and speleothems from this cave are likely to record the history of seasonal and longer (multi-annual) droughts in Normandy.

2.7 Conclusions

A monitoring study in the Caumont cave and quarry site (Normandy, north-western France) was conducted during the years 2019-2021 to better understand the effects of cave environments on calcite deposition and assess the suitability of the site for paleoclimate study from stalagmites. Cave monitoring was carried out every 2 to 4 weeks in Caumont for 20 months between November 2019 and July 2021. The obtained results display constant internal climatic conditions throughout the year, especially in the natural conduit and deep galleries. The recorded temperature in the CAU-3 (Rivière des Robots) and CAU-2 (Salle des Rois) have

a small variability up to 1°C. The $\delta^{18}O_{dw}$ values replicate closely the $\delta^{18}O_{prec}$ values with most of the samples falling close to GMWL and LMWL, based on Fontainebleau GNIP station data. The $\delta^{18}O_{dw}$ signal tends to be more negative compared to Fontainebleau, indicating that it is biased towards the high infiltration season (winter). Furthermore, the low variability in the $\delta^{18}O_{dw}$ values throughout 20 months (± 0.1‰ for CAU-2 and ± 0.2‰ for CAU-3), indicate that the infiltrated waters seem to be well mixed in the epikarst.

A test for kinetic fractionation was done on modern carbonate deposited on a glass flask left at CAU-2 station during the complete monitoring period. The Hendy test performed on the freshly deposited carbonate showed that in the cave no discernible kinetic isotope fractionation is occurring, and hence the $\delta^{18}O$ signal comprises the original signature of the infiltrating water. The carbonate $\delta^{13}C$ signal reflects the processes that occurred in the soil and epikarst, which sometimes (whenever effective recharge is negative) includes epikarst PCP but is not affected by in-cave CO_2 degassing.

We tested (near) equilibrium conditions using both a Hendy test on modern carbonate, and the combination of dripwater $\delta^{18}O$ and modern carbonate $\delta^{18}O$. The former reveals neither increasing $\delta^{13}C$ and $\delta^{18}O$ ratios with distance from the apex, nor a correlation between both isotope ratios. The calculation of the oxygen isotope fractionation factor based on known cave air temperature, water $\delta^{18}O$ and carbonate $\delta^{18}O$ reveals that our modern carbonate maps on or very near the equilibrium regression proposed by Coplen (2007). Together, these tests provide strong evidence for (near)equilibrium isotope fractionation conditions at site CAU-2.

Acknowledgments

We would like to thank the Region Normandy for funding the PhD project and RIN-PALECONOR (2019-2022) project that funded the analysis and fieldwork. We are grateful to the department of Geography and Environmental Sciences, Northumbria University, Newcastle, United Kingdom for stable isotope analysis and for providing the facilities for the preparation and measurements. Similarly, to the Alfred Wegener Institute for Polar and Marine Research, in Potsdam, Germany for the water sample analysis. A special thanks to Kim Genuite and Daniel Ballesteros for their assistance during fieldwork and the French Federation of speleology and canyoning for providing access to the quarry. We appreciate the input we received from the two anonymous reviewers, whose revisions allowed us to improve our work.

CHAPTER 3: A multi-proxy stalagmite record indicates a shift in forcing of 20th Century drought events in Normandy

Recent stalagmites growing in the floor of Salle de Rois gallery.

This chapter was submitted as: Bejarano-Arias, I., Nehme, C., Breitenbach, S.F.M., Ionita, M., Baldini, J., Pons-Branchu, E., Modestou, S., Umbo, S., Mouralis, D. A multi-proxy stalagmite record indicates a shift in forcing of 20th Century drought events in Normandy, to the journal *Scientific Reports*.

Authors contributions

CN and DM designed and directed the study. IB did the fieldwork under the supervision of CN, and wrote the manuscript (original version). The sampling of the stalagmites was done by IB under the guidance of CN. The measurements and analysis of modern carbonate was done by IB with the supervision and assistance of SB, SM and SU. U/Th dating were done by EP-B and the trace element measurements by JB. The modelled climatic data (SPEI) for the study area was provided by MI as well as the guidance for their interpretation. All authors contributed to discussion of the results and to the review of the manuscript.

3.1 Abstract

Drought events are increasingly impacting Europe. The study of past droughts helps disentangle the different factors that trigger hydrological drought, helping to forecast future drought severity. Here we identify the historical drought events of the 20th and 21st centuries in geochemical records of a stalagmite from Caumont cave in northern France and develop a mechanistic understanding of their root causes. Subannually-resolved stable isotope records ($\delta^{13}C$ and $\delta^{18}O$) and trace element data are directly compared with historical climatic records. $\delta^{13}C$, $\delta^{18}O$, Mg, and Sr peaks align well with most of the historical drought events of the 20th and 21st centuries. The comparison reveals a good correspondence between summer effective rainfall and $\delta^{13}C$, Mg, and Sr concentrations. Further comparison of geochemical records with the precipitation-evapotranspiration index (SPEI) reveals a change in the drought forcings for the past two decades. During most of the 20th century, droughts appear driven by a pluvial regime, whereas since the late 1990s, drought was driven by higher evapotranspiration due to increased temperature.

3.2 Introduction

Historical records highlight the extended dry phases in north-western France during 20th century. These dry episodes affected not only Normandy (northern France), but large parts of Western and Central Europe (Vidal et al., 2010; Vicente-Serrano et al., 2021). Droughts events are amongst the natural hazards responsible for the most significant economic losses (World Meteorological Organization (WMO), 2021), affecting ecosystems (Smith and Matthews, 2015), agriculture, water and energy supply (Bakke et al., 2020). Droughts are mainly driven by regional precipitation deficits and/or increased temperature (Van Loon et al., 2016; Dai et al., 2018). A precipitation deficit is classified as lower than normal conditions in the hydrological system in combination with high (potential) evapotranspiration (Bakke et al., 2020). Droughts can be classified into four categories, depending on the type of impact: i) meteorological (precipitation deficit over a specific period), ii) agricultural (as a consequence of meteorological conditions that affect crops), iii) hydrological (manifested as reduced river runoff and lake levels after meteorological and agricultural droughts), and iv) socio-economic (negative economic impacts on population) (Wilhite and Glantz, 1985).

Given the increasing impact of recent droughts in Europe, resources are being directed towards the reconstruction of past droughts using paleoclimate archives (Labuhn, 2014; Büntgen et al., 2021). Tree ring records from the Tatra region, north-west Carpathian mountains, show that during the last millennia, lower temperature align with pandemic episodes across Europe (Büntgen et al., 2013). Additionally, tree rings based reconstructions from the eastern part of Europe indicate that the recent drought events are unmatched over the last 700 years (Nagavciuc et al., 2022).

With global warming as a backdrop, droughts are becoming an increasing concern for modern societies. The recent report from the Group of Intergovernmental Experts about climate evolution (GIEC, 2023), confirms a clear trend of increasing European drought, affecting water resources, aquifer recharge, and soil. The droughts of the recent years in France have left many towns with water shortages during the summer (Valo, 2022) and caused the shutdown of nuclear reactors along the Franco-Belgian border (Woods, 2020).

Droughts are well documented in European historical data (Camenisch and Salvisberg, 2020; Cook et al., 2022), but speleothem records can extend records back further in time, and provide insight where historical records are lacking. Speleothems (secondary carbonates deposited in caves) are highly sensitive terrestrial archives that allow the reconstruction of past hydrological conditions at subannual timescales (Genty et al., 2003; Cheng et al., 2012; Fairchild and Baker, 2012). A wide range of environmentally sensitive proxies hosted in stalagmites enable comparisons with contextually robust evidence from historical studies, and the attribution of local environmental changes to regional and pan-regional climatic forcings (Carolin et al., 2019; Nicholson et al., 2021).

Here we investigate a recent, well-dated, and highly-resolved stalagmite record from Normandy, north-western France. We investigated the sensitivity of the stalagmite (CCB-1) to drought events and used the stalagmite record combined with historical data to examine the causes of regional 20th century drought events. Understanding the mechanisms behind drought events will enable assessment of whether the causes have been the same during the 20th and 21st century, or if there has been a change in drought dynamics. We combined stable carbon and oxygen isotope ratios ($\delta^{13}C$, $\delta^{18}O$) with trace elements (Mg, Sr) to reconstruct changes in local hydrology. We used the Mg and Sr records as recorders of prior carbonate precipitation (PCP) which is enhanced during drier periods (Fairchild et al., 2000; Sinclair, 2011;

Wassenburg et al., 2020). We then compared these data with historical and meteorological records (temperature, effective infiltration) and the 20th century standardized potential evapotranspiration index (SPEI)(Vicente-Serrano et al., 2010). This combination of data allows for differentiation of the mechanisms of drought, whether by pluvial or temperature regime.

Normandy, northern France (Fig. 3.1a) rests largely on a chalk plateau incised by the Seine River. This incision has resulted in long-term groundwater table lowering along a 120 m deep valley, facilitating vadose cave system formation (Nehme et al., 2020) such as our study site, the Caumont quarry and cave system (CQCS) (Fig. 3.1b). The CQCS is located ca. 25 km southwest of Rouen (N 49°22'41"; E 0°54'47"; 15 m above sea level) (Ballesteros et al., 2023; Bejarano-Arias et al., 2024) (Fig. 3.1c), with ~115 m of limestone overburden (Chevalier, 2022). Exploited for building stone since the Middle Ages, CQCS today reaches a total length of ca. 13 km, accessible via the main entrance, located ca. 200 m from the Seine River (Fronteau et al., 2010) (Fig. 3.1c). Inscriptions on the gallery ceiling at the sampling site, indicate opening and excavation dates, providing direct age information (Fig. 3.1b).

The climate of Normandy is temperate oceanic (Ballesteros et al., 2020), with the driest period between March and July and the wettest from October to January (Cantat, 2004). The closest meteorological station, Rouen-Boos, located 20 km from CQCS, records total annual rainfall between 418 and 1065 mm (Cantat, 2004). Effective infiltration describes the precipitation amount infiltrating the soil, layers above the cave, and entering the cave (Fairchild and Baker, 2012). In Caumont, the highest effective infiltration is during autumn and winter (Bejarano-Arias et al., 2024). Surface air temperatures range from 4°C to 18°C, with July and August being the warmest months, and January the coldest (Fig. 3.1d). Potential evapotranspiration (PET) is highest in spring and summer (Diomard and Chéron, 2020), resulting in minimal effective infiltration into the epikarst above the cave during the summer season. Cave air temperature at the sampling site is very stable (10-11°C) and very close to the mean annual air temperature (10.6°C) (Bejarano-Arias et al., 2024).

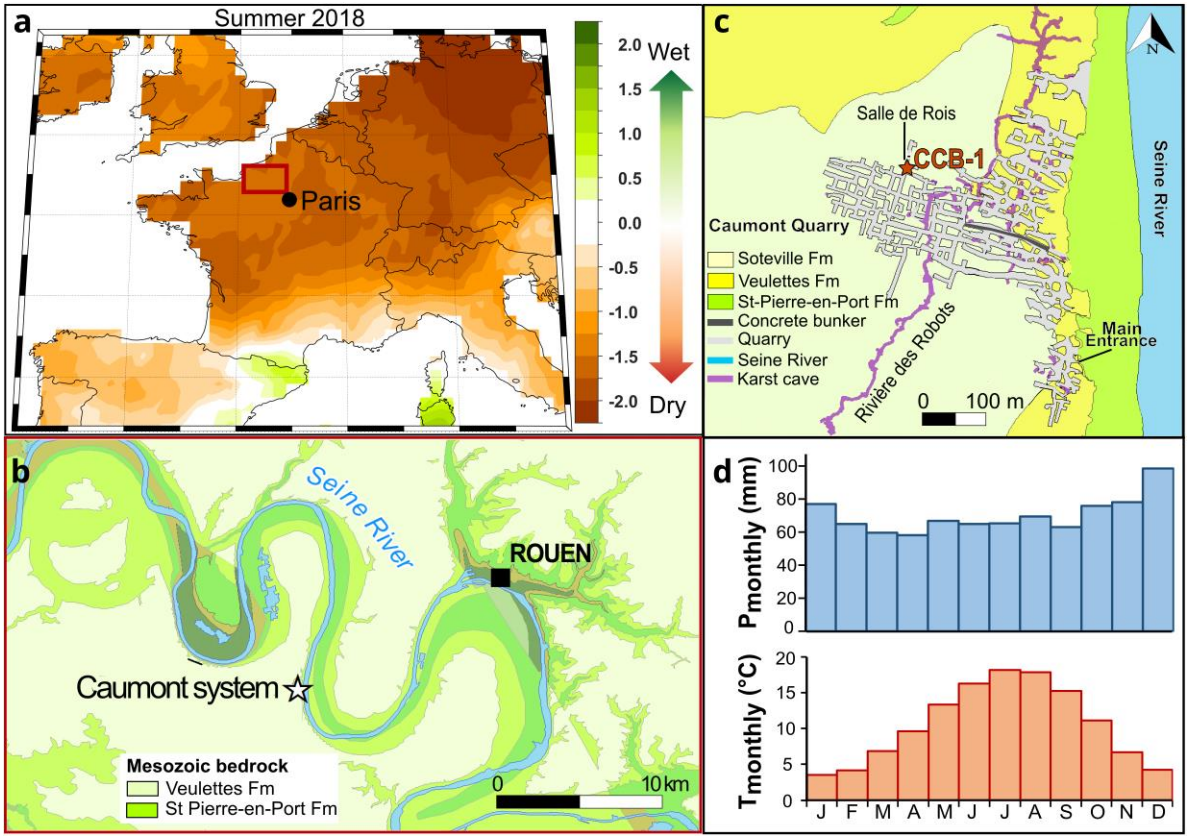

Figure 3. 1. Location map of the study area. Map of western Europe of October SPEI6 displaying drought conditions during summer 2018, and the location of the Seine River (red rectangle) (a). Location of the CQCS (white star) (b), and the sampling site of the stalagmite CCB-1 (red star (c)), in Salle des Rois located 800 m from the quarry entrance. Map modified from Ballesteros et al., (2020) [35]. Monthly values of precipitation and temperature in Rouen meteorological station from 1990-2018 (d).

3.3. Results

3.3.1 Dating and age model for stalagmite CCB-1

The chronology of stalagmite CCB-1 (4 cm in length) is based on U-series dating and constrained by historical information. Three U-series dates suggest continuous growth since ~1907 (Appendix 2 Figure 1, Table 1). Age correction was applied to the detrital ^{230}Th based on stratigraphic constraints using the STRUT ages routine (Roy-Barman and Pons-Branchu, 2016). Due to the moderate U concentration of 0.2 to 0.4 ppm and relatively low Th content (0.3 to 8.9 ppb), corrected ages (Appendix 2 Table 1) include uncertainty of ±40 to ±60 years. To further improve the chronology, we counted individual laminae through greyscale analysis, assuming that these represent seasonal changes in carbonate deposition. This layer counting

chronology was linked to calendar age by assigning the top of the stalagmite to 2019 CE (the year of sampling) as maximum age. The final age model was constructed using the layer counting information and the COPRA routine (Breitenbach et al., 2012).

The age-depth model reveals that the stalagmite grew over the period of 1914 to 2018 CE. The layer counting age model agrees well with the U-series growth estimate, but is internally more precise because most individual layers are easily identified in the grey scale record. The layer counting model is also consistent with an inscription (1901 CE) on the ceiling of the sampling chamber that indicates the year when this gallery was excavated. Thus, the stalagmite growth is constrained by the two ages of 1901 and 2019 CE (Appendix 2 Figure 2). The fact that carbonate deposition began a few years after the chamber was opened is likely explained by ongoing quarrying works that disturbed the floor in this chamber and hindered speleothem deposition between 1901 and 1914 CE. This effect has been previously observed at Brown's Folly mine, UK; where stalagmite growth lagged after closure of the mine combined with a delay in soil recuperation (Baldini et al., 2005). Stalagmite CCB-1's growth rate was relatively high, 0.40 mm/a, with the highest growth rate occurring from 1926-1927 and 1944-1945 CE (0.74 mm/a). The lowest in 1940 CE (0.12 mm/a). The fact that stalagmite CCB-1 is modern permits comparison of the stalagmite's records with instrumental data of the 20th and 21st century.

3.3.2 Instrumental records and drought events in the 20th and 21st century

Normandy receives ca. 750 mm of precipitation annually. The first half of the 20th century was generally drier; the lowest annual precipitation totals were 418 mm in 1921 and 431 mm in 1953 (Fig. 3.2). The highest precipitation on record fell in 1999, 2000, and 2001, with annual totals of 1041, 1065 and 1057 mm respectively. After 1977, rainfall at the site increased from 804 mm/yr to 1065 mm/yr in 2000, with a below average decrease in precipitation of 524 mm/yr in 1989 (Fig. 3.2b). Effective infiltration is estimated by subtracting evapotranspiration from total precipitation (Fairchild and Treble, 2009). The lowest effective infiltration in Normandy is estimated to have occurred in 1921 (418 mm) and the highest in 1910 with 1048 mm (Fig. 3.3e).

The mean annual temperature (MAT) over the instrumental record is 10.6 °C, with a maximum MAT of 12 °C (1949) and a minimum of 9.1 °C (1963, 1985 and 1987) (Fig. 3.2). From 1921 until 1961, MAT were higher (averaging 10.9 °C), then reducing to 10.6 °C between 1962 and1995. From 1996 onwards, there is a clear trend towards higher temperatures (Fig. 3.2c), with consistently warmer MAT (reaching 11.9 °C during 2014 and 2018).

The most significant 20th and 21st centuries (meteorological) drought events in Europe occurred in 1921, 1934, the 1940s, 1976, 1989, 2003 and 2018 (Fig. 3.3h, Appendix 2 Table 2) (Trzpit, 1978; Séchet, 2003; Ionita et al., 2017; van der Schrier et al., 2021; Vicente-Serrano et al., 2021; Mazuir and Bibily, 2022; Lestienne, 2023). These droughts have been described as severe calamities that impacted economies and agriculture in France and elsewhere (Barker et al., 2019; Ionita et al., 2021; Markonis et al., 2021; Hänsel et al., 2022). Drought events affect hydrology and water resources, which directly impact agriculture by reducing crop yields and production, thereby the economy (Spinoni et al., 2017; Hanel et al., 2018). The most extreme drought of the 20th Century occurred between 1920 and 1922 (van der Schrier et al., 2021; Lestienne, 2023). During this event, a minimum discharge of 20 m^3s^{-1} was recorded in the Seine River (Flipo et al., 2021). During the 2003 drought, French maize and wheat fields experienced historical lows in production (van der Velde et al., 2012).

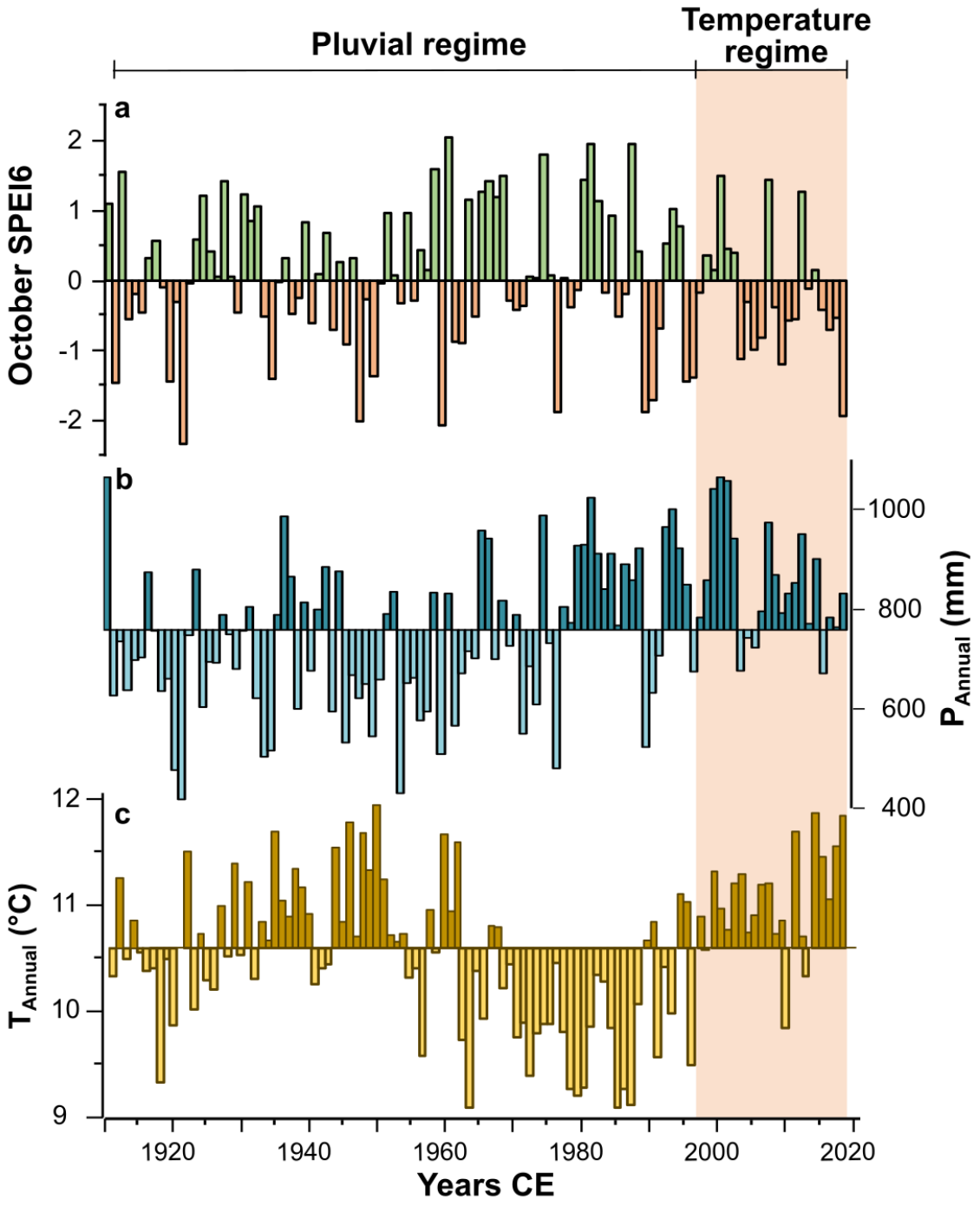

Figure 3. 2. Since the late 1990s (orange shading), Normandy remains water stressed (a), despite above average rainfall (b); likely due to increased air temperature (c) which enhance evapotranspiration. Dry events (negative SPEI values) are mostly correlated to higher temperatures (and thus higher evapotranspiration; 'Temperature regime'), compared to previous periods where negative SPEI appears correlated to decreased precipitation ('Pluvial regime').

3.3.3 Stable isotope and trace element composition of CCB-1

The $\delta^{13}C$ record displays significant variations, with a maximum of -7.8 ‰ and minimum of -12 ‰. Distinct higher excursions, occur at ca. 1921 and 1936, and double peaks of higher values around 1948-1953, 1973-1976, and 1995-2001 CE (Fig. 3.3a). These years are close to several low rainfall periods noted above (Fig 2). Since ~2003 CE, the $\delta^{13}C$ profile shows a trend to higher values.

The magnesium (Mg) and strontium (Sr) records are positively correlated with $\delta^{13}C$ (r = 0.66 and 0.58, respectively), with distinctive peaks during the early 1920s, and 1930s, late 1940s and 1950s and 1973-1976 CE. Mg exhibits the highest correlation with $\delta^{13}C$ and ranges between 58.3-950.8 ppm (Fig. 3.3c), Sr ranges between 3.6-80.6 ppm (Fig. 3.3d).

The $\delta^{18}O$ record lower amplitude variability compared with $\delta^{13}C$ record, varying between -4.1 ‰ and -6 ‰. Elevated values, aligning with $\delta^{13}C$ excursions are also identifiable, especially in the early half of the 20th century (Fig. 3.3b). After 1954 CE, $\delta^{18}O$ excursions become less distinct, although a trend towards higher values exists after ~2003 CE, similarly to the $\delta^{13}C$ record.

Previous studies have shown that the stable isotope and elemental records are highly influenced by infiltration processes in the epikarst. Cave monitoring at the CQCS site has shown that seasonal precipitation amount controls infiltration and that $\delta^{13}C$, Mg, and Sr speleothem records are generally driven by infiltration dynamics during the summer months (Bejarano-Arias et al., 2024). During the summer both evapotranspiration and a longer water residence time in the epikarst enhance PCP and increase isotope ratios (Genty et al., 2001; Fohlmeister et al., 2020; Braun et al., 2023). The monitored modern calcite $\delta^{18}O$ record, from CQCS, shows a clear bias towards the higher infiltration winter months (November to February) and is anticorrelated with infiltration amount (Bejarano-Arias et al., 2024). We use $\delta^{13}C$, $\delta^{18}O$, Mg and Sr as hydrological indicators with higher values reflecting drier conditions above the CQCS site. We find the covarability between the proxy records of CCB-1 with the instrumental data convincing (Fig. 3.3)

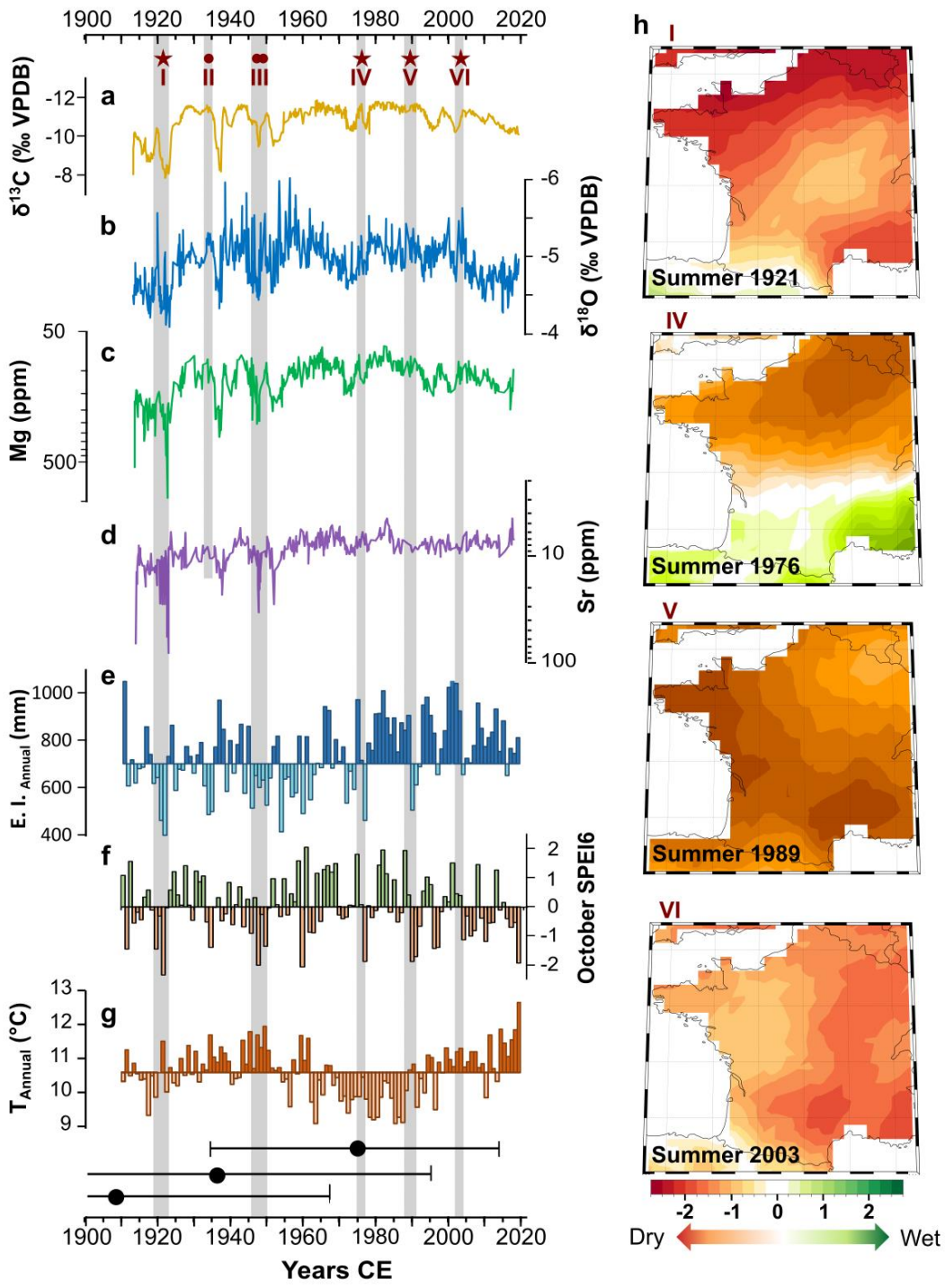

Figure 3. 3. Speleothem multi-proxy record reflects local hydroclimate. Geochemical time series include $\delta^{13}C$ (a), $\delta^{18}O$ (b), Mg (ppm) (c) and Sr (ppm) (d). Note that the y-axis is inverted. Climate time series: effective infiltration (e), October SPEI6 (f) and annual temperature of the 20th century (g). Black dots are U/Th ages (1907 ± 60, 1935 ± 40, 1974 ± 40). Grey shades represent historical droughts with the dark red dots corresponding to local scale and dark red stars correspond to regional scale. Maps of October SPEI6 that correspond to the intensity of the dry conditions, centred over France, during the years 1921, 1976, 1989 and 2003, which represent four of the historical droughts of the 20th and 21st centuries (h).

3.3.4 Links between the drought index and the stalagmite proxy record

For the current study we tested different accumulation periods for SPEI (e.g., 6-months and 12 months) and the highest correlation between our record and the drought index was found with October SPEI6 (Fig. 3.2a) (see methods section for more details). Consequently, to identify the summer dry events of the 20th century, we use the October SPEI6 record. This record ranges from -2.34 in 1921 (extreme dry) to 2.05 in 1960 (extreme wet). Between 1919 and 1959, the October SPEI6 record also shows several multi-annual phases of below-average infiltration (e.g., 1919-20, 1933-34, 1937-38, 1947-49) (Fig. 3.2a). Between 1959 and ~1985, the October SPEI6 record indicates overall wetter conditions, except for 1976 which recorded well below average infiltration (-1.87). Since the 1990s, October SPEI6 indicates regional conditions became increasingly drier, with an increasing frequency of dry events and very few positive infiltration years (e.g., 2018).

October SPEI6 dry events align with $\delta^{13}C$ peaks during severe (-1.5 to -2) and extreme dry conditions (<-2) (Fig. 3.3). This is most apparent for the years 1921, 1947, 1976 and 1995 CE (Appendix 2 Table 2). Likewise, the peaks of higher Mg and Sr values are identified for years 1921, 1937 and 1946-47. Moreover, some of the higher $\delta^{18}O$ peaks correspond with dry events from October SPEI6, more specifically for years 1921 and ~1972-1976 CE, although the relationship is less clear for the rest of the $\delta^{18}O$ peaks in the CCB-1 record (Fig. 3.3b). However, the positive trend of both $\delta^{13}C$ and $\delta^{18}O$ since 2003 agrees with a higher frequency of dry years, reflected in the October SPEI6 timeseries. In the last two decades, relatively dry conditions occurred almost every year, except for years 2007 and 2013 (Fig. 3.3f).

3.4 Discussion

Precipitation and potential evapotranspiration are used as the indicators for SPEI (Spinoni et al., 2017), which allows us to use this index as a regional record of effective moisture budget, with elevated SPEI indicating wetter conditions. The total annual rainfall has increased since the 1970s, reducing the number of years with negative rainfall anomalies (Fig. 3.2b). A closer look into the temperature record shows continuously warmer conditions since the late 1990s, which is supported by a higher frequency of negative October SPEI6 values in this region since 1989 (Fig. 3.2a). This appears at odds with the increase in total precipitation in the region (Fig. 3.2b), but we propose the discrepancy between increasing rainfall totals and

infiltration deficit, reflected in the October SPEI6 timeseries (Fig. 3.3f), could be explained by the rise in temperature since the 1990s (Fig. 3.3g).

Below, we evaluate how these hydrological changes are recorded in stalagmite CCB-1 over the 20th century. Lower effective infiltration increases PCP, which then increases $\delta^{13}C$ and Mg concentration in the stalagmite (Fairchild and Treble, 2009; Allan et al., 2018a). Since effective precipitation is lowest during the summer months when evapotranspiration is highest, the PCP signal is biased towards the warm season (Bejarano-Arias et al., 2024). We find a very good correspondence between the PCP indicators ($\delta^{13}C$, Mg and Sr) and effective precipitation, with higher ratios correlating to periods of effective infiltration deficit (Fig. 3.3e). Our reconstruction reveals a striking pattern of infiltration minima double peaks (Fig. 3.3a, b), which can be directly related to infiltration minima (e.g.: 1920-21, 1932-34, 1945-50, 1953-57, 1971-73, 1989-91) as seen in the October SPEI6 record, especially in the first half of the 20th century, e.g., in 1921 CE (Fig. 3.3f). The link between years of deficient effective infiltration and higher $\delta^{13}C$ and Mg values in ca. 1934-1937 CE and both the 1940s and 1950s is less obvious but still discernible. In the second half of the 20th century, PCP periods are detected in the intervals 1972-1976 and 1994-2003 CE.

The CCB-1 $\delta^{18}O$ record shows elevated values during years of increased PCP, but is also influenced by additional factors that result in higher variability and a less clear response to below-average infiltration. Monitoring of modern calcite in the CQCS shows that $\delta^{18}O$ is biased towards the winter season when infiltration is highest (Bejarano-Arias et al., 2024), which renders $\delta^{18}O$ less susceptible to infiltration changes. This is consistent with the way the $\delta^{18}O$ proxy works, reinforcing our argument.

The link between elevated $\delta^{18}O$ values and effective infiltration minima is noticeable in 1921, the 1940s, 1972-1974 and 1976 CE, but less evident during 1933-1937, 1987-1990 and 2003 CE. The correspondence of $\delta^{13}C$, $\delta^{18}O$, and Mg maxima with minimal effective infiltration seems less evident during the second half of the 20th century, although both $\delta^{13}C$ and $\delta^{18}O$ records still display a trend towards higher values from ca. 2003 that suggest declining infiltration (Fig. 3.3). It is possible that crossing a certain infiltration threshold is needed to initiate PCP-associated Mg and Sr shifts.

The CCB-1 multi-proxy record ($\delta^{13}C$, $\delta^{18}O$, Mg, and Sr) shows distinct and repeated positive excursions for the years 1921, the late 1930s, the late 1940s, the late 1970s, and 2003 that reflect a lack of infiltration (Fig. 3.3). These one-to-four year long excursions can be linked to: i) reduced effective infiltration in the epikarst above the cave, ii) enhanced PCP in the epikarst and cave, and iii) lower drip rates and enhanced CO_2 degassing (Sinclair et al., 2012; Fohlmeister et al., 2020; Wassenburg et al., 2020; Baldini et al., 2021; Bejarano-Arias et al., 2024). The fact that the Mg, Sr, and $\delta^{13}C$ records all show similar dynamics support our interpretation that PCP is a key influencing parameter which itself is driven by local hydroclimatic conditions above the cave.

The clear relation between the isotopic and trace element records and the October SPEI6 timeseries strongly support the fidelity of the stalagmite archive to record seasonal to multiannual climate conditions, and especially droughts. Consequently, the agreement between stalagmite-based geochemical records, instrumental data, and the October SPEI6 help to recognise historical drought events of the last ca. 120 years, including 1921, late 1940s, 1976, and 2003. The faithful record of climate variations of the 20th and 21st centuries in CCB-1, indicates that we could confidently extend the record further back in time in the CQCS.

Droughts are complex climatic events which are driven by precipitation deficit or temperature (Kingston et al., 2015; Ionita et al., 2021; Cook et al., 2022). The comparison with the instrumental temperature records shows that the years of high values correspond with both heavier $\delta^{13}C$ and $\delta^{18}O$ signal peaks for the years 1921, late 1930s, late 1940s and late 1990s (Fig. 3.3a, b). The first peaks from the Mg and Sr records are also in agreement with warmer years of 1921, late 1930s, late 1940s and 1950s (Fig. 3.3c, d). This provides further evidence that high temperatures during the summer months enhance evapotranspiration which consequently influences the isotopic signal in the epikarst and leads to higher PCP. Figure 3.3 highlights the correspondence between increasing $\delta^{13}C$ and $\delta^{18}O$ ratios, high Mg and Sr values, low effective infiltration, severe and extreme dry events according to the October SPEI6 index, and higher temperatures. These parameters align well with the historical droughts of the years 1921, the end of 1940s and 1976 CE, suggesting that the drought events for the first part of the 20th century are related to a precipitation deficit, (pluvial regime). However, the correspondence is less evident for both years 1989 and 2003 CE.

From the year 1996 onwards, we observe an increasing temperature trend (Fig. 3.2b), with higher MATs (reaching 11.9 °C during 2014 and 2018). This trend aligns well with the trend of higher $\delta^{13}C$ and $\delta^{18}O$ values (Fig. 3.3) since the early 2000s onwards. Constant warmer conditions since the late 1990s could explain the trend of elevated $\delta^{13}C$ and $\delta^{18}O$ records, even if precipitation records for the last two decades show no major precipitation reduction (Fig. 3.2b). This relationship reinforces that higher surface temperature since that time has a more significant influence on the stable isotope signal (temperature regime) than precipitation deficit (Markonis et al., 2021). Other studies have also shown the shift in drought regime over the last 120 years, where surface temperature and potential evapotranspiration in soils have a significant effect on drought dynamics in Europe (Ionita and Nagavciuc, 2021). Vicente-Serrano et al., (2010), suggested increasing drying trends from global SPEI datasets, partially due to increasing temperature from the mid-1980s (Ionita et al., 2015).

Further analysis of isotopic records shows that, among the higher values classified as drought, we identified a variation in the isotopic signal separating the points in two clusters, of higher (orange dots) and lighter isotopes (yellow dots) (Fig. 3.4a). This difference between the drought clusters is more evident within $\delta^{13}C$ record, with a 1.28 ‰ difference (between heavier and lighter), than for $\delta^{18}O$ (0.18 ‰) (Fig. 3.4b). Comparing the drought clusters to the temperature record, it is apparent that years with the lighter signal (yellow dots), match with the increasing trend in the temperature record after 2000s. Increasing temperatures usually enhance soil respiration, producing a lighter $\delta^{13}C$ signal (Fairchild and Baker, 2012; Fohlmeister et al., 2020), which is in accordance with a lighter drought $\delta^{13}C$ values compared to the heavier drought cluster at the beginning of the 20th century. However, the average of the lighter $\delta^{13}C$ cluster (-10.31‰), still shows a heavier signal than the rest of the record (mean = -10.75 ‰). This reflects the impact that increasing temperature has at the surface over recent decades, by enhancing evapotranspiration even though there is no deficit in precipitation. The lighter isotopic drought cluster reflects then the change in drought dynamics from a pluvial regime to a more temperature and evapotranspiration related process.

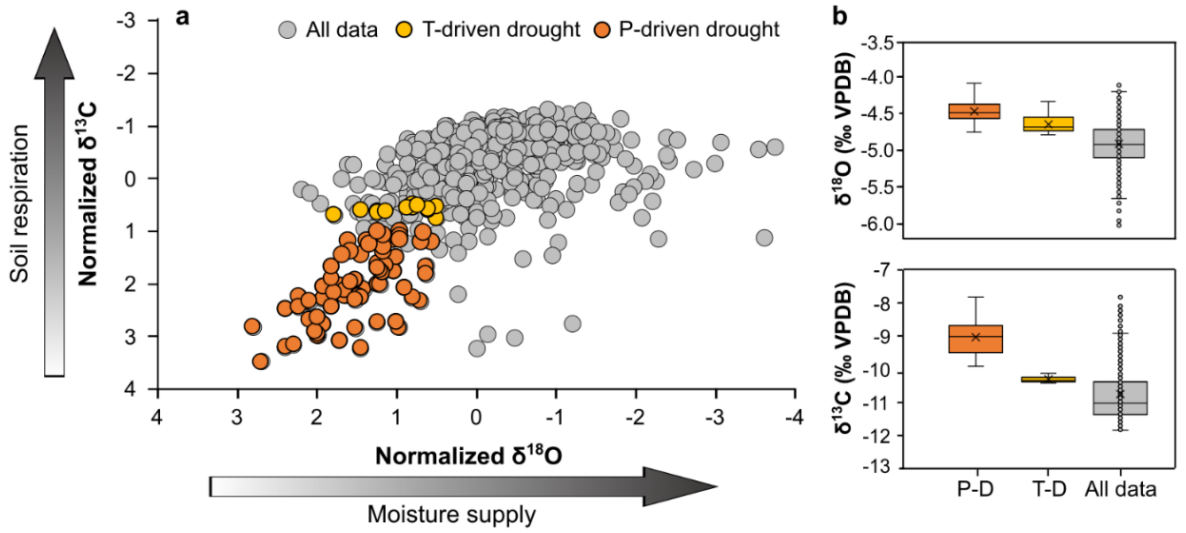

Figure 3. 4. Precipitation-driven droughts can be differentiated in $\delta^{18}O$ – $\delta^{13}C$ space. $\delta^{13}C$ vs $\delta^{18}O$ relationship in stalagmite CCB-1 (a) (Isotope values are z-score normalised). Drought years are identified as positive values, which can be further subdivided in two clusters corresponding to i) pluvial (P-D) and ii) temperature (T-D) drought regimes. Arrows indicate the direction of the main forcings (soil respiration and moisture supply). Box plots for $\delta^{18}O$ and $\delta^{13}C$ signals depict the signal difference between the two drought clusters (b).

A study based on SPEI and other drought indexes in Europe for the last 104 years (e.g., Standardized precipitation index – SPI; Palmer drought severity index - PDSI) also identified an increase in severe and extreme droughts since ca.1990 (Ionita and Nagavciuc, 2021; Bakke et al., 2023). The central and southern parts of Europe are becoming dryer as a result of increasing PET and mean air temperature (Ionita and Nagavciuc, 2021). This drying trend in soil and in the epikarst is confirmed in Normandy, through the convergence of the geochemical proxies evidenced in the stalagmite CCB-1, with the SPEI index and historical data. Our results show that the climatic conditions of the past century recorded within the CQCS are consistent with the regional paleoclimate dynamics of north-western Europe.

Analysis of the different drought events recorded in CQCS shows the complexity of drought events, their irregularity and how different climatic parameters (i.e., precipitation and temperature), can change over time. We show that using these proxies together ($\delta^{13}C$, $\delta^{18}O$, Mg and Sr) is critical to disentangle the complex mechanisms underlying drought events. In the case of CC1-B, this combination made it possible to differentiate the impact of effective infiltration versus temperature changes. Additionally, to identify the shift in drought dynamics, transitioning from primarily precipitation-controlled events in the 20th century to a regime

increasingly dominated by rising temperatures in recent decades. Our results align with observed trends of more frequent droughts and future climate projections, emphasizing the escalating influence of rising temperatures due to climate change on European drought patterns and the urgent need for adaptive water management strategies.

3.5 Methods

3.5.1 Stalagmite CCB-1 and sample preparation

The stalagmite CCB-1 was collected in 2019 from the "Salle des Rois", a quarry chamber of the CQCS. At the time of collection, the stalagmite was still actively growing and the Salle des Rois had current drip. CCB-1, composed of calcite, was cut in four parallel slabs, from which the centre slab (110 mm wide and 38.6 mm long) was placed in epoxy resin, polished to improve appearance of growth laminae and other structures, and subsampled. Polishing was performed with silicon carbide sandpaper, from 120 to 2400 µm. Subsampling was performed for geochronological (U-Th) and geochemical ($\delta^{18}O$, $\delta^{13}C$, trace element) analysis.

3.5.2 U/Th dating

Three powder samples were taken for U-Th dating at 1, 22, and 34 mm from top of the stalagmite CCB-1 using a 1 mm drill bit (Appendix 2 Figure 1). Powder samples of 90 to 150 mg were dissolved in PTFE beakers and mixed with a ^{229}Th-^{236}U spike. This spike solution was calibrated against HU-1 uraninite, assumed to be at secular equilibrium. After co-precipitation with $Fe(OH)_3$, the uranium (U) and thorium (Th) fractions were separated and purified using U-TEVA® in nitric media (HNO_3 3N), with Th and U elution in hydrochloric acid (3N and 1N HCl, respectively). The U and Th isotopic composition was analysed at the Laboratoire des Sciences du Climat et de l'Environnement (LSCE, France), on a Multi-Collector Inductively Coupled Plasma Mass Spectrometer (MC-ICPMS) Thermo Scientific™ NeptunePlus fitted with an Aridus II™ introduction system and a jet pump interface. The detailed chemical treatment and MC-ICPMS analysis are outlined in (Pons-Branchu et al., 2014, 2022). After corrections for mass fractionation (using an exponential law), peak tailing, hydrate interference, and chemical blanks, $^{230}Th/^{234}U$ raw ages were calculated through

iterative age estimation using the ^{230}Th, ^{234}U and ^{238}U decay constants of Cheng et al., (2013) and Jaffey et al., (1971).

3.5.3 Laminae counting and greyscale analysis

The stalagmite exhibits growth layers that are visible to the naked eye. The growth layers have been identified by grey value changes, with dense translucent layers being deposited in one season, and more milky-white layers being formed in another season. Although it currently remains impossible to unambiguously ascertain when exactly each layer is formed, we counted greyscale value maxima to develop a layer counting chronology following the method outlined in Breitenbach and Marwan, (2023). To extract greyscale data from a high resolution scan we used the free software ImageJ (https://imagej.nih.gov/ij/index.html; (Schneider et al., 2012). We extracted a record of grey intensity values ranging from black (grey value 0) and white (grey value 255) at a spatial resolution of 20 μm following the procedure given in Breitenbach and Marwan, (2023). The greyscale record follows the growth axis, and for layer counting we developed several lines parallel to the master profile. Using the master grey scale profile, we then counted grey maxima throughout the stalagmite, assuming that couplets of darker and brighter laminae represent one year of deposition. In stalagmite CCB-1 we counted 104 years back from 2019, the year of collection.

3.5.4 Age modelling

The age model for CCB-1 was constructed using the COPRA software (Breitenbach et al., 2012). Using 2,000 Monte Carlo simulations for the $\delta^{18}O$ and $\delta^{13}C$ records, COPRA calculates median ages and 95% confidence intervals. For the age model we used the layer counting results and the U-Th dates as absolute ages. The year of collection and inscription in the chamber were used as maximum and minimum ages.

3.5.5 Stable isotope analysis

Six hundred powder samples were collected for stable isotope analysis by continuously milling at 50 μm resolution using a high precision micromill (Sherline 5400 Deluxe) at the Université de Rouen Normandy. Samples were analysed for $\delta^{18}O$ and $\delta^{13}C$ using an

ThermoFisher Scientific Delta V Advantage isotope ratio mass spectrometer (IRMS) coupled with a ConFlo IV and a Gasbench II at the Department of Geography and Environmental Sciences, Northumbria University, following the methodology of Spötl (2004) and Breitenbach & Bernasconi (2011). The raw isotope values were corrected using the in-house carbonate standard Plessen (for sample size and drift; n=10 per run) and the international standards NBS18, NBS19, and IAEA603 (for 'stretching' correction; n=> 3 per standard, per run). In-house standard Pol-2 was measured in each run as control for long-term accuracy. Isotope results are reported in delta notation against the international Vienna Peedee Belemnite (VPDB) standard. The long-term external precision of both $\delta^{18}O$ and $\delta^{13}C$ is 0.1 ‰ (1 standard deviation) or better.

3.5.6 LA-ICPMS analysis

Laser Ablation Inductively Coupled Plasma Mass Spectrometry (LA-ICPMS) was used to quantify the trace element concentrations of the stalagmite along a track parallel to the growth direction. The analyses were conducted at Department of Earth Sciences, Durham University, using a 193 nm ArF Teledyne Analyte Excite+ excimer laser system coupled with a ThermoFisher iCAP TQ ICP-MS. The laser ablated material within a 10 x 140 µm rectangular spot, with the spot's long dimension oriented perpendicular to the growth axis, parallel to growth horizons (Müller et al., 2009). Concentration data were obtained for 11 elements (Mg, Al, Si, P, Ca, Cu, Sr, Ba, Pb, Th, and U) along the entire growth axis of CCB-1 at a sample advance rate of 10 µm s^{-1} and a 15 Hz laser repetition rate. NIST 610 and 612 glasses were used as external standards to quantify any instrumental drift and to derive elemental concentrations. The sample was cleaned thoroughly prior to analysis, and a pre-ablation track run to remove any remaining impurities. A secondary parallel track was run to replicate the results of the main track. Dynamic time warping (DTW) techniques were used within Matlab to wiggle match the trace element to the $\delta^{13}C$ data, thereby correcting for lateral offsets in the stalagmite laminae. The DTW reduced the resolution of the trace element data but ensures its temporal consistency with the $\delta^{13}C$ dataset.

3.5.7 Modelled data for drought index

The few available local instrumental data of the study area (Appendix 2, methods), drove us to search for modelled climate data and we chose to work with the standardized

precipitation evapotranspiration index (SPEI). This index was used for drought analysis and measures the normalised differences of the climatic water balance, by subtracting potential evapotranspiration of precipitation (P-PET) (Bakke et al., 2022). The PET is part of the CRU (Climatic Research Unit) v4 dataset (Harris et al., 2020) and is computed with the Penman–Monteith equation (Vanderlinden et al., 2008). PET values were extracted from this dataset using the coordinates of Caumont cave. Values were normalised to log-logistic probability distributions (Vicente-Serrano et al., 2010) using the R package SPEI (https://cran.r-project.org/web/packages/SPEI/index.html). The obtained SPEI record covers the period 1902 – 2021, with a spatial resolution of 0.5° x 0.5°. SPEI numbers are given per monthly values (January to December) with different accumulation periods (3, 6, 9, and 12 months). For this study we used the accumulation period of 6 months until October (dry period). SPEI data is given in positive values, corresponding to positive infiltration, and negative values for dry conditions (water loss to evapotranspiration). Here we focused on October SPEI6 negative values, classified as: i) moderate drought (-1 to -1.5), ii) severe drought (-1.5 and -2), and iii) extreme drought (< -2) (Ionita and Nagavciuc, 2021). The combined dataset Rouen-Boos and PET extracted from CRU V4 were used to estimate effective infiltration.

Acknowledgements

We would like to thank the Region Normandy for funding the PhD project and RIN-PALECONOR (2019-2022) project that funded the analysis and fieldwork. Similarly, to the laboratory team at the department of Geography and Environmental Sciences, Northumbria University, Newcastle, United Kingdom for stable isotope analysis and for providing the facilities for the preparation and measurements. We are grateful to the Panoply technical platform for the U/Th measurements, to A. Dapoigny for assistance during MC-ICPMS measurement and the Department of Earth Sciences, Durham University, UK for the trace elements analysis. Lastly, we thank the French Federation of speleology and canyoning for providing access to the Caumont quarry and cave system.

Data availability

Upon acceptance of the manuscript the data used in this manuscript will be available in a public repository. This is currently under work with the possible repository being NOAA or Zenodo.

CHAPTER 4: Paleoclimate evolution over the last 10,000 years in Caumont cave in Normandy, France

La Jacqueline natural conduit, where part of the Holocene stalagmites were sampled, photo by Carole Nehme.

4.1 Introduction

The Holocene, current interglacial, has been generally categorized as a period with relatively stable and warm climate, in comparison to the previous Quaternary glacial/interglacial changes. High-resolution global paleoclimate records were examined to determine whether the Holocene (from 11.7 ka BP until present) presented climatic fluctuations (Mayewski et al., 2004). Among the different types of climatic proxies that were used are stable isotopes ($\delta^{18}O$ and $\delta^{13}C$), trace elements and pollen, taken from various geological archives as peat (Kalis et al., 2003; Cubizolle et al., 2013), speleothems (Genty et al., 2003; Verheyden et al., 2008; Fairchild and Baker, 2012), lake sediments (Magny, 2004; Litt et al., 2009) and tree rings (Büntgen et al., 2010, 2011). The analysis of the Holocene paleoclimatic proxies revealed several climatic oscillations or "cold events" in a multi-century to multi-

decadal timescale, as described by Wanner et al., (2011), during 8.2 ka, 6.3 ka, 4.7 ka, 2.7 ka, 1.5 ka and 0.5 ka BP. Nevertheless, the identification of these events presented spatial disparities (Lechleitner et al., 2018). The major drivers of the Holocene climatic changes have been ascribed to orbital forcing, volcanic and/or solar activity (Wanner et al., 2008), freshwater outbursts into the North Atlantic ocean and changes in the Atlantic meridional overturning circulation (AMOC) (Bond et al., 2001). While Holocene climate variations are well-studied in north-western Europe, paleoclimate investigations in some archives, such as speleothems, remain poorly studied, specifically in north-western France. Therefore, there is a need to investigate well dated and highly resolved speleothem records to better understand the links between Holocene climate and forcing mechanisms.

Speleothem-based paleoclimate studies increased globally due to the high potential of stalagmites as paleoclimate archives. The stalagmites chemical properties provide a wealth of information about temperature, precipitation, water availability and vegetation above the cave that allows us to put climate reconstruction into a long-term perspective. Additionally, recent studies highlight the significance of speleothem records, in particular for achieving precise chronologies of continental climate changes (Genty et al., 2003; Fairchild et al., 2006; Cheng et al., 2016).

In Normandy and north-western France, few well-dated research is available on the Holocene climate variability. Some studies focus on paleoenvironmental reconstruction, through the evolution of pedo-sedimentary archives, such as loess sediments on the plateaus, marsh and peat land along the Seine and Caen low plains, and fluvial sediments of the Seine River' tributaries (Lespez et al., 2005; Frouin et al., 2010; Gonnet et al., 2023). There are no speleothem records, spanning the Holocene, that have been investigated yet in north-western France (Lechleitner et al., 2018). Whereas several speleothem-based paleoclimate studies were completed in surrounding areas as north Spain (Domínguez-Villar et al., 2008), United Kingdom (Roberts et al., 1998), Ireland (McDermott et al., 2001), Belgium (Verheyden et al., 2000), Western and Southern Germany (Breitenbach et al., 2019), South-Western France (Genty, 2008), Italy (McDermott et al., 1999).

The cave and quarry system of Caumont (Normandy) comprise detrital infill covered by speleothem formation, spanning many glacial and interglacial cycles. The deposition and preservation of flowstones and stalagmites during the past 600 ka BP (Nehme et al., 2020;

Ballesteros et al., 2023), renders Caumont cave a potential site for paleoclimate reconstruction of glacial and interglacial periods, more specifically for the present interglacial, the Holocene.

Here, we focus on 5 stalagmites collected from the Robots stream and La Jacqueline passages in Caumont cave. The 5 stalagmites have been dated using U-Th method, sampled for stable isotopes - SI ($\delta^{18}O$ and $\delta^{13}C$), and one stalagmite, from the Robots stream, was analysed for trace elements. We present new highly resolved stalagmite-based records (SI and trace element data) with the aim to reconstruct the environmental and climatic evolution, in a regional scale and in north-west European level. Moreover, to understand the forcings causing environmental change as well as the underlying causes for hydrological change, during the Holocene. The resulting Caumont geochemical records enabled us to compare them with other proxy records from Normandy and north-western Europe.

4.2 Site setting

The Caumont cave system (CCS), located in the Normandy region (Fig. 2.1 and 3.1), is developed in dolomitized chalk (cf. section 2.3 and 3.2 for more details). In Normandy, the Chalk aquifer properties are a result of its specific lithology: a soft coccolith biomicrite with low primary permeability and high primary porosity (20–40 %), yet it has an important transmissivity through fractures and karstic conduits (El Janyani et al., 2012; Descamps et al., 2017).

The CCS development is related to the incision of the Seine valley and the speleogenic model was suggested by Nehme et al. (2020), based on fluvial terrace and cave sediments studies, coupled with speleothem and paleomagnetic dating. The cave passages along the Seine valley, such as Caumont (Fig. 4.1A), were formed in a shallow epiphreatic setting, which started at ~1 Ma. Caumont has two cave levels (Nehme et al., 2020), at 50 m and 15 m a.s.l. (Fig. 4.1B) where the lower level is very low-gradient branch-work and maze systems (Rodet, 2013). The cave system is fed by recharge from the surrounding plateau, often through discrete sinks known locally as “bétoires”, or large faults (Nehme et al., 2020; Ballesteros et al., 2021).

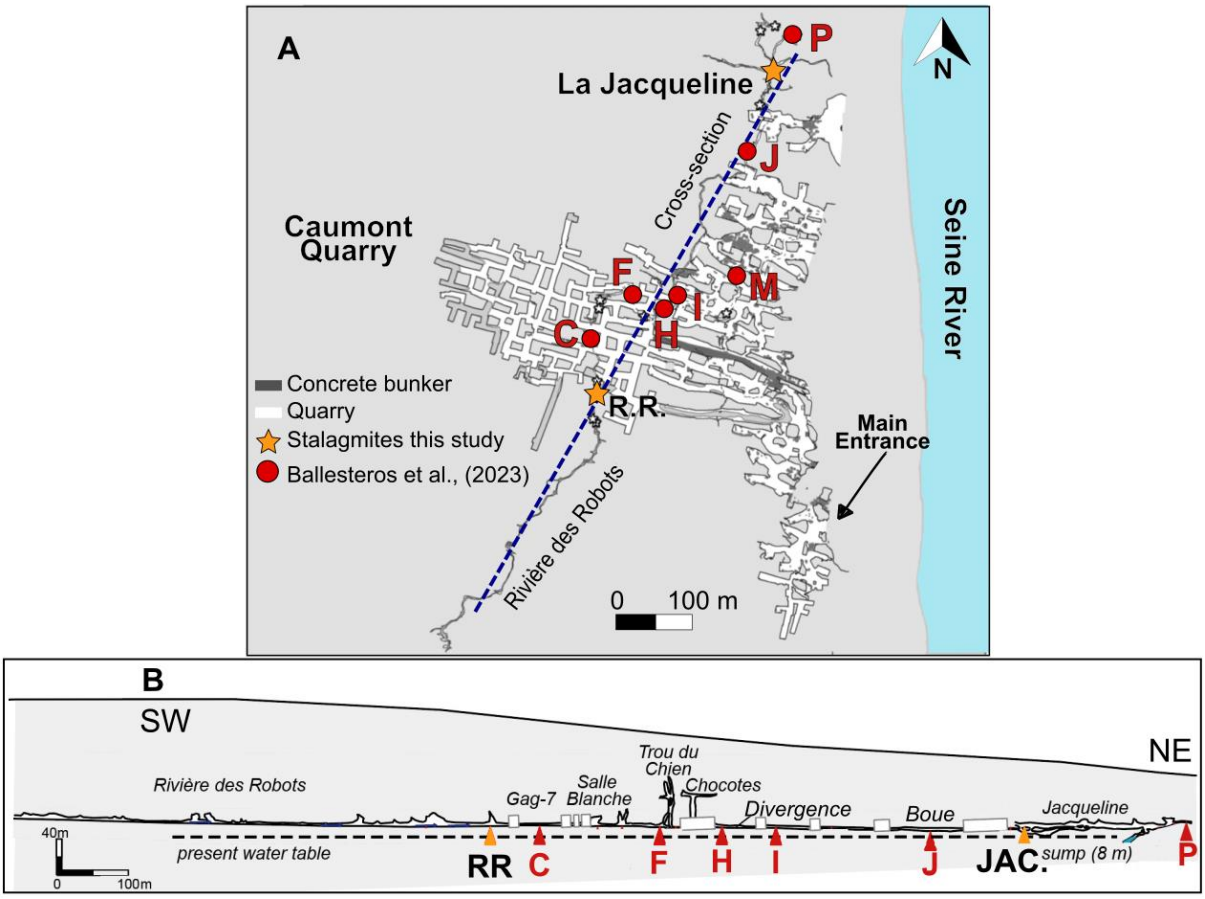

Figure 4. 1. Map of speleothem sampling locations in Caumont cave, from Ballesteros et al, 2023 (red dots) and from this study (orange stars), (A). The cross-section, traverses the natural conduit in a SW-NE direction (B). RR: Rivière des Robots; JAC.: Jacqueline cave.

Ballesteros et al., (2023), shows that the lower level (Fig. 4.1B), has different episodes of detrital infill, erosion, and speleothem deposition. The depositional phases of detrital infill and speleothems (e.g. flowstones and stalagmites), in CCS were identified since Marine isotope stage (MIS) 13, mostly during Interglacial periods, except for the MIS 6 (Fig. 4.2). Moreover, the karstic conduits at Caumont were significantly influenced by the detrital deposition and the chalk aquifer groundwater flow. As a result, the dissolution and enlargement of conduits was enhanced by sedimentary aggradation (Ballesteros et al., 2023). This led to the development of the main conduit of the study area, the Riviere de Robots (RR), located at 15 m.a.s.l. (Fig. 4.1). The RR stream is filled with clay silt and sand deposits, which were partly removed by the current stream as well as by the first explorers at Caumont (Nehme et al., 2020). The current access to one of the sampling sites of this study, (RR) was only possible after the removal of the detrital deposits by the workers in the quarry during the medieval period (cf. section 3.2 for

details). The access to La Jacqueline sampling site remains via the natural conduit, towards the NE of the cave (Fig. 4.1).

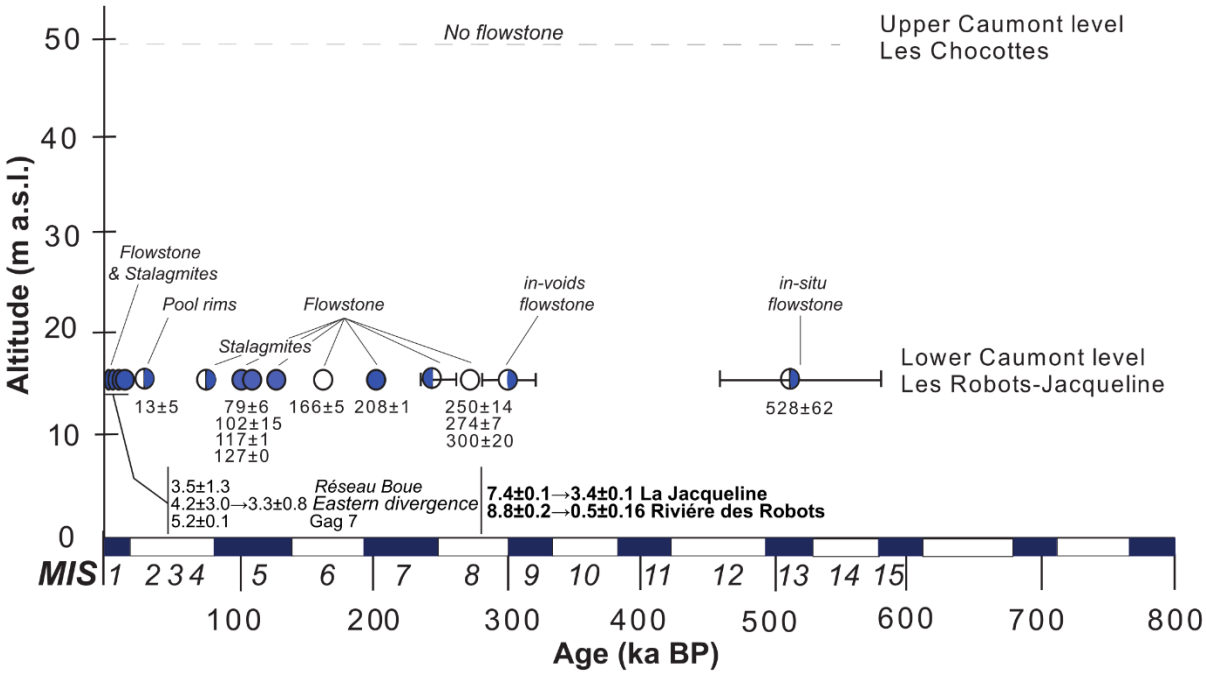

Figure 4. 2. Synthesis of speleothem ages sampled at Caumont cave. The white circles represent the speleothem deposition during glacial periods and blue during interglacial periods. Ages in bold are the ones considered for this study, the other ages are analysed in Ballesteros et al., (2023).

4.2.1 Holocene state of the art in Normandy

In the Normandy region, north-western of France, the common archives, for paleoenvironmental studies, are sediments from plateaus, river valleys or marshes. One of the main sources of information is the Seine River and its tributaries, where different fluvial deposits, peat bogs and soils have been studied to investigate the Holocene paleoclimate. The main proxies used for this purpose are pollen and sedimentological analysis (Frouin et al., 2009; Germain-Vallée and Lespez, 2011; Gonnet et al., 2023). Geochemical proxies such as stable isotopes ($\delta^{18}O$ and $\delta^{13}C$) were used to a less extent in tufa deposits (Dabkowski, 2011). The Normandy study sites are located in the floodplains of Caen, the Marais Vernier, and tributary valleys of the Seine River (e.g., Alizay and Viller-Écalles). The floodplains of Caen are located ca. 96 km southwest of Caumont, whereas the Marais Vernier is situated 37 km to the west of Caumont and Alizay valley at 25 km east of our studied site (Fig. 4.3).

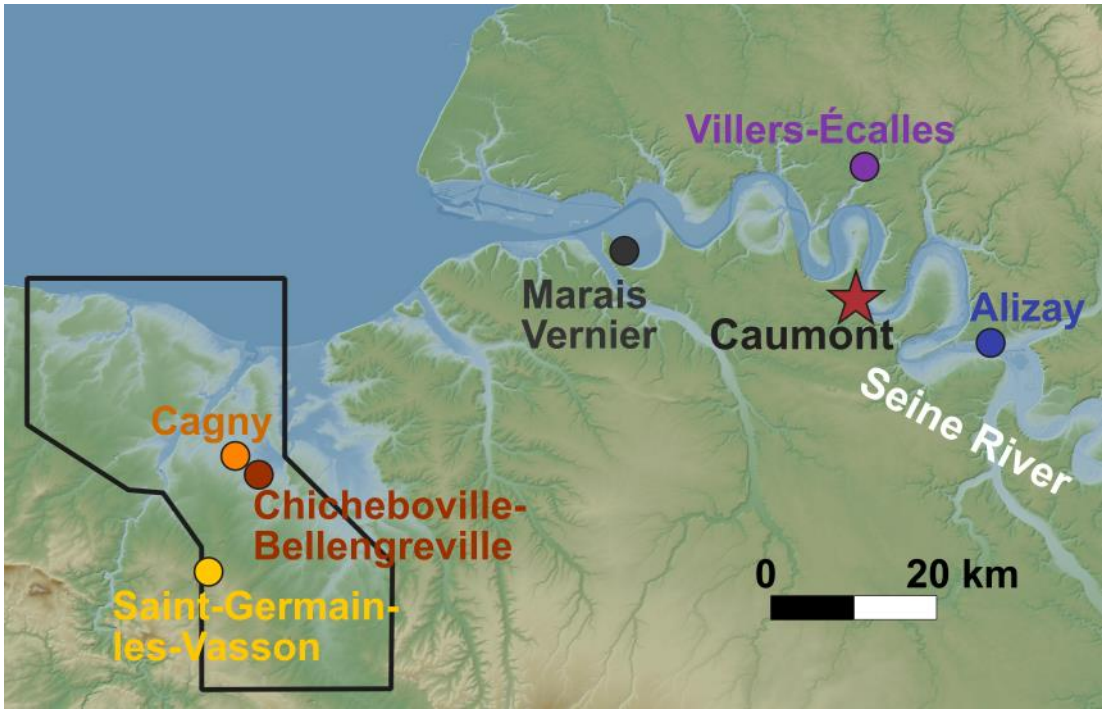

Figure 4. 3. Location map of the main study sites for Holocene paleoclimate in Normandy. Along the Seine River are the studies of Marais Vernier (black dot), (Frouin et al., 2007, 2009, 2010) and in floodplains are Alizay (blue dot), Villers-Ecalles (purple dot) (Gonnet, 2017; Gonnet et al., 2023) and Caumont cave (red star). In the plains of Caen are Cagny (orange dot) (Germain-Vallée and Lespez, 2011) and Chichebovile-Bellengrville (Lemer, 2024).

The Marais Vernier, situated in the Lower Seine valley, is one of the cut-off meanders (Frouin et al., 2010 and references therein). In the early-Holocene, the site is considered as a remnant fluvial channel, occupied by wetlands. The Holocene evolution of the Marais Vernier is based on sedimentary logs and pollen analysis. The paleoenvironment reconstruction, summarized by Frouin et al., (2009, 2010), is divided in 5 stages:

1) Prior to 8950-7950 BP, deposition of terrestrial material occurred in the abandoned fluvial channel, coming from the colluvium fans.

2) In parallel, an estuarine environment started to develop with a reed-swamp surrounded by deciduous trees (e.g. oak, elm and hazel).

3) Around 7800-7660 BP, estuarine deposits accumulated in the site and a maximum flooding event occurred during this phase.

4) From 74070-5650 BP, a thick peat accumulation developed as a result of the regional high water-table level.

5) From 3080-2850 BP, peat accumulation continued but from 3050 BP onwards, an increase in detrital deposits occurred, plausibly related to deforestation as a consequence of higher human pressure on the landscape.

The studies at the plain of Caen (Germain-Vallée and Lespez, 2011), (e.g., Cagny valley) and Seine river tributaries, such as Alizay and Viller-Écalles valleys (Fig. 4.3), have been synthesized in Gonnet et al., (2023). The comparison of regional data, allowed to illustrate the Holocene landscape evolution. The analysis of archaeological, pedological and geomorphological data completed in Gonnet et al., (2023), for the past 10,000 years BP, yielded 6 phases of geomorphological evolution, three of which are relevant for our study:

1) The late glacial/Holocene transition period, resulted in climate warming and the onset of soils development with the progressive evolution of luvisols and expansion of vegetation cover.

2) The middle Holocene presented a gradual development of forests (Leroyer et al., 2011) and thickening of luvisols as a result of climate forcings. In parallel, the pollen reconstruction shows the first indices of agriculture during the onset of the Neolithic (before 6500 cal. BP). This is interpreted by the authors as evidence of the potential onset of anthropogenic forcing.

3) From the protohistoric period to the end of Middle Ages, the first impacts of human settlements on the slopes of the valleys in Normandy were detected in the sediment profiles: high erosional processes lead to soil run-off and to the deposition of fine-grained sandy silt sediments in valleys as colluvium fans. The impact of human settlements on the landscape was intensified, during the post-medieval to late-modern era, with enhanced soil erosion detected in the log profiles. (Gonnet et al., 2023).

Recent geomorphological investigations and biological proxies study (Lemer, 2024), at the Chicheboville-Bellengreville marsh in the low plains of Caen, revealed the landscape environmental conditions throughout the Holocene. Moreover, based on the sediment and chemical analysis from the sampled cores, Lemer, (2024) identified seven periods of elevated water table in the marsh, throughout the Holocene. Two episodes (10500 – 9000 cal. BP; 8400 – 7500 cal. BP) were identified in the early Holocene, three in the Middle (6800 to 6700 cal. BP; 6000 – 5500 cal. BP; 5300 – 4750 cal. BP) and two in the late Holocene (4250 – 3550 cal. BP; 3000-2500 cal. BP). These periods with high water-table were intercalated by stable periods of soil development.

The marsh general evolution phases were synthesized by Lemer, (2024) as follows:

1) Between the Early (10500 cal. BP) and Middle Holocene (7520 cal. BP), the studied site was characterised by a progressive water table rise, associated with the development of peat bog and palustrine herbs increase. Meanwhile, on the flanks surrounding the marsh, the forest composed of mixed oak groves developed.

2) During the Middle Holocene, a general stabilisation of the water table is seen from 7500 to 6000 cal BP. The pollen records at the Chicheboville-Bellengreville show that the site was covered by forests. From 6000 to 4250 cal. BP, longer periods of water-table rise increased the organic matter and resulted in the accumulation of peat bog soil.

3) The Late Holocene period is characterized by two new phase of water table rise and return to more humid conditions. In parallel, the development of agropastoral activities was evidenced after 3570 cal. BP (Early Bonze Age), with the first occurrence of cereals and ruderal taxa identified in the peat cores. The detrital contribution into the peatland, associated with the impact of agricultural activities on the landscape, was significant after 3570 cal. BP.

A study based on riverine tufa deposits was also conducted in the plains of Caen, at Saint-Germaine-les-Vassons (SGV) and provided one of the first Holocene isotopic record on terrestrial carbonates in Normandy. Stable isotopes ($\delta^{13}C$ and $\delta^{18}O$) and malacology analysis were conducted along the profile of the tufa section, which covers the early to middle Holocene (Dabkowski, 2011). The tufa $\delta^{13}C$ record at SGV was interpreted as indicating humid/dry conditions and the $\delta^{18}O$ as being temperature driven. The obtained results were described by Dabkowski, (2011) as follows: at the base of the record, the $\delta^{13}C$ and $\delta^{18}O$ records on tufa were found in agreement with the mollusc and pollen assemblages, showing cooler and wetter conditions during the early Holocene (Preboreal). Followed by a transition to higher atmospheric temperatures and a decrease in precipitation during the Boreal. At the top of the sequence, the $\delta^{13}C$ and $\delta^{18}O$ records were found inconsistent with the mollusc assemblages. Although the tufa profile shows a general trend of isotopic variability from the early to middle-Holocene, the record is not well-dated and at low resolution, preventing from showing a clear isotopic trend for the whole Holocene. Also, the geochemical signal is not well-preserved and the change in the isotopic signal, specifically at the top of the profile is attributed to the effect of evaporation processes and a covariation between $\delta^{13}C$ and $\delta^{18}O$ signals.

The studies in Marais Vernier, the fluvial deposits in tributaries of the Seine River as well as the peat bog deposits in the plains of Caen show mainly a fluvial and drainage response to the climate change at the onset of the present interglacial (Holocene). The geomorphological and palynological investigations on sediments cores in all three sites revealed, from 5000 - 3000 yrs BP onwards, a change in the landscape due mainly to agropastoral activities, resulting in higher runoff. However, the studies show mainly local responses to climate- or human-driven changes throughout the Holocene. Pollen proxies reflect a regional vegetation trend, but the studied records are at low resolution. A highly-resolved record is needed to complement and improve the Holocene climate variability in Normandy and north-western Paris Basin. The highly resolved stalagmite stable isotope records from Caumont have a more regional scale significance in comparison to the lower resolution studies, which allows for a better comparison with other extra-regional (north-western Europe) proxies. The comparison with other north-west European proxies can help understand the climate variability drivers at a more regional scale.

4.3 Methods

4.3.1 Stalagmites collection and sampling

The five stalagmites collected for this study were taken from two different parts of the natural conduit at CCS (Fig. 4.1). Two stalagmites were taken from Rivières des Robots, CAU-1 and CAU-2 in 2019. The stalagmites were then cut in half, lengthwise, and one of the cut slabs was placed in epoxy resin and then polished (Fig. 4.4). Stalagmites CAU-1 measures 13 cm, CAU-2 12.6 cm and both present a monocrystalline structure. At La Jacqueline, three stalagmites were collected in 2021, then cut and polished (Fig 4.5). JAC-1 measures 14.7cm, JAC-3 10 cm and JAC-4 12.5 cm. Samples JAC-1, JAC-3 and JAC-4 present a clear lamination with grey colours and JAC-3 was broken at the top, losing the first 2 cm.

4.3.2 U/Th dating and age model

Nine U-series samples were taken from CAU-1 at 12, 22, 38, 45, 59, 68, 78, 98 and 120 mm depth and 7 samples from CAU-2 at 5, 22, 62, 76, 93, 104 and 119 mm depth (Fig. 4.4). Four samples were taken from JAC-1, at 15, 53, 77 and 135 mm from top. 5 samples from JAC-3 at 14, 68, 76, 90 and 106 mm, and 5 samples from JAC-4 at 13, 37, 49, 85 and 113 mm

(Fig. 4.5). The first set of measurements of calcite samples were taken by extracting a small piece of calcite, between 30 and 230 mg, using a dental drill, at the Laboratory Environnements, Dynamiques et Territoires de Montagne (EDYTEM), at Savoie University, France. These first set of subsamples were dissolved in isolation using 1.5 M HNO_3, spiked with a measured quantity of $^{233}U/^{229}Th$ or $^{236}U,^{233}U/^{229}Th$ mixed synthetic isotopic tracer (Hellstrom, 2003; Drysdale et al., 2012) and allowed to balance out on a hotplate overnight. U and Th were separated from the carbonate matrix using Eichrom TRU ion exchange resin and established methods (Luo et al., 1997), modified to collect U and Th in the same fraction using 0.1 M HCl –0.2 M HF (Hellstrom, 2003). Mass spectrometric analysis was undertaken at the University of Melbourne, Australia, using either a Nu Instruments Plasma MC-ICP-MS with standard collector block or a similar instrument with modified collector block placing simultaneously using the high- and low-mass SEM ion counters for each situation (Hellstrom, 2003).

The second set of subsamples were taken with a 1 mm drill bit, where powder was collected between 90 to 150 mg, at the Université de Rouen Normandy, France. This set of ages were analysed following the same protocol presented in Chapter 3, section 3.6.2 at the Laboratoire des Sciences du Climat et de l'Environnement (LSCE), France (Pons-Branchu et al., 2014, 2022). The age model for the 5 stalagmites was computed with COPRA software (Breitenbach et al., 2012), using 2000 Monte Carlo simulations for the $\delta^{18}O$, $\delta^{13}C$ and trace elements records. COPRA calculates the median and 95% confidence intervals and we used the U-Th dates as absolute ages.

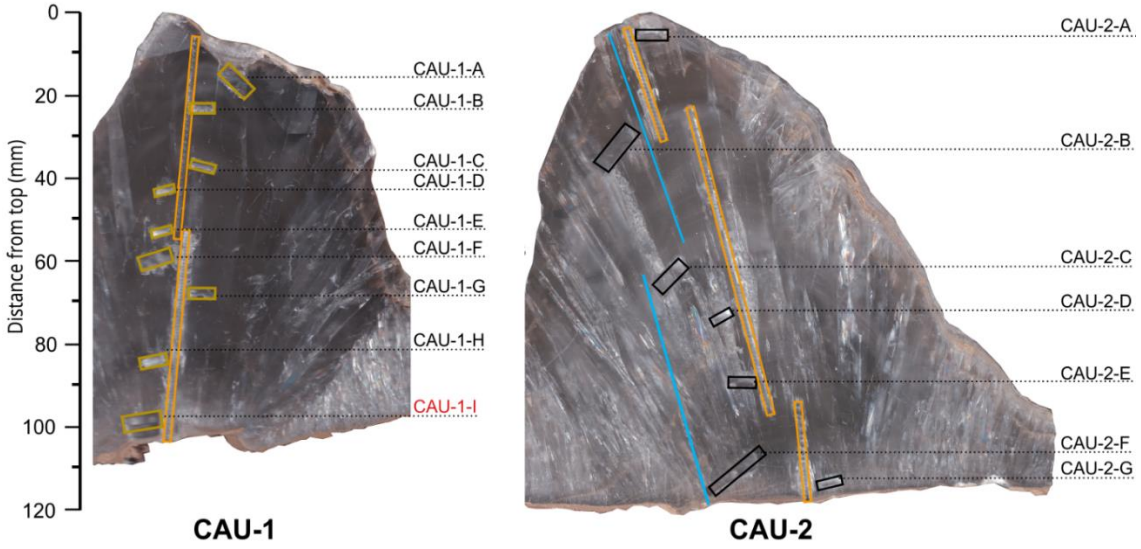

Figure 4. 4. Scan of the polished stalagmite slabs from Rivière de Robots, CAU-1 and CAU-2 depicting the sampling track for stable isotopes (orange rectangle), trace elements laser track (blue line) and the location of U/Th ages.

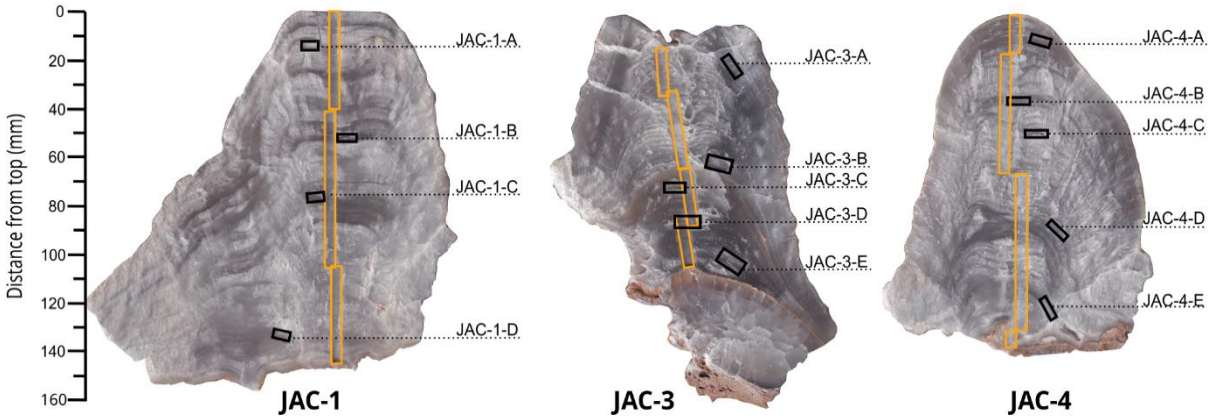

Figure 4. 5. Scan of the stalagmites polished slab from La Jacqueline, JAC-1, JAC-3 and JAC-4 with sampling track for stable isotopes (orange rectangle) and locations of U/Th samples plus ages.

4.3.3 Stable Isotope analysis

Powder samples were collected for stable isotope analysis, by continuously milling at 1 mm resolution for CAU-1 and CAU-2 at EDYTEM laboratory, Savoie University (France). The temporal resolution of CAU-1 is 59 a/mm (each sample representing ~59 years) and for CAU-2 is ~53 a/mm (each sample representing 53 years). The analysis of the samples for $\delta^{13}C$ and $\delta^{18}O$ was done using 0.7–0.8 mg aliquots, on an Analytical Precision AP2003 continuous-flow isotope-ratio mass spectrometer at the University of Melbourne following the protocol of Drysdale et al., (2007). An internal standard of Carrara marble (NEW1), which was previously calibrated against the international standards NBS18 and NBS19, was used to normalize the stable isotope values to the Vienna Pee Dee Belemnite (VPDB) scale. The mean analytical precision is 0.05 ‰ for $\delta^{13}C$ and 0.1 ‰ for $\delta^{18}O$ (Fig. 4.4).

For stalagmite JAC-1 145 powder samples (between 90 and 120 µg), were collected, 270 from JAC-3 and 172 from JAC-4, using a high precision micromill (Sherline 5400 Deluxe) at the Université de Rouen Normandy (Fig. 4.5). JAC-1 and JAC-4 were sampled at 1 mm and JAC-3 at 0.2 mm resolution. The resulting temporal resolution of the three stalagmites is almost decadal, with 6 a/mm (each sample representing ~6 years) for JAC-1, 10 a/mm (each sample representing ~10 years) for JAC-3 and 15 a/mm (each sample representing ~15 years) for JAC-4. Samples were analysed for $\delta^{13}C$ and $\delta\ ^{18}O$, at the Department of Geography and Environmental Sciences, Northumbria University (UK), following the methodology of Spötl, (2004) and Breitenbach and Bernasconi, (2011), explained in detail in Chapter 3, section 3.6.5.

4.3.4 LA-ICPMS analysis

Stalagmite CAU-2 was analysed for trace elements, quantified by Laser Ablation Inductively Coupled Plasma Mass Spectrometry (LA-ICPMS). The analysis was conducted at Department of Earth Sciences, Durham University (UK), with a 193 nm ArF Teledyne Analyte Excite+ excimer laser system coupled with a ThermoFisher iCAP TQ ICP-MS. The measurements were done every 10 µm (representing a sub-annual resolution), following the protocol of Müller et al., (2009) and it is described in detail in Chapter 3, section 3.6.6.

4.4 Results

4.4.1 Age model

The resulting ages from CAU-1 had an average error of ± 0.13 ka (2s), except for the bottom age 6.8 ± 4.5 ka BP, which was not considered for the age model calculations. The final age model ranges from 4.37 to 8.84 ka BP (Fig. 4.6). The ages for CAU-2 ranged between 0.54 and 8.84 ka BP with an average an error of ± 0.14 ka (2s) (Table 4.1). The resulting ages from JAC-1 had an average error of ± 0.06 ka (2s), and spanned between 3.39 and 4.11 ka BP (Fig. 4.6). For JAC-3, the average error is ± 0.11 ka (2s), and covered from 5.37 to 7.36 ka BP, with a hiatus from 6.99 to 5.87 ka BP. Lastly, JAC-4 had an average error of ± 0.10 ka (2s), and spanned between 3.68 and 4.59 ka BP (Table 4.1). Depth age models for the 5 stalagmites are shown in Figure 4.6. CAU-1 and CAU-2 both present an average growth rate of 0.02 mm/a, which is smaller than the average growth of JAC-1 (0.20 mm/a), JAC-3 (0.10 mm/a) and JAC-4 (0.13 mm/a).

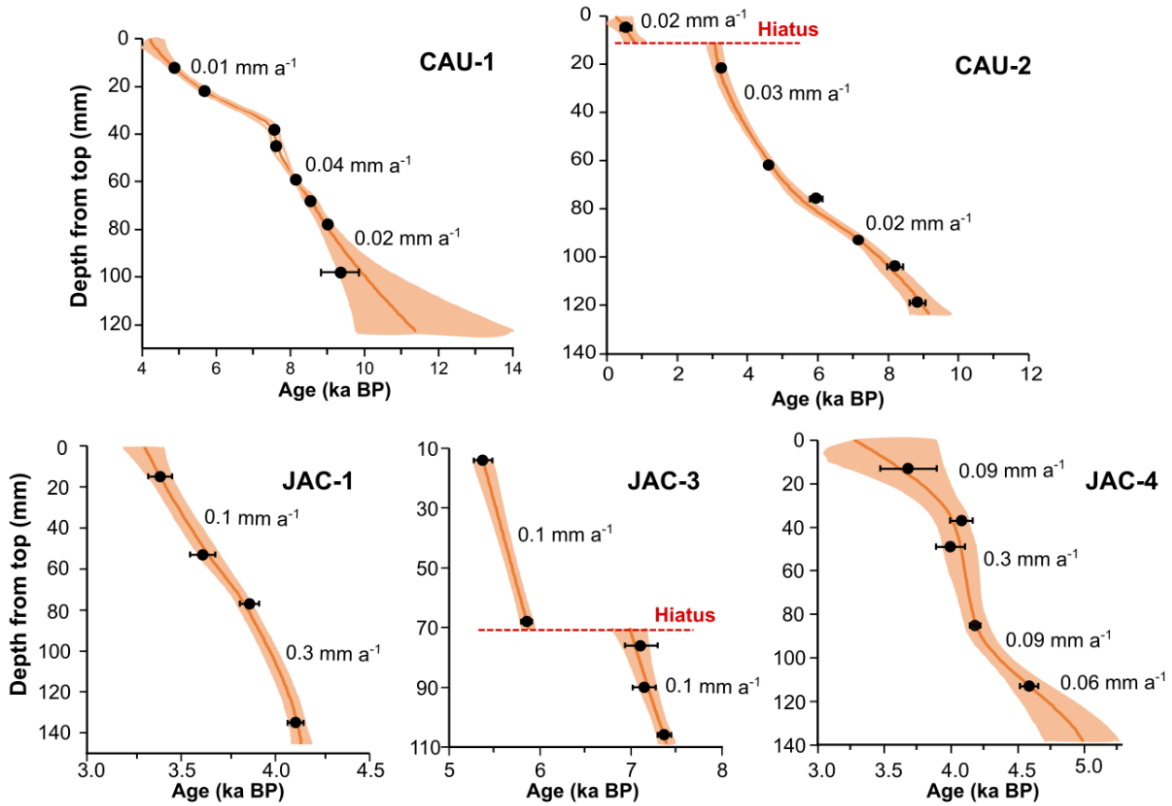

Figure 4. 6. Age depth models of all stalagmites, CAU-1, CAU-2, JAC-1, JAC-3 and JAC-4. CAU-2 and JAC-3 were the only two to present hiatuses but CAU-2 was the only one to start growing after the 3ka. Age models were computed with COPRA (Breitenbach et al., 2012).

Table 4. 1. U-series dates from stalagmites CAU-1, CAU-2, JAC-1, JAC-3 and JAC-4. The ages are given BP and the errors in 2s. The samples with (*) were measured at the Laboratoire des Sciences du Climat et de l'Environnement (LSCE, France) and the other samples at the University of Melbourne, Australia. Sample in bold, CAU-1-I, was not used due the wide error range.

Sample ID	Depth (mm from top)	230Th/238U	Error (2s)	234U/238U	Error (2s)	232Th/238U	Error (2s)	Age (ka)	Error (2s)	230Th/232Th	Age corrected (ka)	Error (2s)	Age corrected (ka BP)	Error (2s)
CAU-1-A	12	0.042	0.0005	1.057	0.0027	7.836E-05	1.6E-06	-	-	539.4	4.44	0.05	4.37	0.06
CAU-1-B*	22	0.050	0.0000	1.058	0.002	0.0501	0.0004	5.295	0.050	162.3	5.248	0.07	5.17	0.075
CAU-1-C*	38	0.067	0.0000	1.056	0.001	0.0675	0.0005	7.206	0.058	171.1	7.144	0.09	7.07	0.088
CAU-1-D	45	0.068	0.0007	1.055	0.0021	2.19E-04	5.28E-06	7.209	0.078	309.7	7.17	0.09	7.11	0.09
CAU-1-E	61	0.074	0.0007	1.053	0.0018	1.38E-03	4.43E-05	7.905	0.078	53.6	7.69	0.23	7.63	0.23
CAU-1-F	70	0.076	0.0007	1.058	0.0027	7.472E-05	1.5E-06	-	-	1014.9	8.10	0.08	8.03	0.08
CAU-1-G*	82	0.080	0.001	1.059	0.001	0.0804	0.0005	8.622	0.070	283.0	8.578	0.091	8.50	0.091
CAU-1-H	103	0.087	0.0008	1.055	0.0016	3.24E-03	6.88E-05	9.410	0.092	27.0	8.91	0.51	8.84	0.52
CAU-1-I	121	0.103	0.0007	1.055	0.0015	2.768E-02	5.5E-04	-	-	3.7	6.84	4.50	6.80	4.50
CAU-2-A	17	0.008	0.0004	1.076	0.0017	0.001033	0.000018	0.762	0.041	7.5	0.61	0.16	0.54	0.16
CAU-2-B	32	0.032	0.0003	1.060	0.0014	4.965E-04	9.9E-06	-	-	65.4	3.31	0.08	3.25	0.09
CAU-2-C	59	0.044	0.0005	1.053	0.0027	2.769E-05	5.5E-07	-	-	1593.0	4.66	0.06	4.59	0.06
CAU-2-D	71	0.058	0.0005	1.057	0.0017	1.04E-03	2.16E-05	6.182	0.055	56.3	6.02	0.17	5.96	0.17
CAU-2-E*	87	0.070	0.0000	1.076	0.002	0.0698		7.316	0.049	139.56	7.241	0.087	7.17	0.087
CAU-2-F	104	0.081	0.0006	1.079	0.0027	1.351E-03	2.7E-05	-	-	59.8	8.27	0.22	8.20	0.22
CAU-2-G	112	0.087	0.0008	1.089	0.0019	1.37E-03	2.73E-05	9.106	0.088	63.9	8.90	0.23	8.84	0.23
JAC-1-A	19	0.037	0.0005	1.158	0.0043	2.69E-04	1.92E-05	3.500	0.050	136.8	3.46	0.06	3.39	0.06
JAC-1-B*	53	0.039	0.0000	1.153	0.001	0.0389	0.0004	3.743	0.040	99.99	3.687	0.067	3.61	0.067
JAC-1-C	83	0.041	0.0005	1.156	0.0040	5.49E-05	2.52E-06	3.915	0.051	745.0	3.91	0.05	3.84	0.05
JAC-1-D	137	0.043	0.0004	1.154	0.0034	3.62E-05	1.61E-06	4.185	0.042	1203.4	4.18	0.04	4.11	0.04
JAC-3-A	20	0.058	0.0005	1.180	0.0049	6.13E-04	5.60E-05	5.528	0.054	95.5	5.44	0.10	5.37	0.10
JAC-3-B	62.5	0.063	0.0005	1.186	0.0037	2.05E-04	1.14E-05	5.955	0.052	308.9	5.93	0.06	5.86	0.06
JAC-3-C*	64	0.077	0.0009	1.184	0.001	0.0772	0.0009	7.352	0.095	64.52	7.187	0.177	7.114	0.177

Table 4. 2 ***(continued)***

JAC-3-D*	77	0.0077	0.0006	1.185	9E-04	0.0772	0.0006	7.344	0.065	85.32	7.219	0.127	7.146	0.127
JAC-3-F	102.5	0.079	0.0006	1.186	0.0041	2.76E-04	1.38E-05	7.474	0.064	285.7	7.44	0.07	7.36	0.07
JAC-4-A	10	0.042	0.0009	1.179	0.0040	1.36E-03	7.27E-05	3.944	0.088	31.1	3.76	0.21	3.68	0.21
JAC-4-B*	36	0.045	0.0006	1.179	0.001	0.0445	0.0006	4.201	0.058	120.29	4.150	0.083	4.077	0.083
JAC-4-C*	48	0.044	0.0004	1.179	0.001	0.0437	0.0008	4.116	0.082	124.23	4.068	0.107	3.995	0.107
JAC-4-D	86	0.045	0.0004	1.179	0.0039	5.23E-05	2.69E-06	4.259	0.041	867.3	4.25	0.04	4.18	0.04
JAC-4-E	117.5	0.050	0.0006	1.184	0.0041	2.53E-04	1.17E-05	4.691	0.060	197.5	4.66	0.07	4.59	0.07

4.4.2 Holocene $\delta^{13}C$ and $\delta^{18}O$ records

The stable isotope record of CAU-1 yields a $\delta^{13}C$ value of -8.15 ‰ at ca. 10.87 ka BP. At 10.68 ka BP it presents a negative peak at with -9.68 ‰ (Fig. 4.7A). There is a general trend after 10.49 ka BP, towards more negative values, reaching the lowest value of -11.20 ‰ at 8.19 ka BP. After ca. 8 ka BP, the record shows a short increase in $\delta^{13}C$ until 7.14 ka BP, presenting a second negative peak of -11.08 ‰ at 7.01 ka BP. From ca. 7 to 3.72 ka BP, the $\delta^{13}C$ values, yielding an average of -10.13 ‰, show no major variability.

For $\delta^{18}O$, the record presents less variation than for $\delta^{13}C$, starting with -4.83 ‰ and reaching the highest value of -4.27 ‰ at 10.31 ka BP. From ca. 10 to 8.56 ka BP, the $\delta^{18}O$ values present a general decreasing trend with the lowest value reaching -5.59 ‰. An increasing trend is noticed from 8.56 to 7.41 ka BP, reaching -4.51 ‰, followed by a rapid decrease of 1.05 ‰ until 7.16 ka BP. After ca. 7 ka BP the $\delta^{18}O$ curve generally shows stable signal until 3.72 ka BP with a variation of ca. 0.5 ‰.

Stalagmite CAU-2 $\delta^{13}C$ record presents in general less variability than CAU-1, with a maximum value of -9.76 ‰ and a minimum of -11.42 ‰ (Fig. 4.7B). The record starts at 9.03 ka BP with -9.53 ‰ and presents a general decreasing trend until 7.48 ka BP and 5.93 ka BP, with two negative peaks of -11.31 ‰ and -11.36 ‰, correspondingly. From ca. 5,93 to 3.77 ka BP, the record shows low variability, followed by an increasing trend until the hiatus at 2.95 ka BP. Finally, CAU-2 stalagmite restarts to grow until from 0.77 ka BP until 0.33 ka BP (modelled age).

The $\delta^{18}O$ record shows a variability of 1.31 ‰ and also presents a decreasing trend at the beginning of the Holocene, from 9.03 ka BP (-4.81 ‰) until 8.56 ka BP, (-5.77 ‰). A general increasing trend is noticeable until 5.80 ka BP and then a rapid negative excursion (-5.72 ‰) is observed at 4.27 ka BP. The record stopped at 2.95 ka BP and restarts at 0.77 ka BP and presents an increasing trend of 0.43 ‰ until 0.47 ka BP.

JAC-1 $\delta^{13}C$ record ranges between -11.55‰ and -9.74 ‰ from 4.14 to 3.31 ka BP. It presents a general trend towards positive values, with the highest value of -9.74 ‰ at 3.32 ka BP, before it stops growing at 3.31ka BP. JAC-1 $\delta^{18}O$ signal varies between -4.64 ‰ and -5.61‰ and does not present major excursions (Fig. 4.7B).

Stalagmite JAC-3 yields the oldest record from La Jacqueline, starting at 7.39 until 5.37 ka BP. As mentioned in section 4.4.1, JAC-3 presents a hiatus at 6.99 ka BP which lasted 1.12 ka. The $\delta^{13}C$ record shows a negative trend from -9.62 ‰ to -10.23 ‰ from 7.39 to 7.01 ka BP, followed by a short increase of 0.77 ‰ until 6.99 ka BP. After the hiatus, the signal starts at -9.77 ‰ and decreases to -11.24 ‰ at 5.46 ka BP, followed by a final increase to -10.47 ‰ at 5.37 ka BP. The $\delta^{18}O$ signal varies between -5.61 ‰ and -4.64 ‰. Prior to 6.99 ka BP, the $\delta^{18}O$ signal has an average of -5.36 ‰. From 5.87 ka BP onwards, the record presents a negative peak of -5.54 ‰ at 5.79 ka BP and then trends towards more positive values, reaching -5.22 ‰ at the top of the stalagmite.

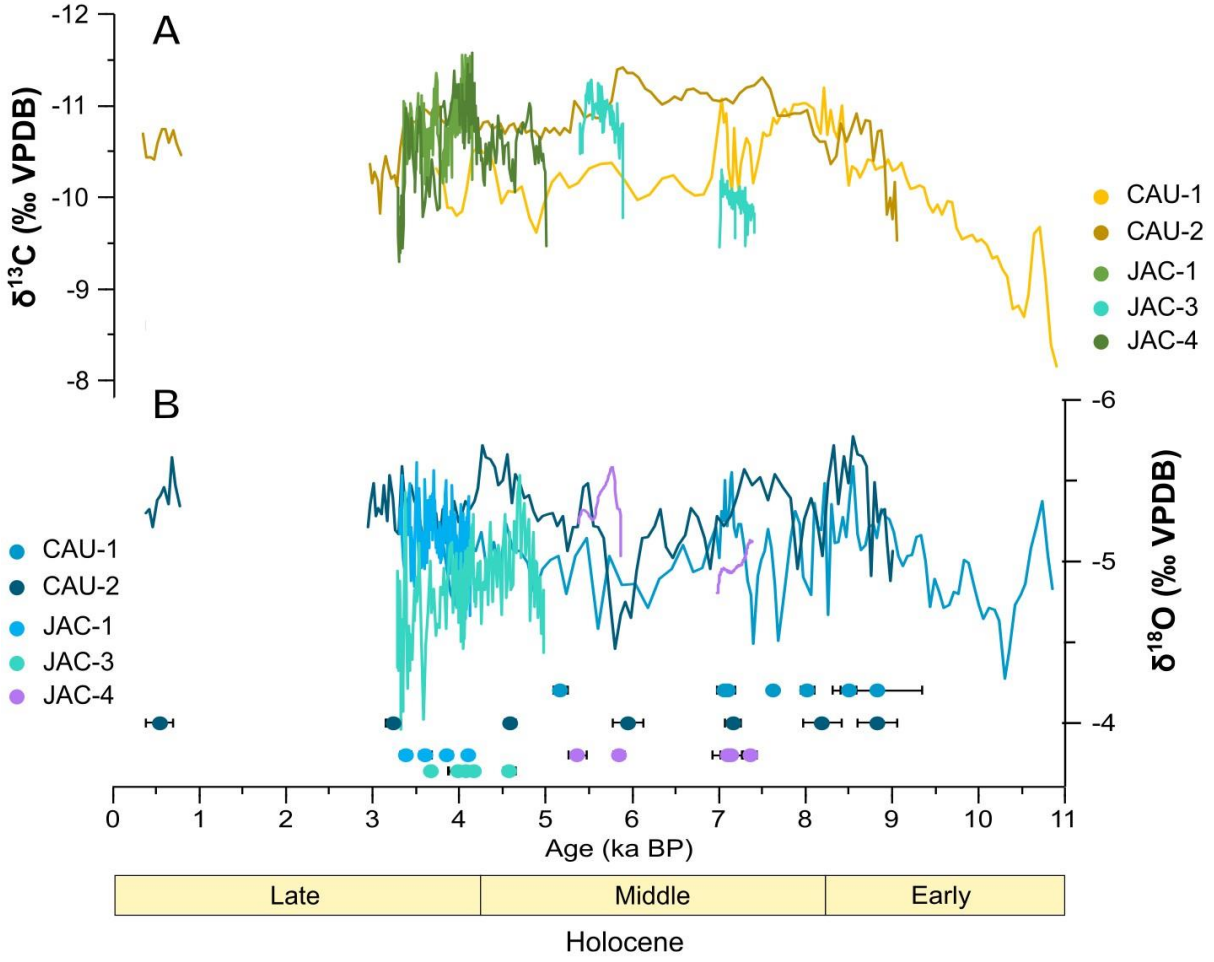

Figure 4. 7. Holocene records of the 5 stalagmites CAU-1, CAU-2, JAC-1, JAC-3 and JAC-4 depicting δ13C (A) and δ18O (B), with their corresponding ages and incertitude.

For JAC-4, the $\delta^{13}C$ record starts at 4.99 ka BP with -9.47 ‰ and the values decrease to -10.98 ‰ at 4.81 ka BP. The $\delta^{13}C$ signal presents an increasing trend to -10.13 ‰ at 4.28 ka BP, followed by a decreasing trend, reaching a negative peak of -11.58 ‰ at 4.14 ka BP. For the remaining 0.86 ka of the record, the $\delta^{13}C$ signal shows a general increasing trend, reaching -9.29 ‰ at 3.29 ka BP. The $\delta^{18}O$ record starts at 4.99 ka BP with -4.83 ‰ and present a decreasing trend, reaching the lowest value of -5.53 ‰ at 4.70 ka. From ca. 4.70 ka BP onwards, the $\delta^{18}O$ signal shows a general increasing trend towards the top of JAC-4, reaching -3.9.6 ‰ at 3.33 ka BP, with the exception of a negative excursion of -5.43 ‰ at 3.38 ka BP.

4.4.3 Trace elements

Stalagmite CAU-2 presented a Mg record that ranged between 38 and 5688 ppm, with an average of 132 ppm and Sr ranged between 14 and 3169 ppm, with 71 ppm average (Fig. 4.8). At the bottom of the record, 9.01 ka BP, Mg and Sr yielded high values of 1700 and 445 ppm, respectively, with a growth rate of 0.04 ka/mm. Then, Mg and Sr concentrations decreased continuously until 7.3 ka BP, with the exceptional peak at ca. 7.8 ka BP, (Fig. 4.8). From ca. 7.3 ka BP until the hiatus (2.95 ka BP), the Mg record had an average of 124 ppm, the Sr record of 69 ppm. After the hiatus, (0.79 ka BP) until the top of the stalagmite (0.40 ka BP), the Mg record presented a range of values from 55 to 2220 ppm, with higher peaks at 0.06 and 0.41 ka BP, and Sr between 16 and 247 ppm. The elemental records yielded a continuous growth rate of 0.02 mm/a from 0.79 to 0.40 ka BP. The record presents a small gap of data between 6.99 and 7.11 ka BP, lost in the post treatment process and does not represent a hiatus.

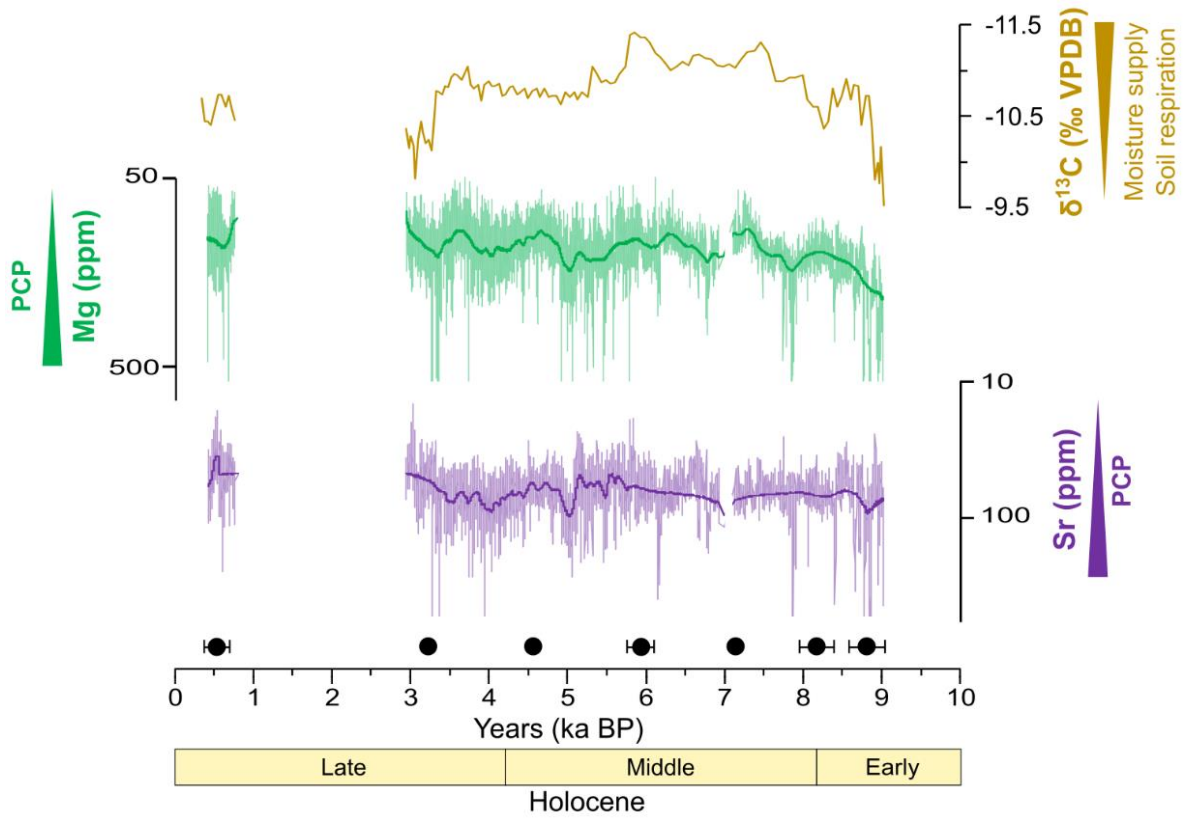

Figure 4. 8. Geochemical records from stalagmite CAU-2, reflect hydroclimate variability during the Holocene. The records include $\delta^{13}C$, Sr and Mg concentrations.

4.5 Discussion

4.5.1 Interpretation of the proxy records

The isotopic signal ($\delta^{13}C$ and $\delta^{18}O$) in speleothems records is influenced by different factors, such as the vegetation/soil overlying the cave, the karst aquifer infiltration dynamics, rainfall amount, crystal growth and secondary alterations (Fairchild et al., 2006). The monitoring studies done on Caumont quarry and cave system (Bejarano-Arias et al., 2024) and analysis of a recent stalagmite (chapter 3), helped to decipher the sources and factors that influence the isotopic $\delta^{13}C$ and $\delta^{18}O$ signal.

At Caumont site, it was identified that the $\delta^{13}C$ record is mainly influenced by a deficit in summer effective infiltration and consequently prior calcite precipitation (PCP) (Bejarano-Arias et al., 2024). This was observed when comparing the modern precipitated calcite with local rainfall records (Fig. 2.6, section 2.5.4) as well the evaluation of the 20th century stalagmite

records with historical climatic data (e.g. precipitation and temperature). We identified that increases in the $\delta^{13}C$ calcite signal were linked to periods of lower effective infiltration, which lead to longer water residence time in the epikarst and enhanced PCP (Riechelmann et al., 2013). Other factors such as CO_2 productivity and soil bio-activity as well as vegetation cover influence the $\delta^{13}C$ calcite signal, but to a lesser extend at Caumont site. The monitoring study at Caumont showed that the $\delta^{18}O$ calcite and drip water signal are biased towards the higher infiltration season, corresponding to autumn and winter months (November to February), in the study area. $\delta^{18}O$ calcite signal is interpreted then, as an indication of changes in precipitation amount.

4.5.1.1 Growth rates

The understanding of the isotopic signal in the previous chapters allows us to interpret the long-term isotopic changes in Caumont speleothems that span the present interglacial (Holocene). The onset of CAU-1 growth at 10.8 ka BP and CAU-2 growth, at ca.9 ka BP (Fig. 4.6), occurred under wet and favourable climate conditions during the early Holocene in north-western Europe (Fairchild and Baker, 2012; Verheyden et al., 2014). Followed by growth increase specially for CAU-1 from ca. 10 to ca 7 ka BP. A growth decrease is seen in CAU-1 stalagmite ca. 7 ka BP, but increases again from 6.9 until 3.7 ka BP, whereas CAU-2 grows constantly, at a lower rate, from ca. 8 ka BP until ca. 2.9 ka BP. Both stalagmites show continuous but slower growth with sufficient effective infiltration conditions to support calcite growth during the mid-Holocene, compared to the early Holocene. The growth start of JAC-1, at 4.1 ka BP, and JAC-4 at 4.9 ka BP (Fig. 4.6), are in agreement with the general increase in growth rate of CAU-2, specially around ca. 4 ka BP, implying higher infiltration conditions from 5 to 4 ka BP which resulted from a general humidity increase seen in north-western Europe (Fairchild and Baker, 2012).

4.5.1.2 $\delta^{13}C$ calcite signal

CAU-1 $\delta^{13}C$ signal shows a decreasing trend, towards lower values, from 10.8 until 8.19 ka. The decrease in $\delta^{13}C$ values reflect mainly higher effective infiltration and reduced PCP, but also the development of the vegetation cover (Fohlmeister et al., 2012) associated with Early Holocene high biogenic soil CO_2 productivity. From ca. 8 to 5.5 ka, a relatively stable $\delta^{13}C$ signal is observed in CAU-1, but less for CAU-2 and JAC-3 records with an overall $\delta^{13}C$ isotopic variability of ±1 ‰. Low isotopic variability reflects stable effective infiltration and

vegetation cover during the Middle Holocene compared to the higher $\delta^{13}C$ signal variability during the Early Holocene. Fairchild and Baker, (2012) suggested fairly steady environmental conditions for the Middle Holocene in north-western Europe, although a high frequency of wet events occurred in the Northern hemisphere form 8.1 to 7 ka BP (Verheyden et al., 2000; Wanner et al., 2015).

At the onset of the late Holocene, we observe a clear increase in $\delta^{13}C$ signal for JAC-1, JAC-4 and CAU-1 from ca. 4 ka BP onwards, except for CAU-2 record where the increasing trend starts later at 3.73 ka BP. The change towards higher isotopic signal around 4 ka BP would reflect lower effective infiltration conditions, higher PCP and a scarcer vegetation cover associated with lower biogenic soil CO_2 productivity above Caumont. During the late Holocene, all stalagmites stopped growing at ca. 3 ka BP, except CAU-2 stalagmite, which was reactivated from 0.77 to 0.33 ka BP. During this short period, the $\delta^{13}C$ signal was stable with a variability of 0.17 ‰ and an average of -10.59 ‰. The low $\delta^{13}C$ signal indicates a return to higher effective infiltration and favourable soil bio-activity above Caumont.

4.5.1.3 $\delta^{18}O$ calcite signal

The resulting Holocene $\delta^{18}O$ record, showed less variation than the $\delta^{13}C$ record, with an average variability of ±1.31 ‰, for CAU-1 and CAU-2, ±1 ‰ for JAC-1 and JAC-4 and ±1.5 ‰ for JAC-3. The interpretation of the 5 records, showed a similar trend than the $\delta^{13}C$ record: early Holocene CAU-1 and CAU-2 records present decreasing $\delta^{18}O$ signal until 8.61 ka BP. The decrease is related to a shift towards more humid winter conditions and it is confirmed by the trend of more negative $\delta^{18}O$ signal (Fohlmeister et al., 2012), reaching minimum values from 8 to 9 ka BP. A general increasing trend of $\delta^{18}O$ signal in both CAU records is noticeable from 8 to 5.5 ka BP, reaching the maximum, around 5.7 ka BP, before decreasing by ca. 1 ‰ until 4.36 ka BP.

JAC-4 also shows a general increasing trend, until it stops growing at 3.28 ka BP. The $\delta^{18}O$ signal increase during the first half of the late Holocene would reflect a shift in the Northern Hemisphere to cooler (Fairchild and Baker, 2012) and drier conditions (Verheyden et al., 2014; Allan et al., 2018a). After the growth stop of all stalagmites, CAU-2 starts regrowing at 0.77 ka BP (modelled age), during the medieval period. The $\delta^{18}O$ signal shows an increasing trend (variation of ca. 0.4 ‰) towards higher $\delta^{18}O$, until it stopped growing at 0.33 ka BP). The $\delta^{18}O$

trend towards higher values, confirms the cooling and drying conditions (Camenisch and Salvisberg, 2020), during the little ice age (LIA) (McDermott et al., 2001) that might have prevented any further precipitation of calcite.

4.5.1.4 Trace elements records

The main factors that influences the Mg and Sr signal in stalagmites are interpreted as water residence changes in the epikarst (Verheyden et al., 2000) and by rainfall variability, influencing PCP along the water flow path in the epikarst (Fairchild et al., 2000; Fairchild and Treble, 2009; Wassenburg et al., 2020). Moreover, the Mg and Sr records present a positive correlation (*r:* 0.55) providing further evidence that PCP is dominant in Caumont (Mischel et al., 2017).

From 9.04 ka BP until 7.35 ka BP (Early and Middle Holocene), the Mg values present a decreasing trend, with the exceptional increase of ca. 31 ppm at 7.85 ka BP. The Sr record also decreased from 8.8 until 8.5 ka BP and then remained relatively stable. The decrease is interpreted as result of the shift from cooler and drier to wetter climate conditions, characteristic of the early Holocene period in north-western Europe (Boch et al., 2009).

In the Middle Holocene, at ca. 6.7 ka BP, there is a minor increase in the Mg values of ca. 300 ppm and Sr values of ca. 150 ppm, which is rather small in comparison to the shift at the onset of the Early Holocene. The small variation could imply a short-term shift to drier conditions, yet not strong enough to pass the PCP threshold that leads to higher Mg, Sr and $\delta^{13}C$ values. A possible explanation for the slight response in Mg and Sr but not in $\delta^{13}C$, is the well-developed vegetation and soil above the cave, resulting from the general humid conditions (Mischel et al., 2017) that predominate during this period. From 6.4 to 6.2 ka BP drier phase was also identified in the Mg and Sr records at Père Noël stalagmite record (Allan et al., 2018), but this dry trend is not clear in the Caumont record.. The PCP threshold is not surpassed until ca. 5.26 ka BP for $\delta^{13}C$, with an increase of ca. 0.7 ‰. Around 5 ka BP, Mg and Sr records present peaks of higher values (Fig. 4.8), that can be interpreted as change to stronger dry conditions, that lead to higher PCP in the epikarst, under low effective infiltration climate conditions (Hellstrom and McCulloch, 2000; Wassenburg et al., 2020).

The Mg and Sr concentrations during Middle and Late Holocene (from ca. 5 to 3 ka BP) present more variability than in the first half of the record. Both Mg and Sr records present a long-term increasing trend until ca. 3.3 ka BP, in line with increased $\delta^{13}C$ values, indicating generally drier conditions. A gradual increase of Mg and Sr concentrations were also identified between 3.5 and 2 ka BP in a Belgium speleothem (Verheyden et al., 2000), confirming a drier period with higher PCP. From 0.77 to 0.33 ka BP (modelled age), both Mg and Sr records, present a similar general trend to $\delta^{13}C$, with low variability and lower than average values (114 ppm for Mg and 49 ppm for Sr), indicating generally humid conditions during the medieval period.

4.5.2 Evaluation of Caumont geochemical records with regional proxies

The comparison of the geochemical records obtained from Caumont site, with the regional records of Normandy, was focused mainly on the CAU-1 and CAU-2, since these two stalagmites present the longest coverage of the Holocene. From the well dated isotopic records, the $\delta^{13}C$ signal shows more variability than the $\delta^{18}O$ record. Moreover, the $\delta^{13}C$ signal is related to soil and the biological activity above the cave (Fairchild and Baker, 2012), unlike $\delta^{18}O$, rendering it more suitable to compare with the sedimentary proxy records from Normandy, related to vegetation and soil dynamics.

In the Early Holocene (10.87 - 8.19 ka BP), the $\delta^{13}C$ record shows a decreasing trend, interpreted as a shift from drier to wetter conditions (Fig. 4.9), with the signal reaching the lowest values from 9 to 8 ka BP, indicating a peak in humid conditions. This coincides with the sediment sections of Alizay, which presents a change at ca. 8.5 ka BP, from detrital sediments deposition (silts), to a pedogenetic stage (Fig. 4.9), composed of neoluvisol and luvisols (Gonnet et al., 2023). The variation in the composition, from silty-clay minerogenic sediments to organic rich sediments (paleosol), reflects a shift into a wetter climate that allowed soil formation (Gonnet, 2017). In the Marais Vernier, an increase up to 75% in the arboreal pollen content was observed, ca. 8 ka BP (Sebag, 2002; Frouin et al., 2009).

Likewise, during this period, the Plains of Caen present peat formation, in the Cagny Valley, from 8.95 to 2.95 ka BP (Germain-Vallée and Lespez, 2011), and in the Marais de Chicheboville-Bellengreville, from 8.7 to 3.9 cal ka BP (Lemer, 2024). Moreover, at Saint-

Germain-Le-Vasson (SGV), the analysis of tufa deposits shows a similar trend: during the first half of the Holocene, humid climate conditions associated with a high water table and a well-developed soil favoured the precipitation of vast tufa deposits (Limondin-Lozouet et al., 2013). The pollen records preserved in SGV tufa deposit, reflected the development of pine forests and later spread of hazel and oak during the Preboreal (Lemer, 2024). Furthermore, the stable isotopes analysis ($\delta^{13}C$ and $\delta^{18}O$) of the SGV tufa showed during the Preboreal lower $\delta^{13}C$ values, reflecting an increase in vegetation cover with wet climate conditions. This interpretation is supported by the malacological data which also developed in a humid environment (Dabkowski, 2011). The interpretations of the isotopic record in SVG tufa are in agreement with the isotopic trend in the CAU record during the early Holocene, since higher temperature enhances soil activity which is reflected in more negative $\delta^{13}C$ values (Fairchild and Baker, 2012; Fohlmeister et al., 2020).

The $\delta^{13}C$ record in Caumont shows a period of relatively stable climatic conditions after the early Holocene. However, three negative excursions are noticeable at 7.5 and 6 ka BP in CAU-2 and at 7.14 ka BP for CAU-1. The decrease in $\delta^{13}C$ in both records coincides with the "Holocene optimum" period, commonly classified between ca. 8.5 to ca. 4.5 ka BP (Johnsen et al., 2001; Wanner et al., 2011; Mischel et al., 2017). In parallel, the wet climate in Normandy is reflected in the continuous peat accumulation in the plains of Caen and the pedogenesis in Alizay. Likewise, the relatively consistent arboreal pollen content (ca. 70%) in the Marais Vernier (Fig. 4.9) shows the expansion of deciduous oak forest (e.g. *Quercus, Tilia, Fraxinus*) and the sporadic increased presence of *Taxus* and *Fagus taxa,* indicating humid forest conditions (Leroyer et al., 2011).

Around 4 ka BP, an increase in $\delta^{13}C$ signal in CAU-1 record, indicates a slight shift towards drier conditions, which coincides with a decrease in the arboreal pollen in the Marais Vernier. The latter shift in pollen record is interpreted to be related to agropastoral activities (Leroyer et al., 2011). In parallel, the increase in $\delta^{13}C$ signal from Caumont stalagmites is in agreement with the change from pedogenetic to erosional phase at Alizay site.

Stalagmite CAU-1 stops growing at 3.76 ka BP, while CAU-2 presents an increasing trend in $\delta^{13}C$ signal at ca. 3.73 ka BP, until it also stops growing at 3 ka BP. The increase in $\delta^{13}C$ signal could reflect a shift to drier climate. At 160 km north-east of Caumont site, the study

of tufa in the Somme valley (Beaumont et al., 2023) showed a shift to cool and dry conditions during the Subboreal. Likewise, around 3 ka BP, the sediment section study in Cagny, East of Caen shows a change from peat accumulation to the deposition of detrital sediment (Lespez and Germain, 2011). The Chicheboville-Bellengreville core, close to Cagny, presents a change from peaty clays to clayey silt sediments around 3 ka BP (Fig. 4.9) (Lemer, 2024). The interpretation of the environmental change around 3 ka BP, in the sedimentary records, was no longer ascribed only to climate forcing but as reflecting a higher influence of human impact (e.g. Germain-Vallée and Lespez, 2011; Gonnet et al., 2023). Moreover, at SGV, the tufa record showed a decrease in the deposition of carbonates after 3.7 ka cal. BP with the evident disrupt of the tufa at ca. 2.6 cal. BP. The soil erosion surrounding SVG site at this period is interpreted to be related to the impact of human activities on the fragile tufa ecosystem, leading to a stop in tufa accumulation (Lespez et al., 2005; Limondin-Lozouet et al., 2013). At the Marais Vernier site, high clastic sediments related to flooding dynamics are noticeable from 3.1 ka BP.

During the late Holocene period, human settlements begin to modify the environment and landscape (Frouin et al., 2010) at the Marais Vernier. Gonnet et al., (2023) explain the substantial impact of early human settlements reflected in the increased erosion processes and associated deposits in the studied area of Alizay and Villers Ecalles (Fig. 4.9). The deforestation on the plateau and slopes of the Seine River enhanced the erosion and run-off of luvisols, subsequently changing the type of sediments in the valley to detrital deposits. Such interpretation is generally in line with the onset of human settlements and their impact on the landscape in Normandy, ca. 3 ka BP (Lespez and Germain, 2011).

4.5.2.1 Analysis of the growth stop in Caumont stalagmites

The collected speleothems in the lower level of Caumont span the Holocene period, and show a general stalagmite growth from ca. 8 to 3.2 ka BP in the Robots and from ca. 7 to 3.4 ka BP in La Jaqueline (Fig. 4.2). The flowstone covering the detrital deposits in the Riviere des Robots spans the early Holocene from 10 to 7 ka BP (Nehme et al., 2020). Moreover, in Ballesteros et al., (2023) the study of the Caumont speleogenesis allowed dating more than 15 speleothem samples. The flowstone samples collected at Salle Blanche, the Eastern divergence and Réseau de la Boue also span the Holocene (Fig. 4.1 and 4.2). Surprisingly, with the 5 collected speleothems in the lower level of Caumont, no sample yielded a younger age than 3.2

ka BP. Coincidently, the 4 out of 5 stalagmites collected for this study stopped growing after ca. 3 ka BP.

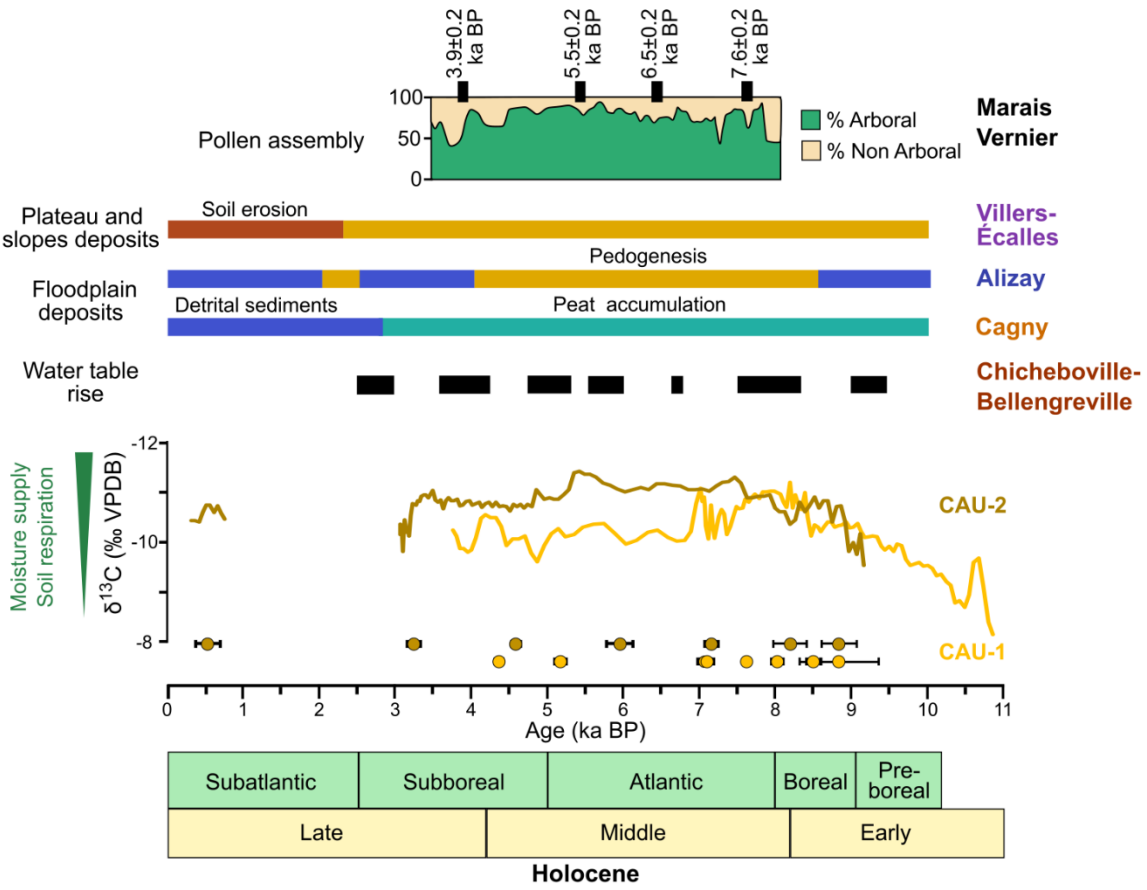

Figure 4. 9. Comparison of stalagmite CAU-2 $\delta^{13}C$ record with proxy records from Normandy, pollen assembly (Sebag, 2002; Frouin et al., 2009) from Marais de Vernier and sedimentary synthesis (for location see Fig. 4.2) (Gonnet et al., 2023). Chronozones defined by Mangerud et al., (1974) and calibrated by Walanus and Nalepka, (2010).

To explore the possible reason for stalagmites CAU-1, CAU-2, JAC-1 and JAC-4 growth stop at fairly the same time (Fig. 4.10A), we take a closer look at CAU-2 stalagmite. CAU-2 record is the only stalagmite that presented regrowth at ca. 0.44 ka BP, after the hiatus at ca. 2.18 ka BP (modelled age). This hiatus is associated with the deposition of a clay layer, along the stalagmite laminae where the renewal of calcite precipitation was dated at 0.77 ka BP (modelled age). The clay layer, located at 10.5 mm from the top of stalagmite (Fig. 4.10B), in addition to the clay deposits found at the base of the stalagmites could indicate a flooding event in the Rivière de Robots. The fact that clay deposits were found on both Rivière de Robots and La Jacqueline sites, covering the floor and stalagmites, suggest that flooding events could have

occurred in the lower level of CCS. The origin of such flooding events is yet to be identified and several hypotheses are suggested below.

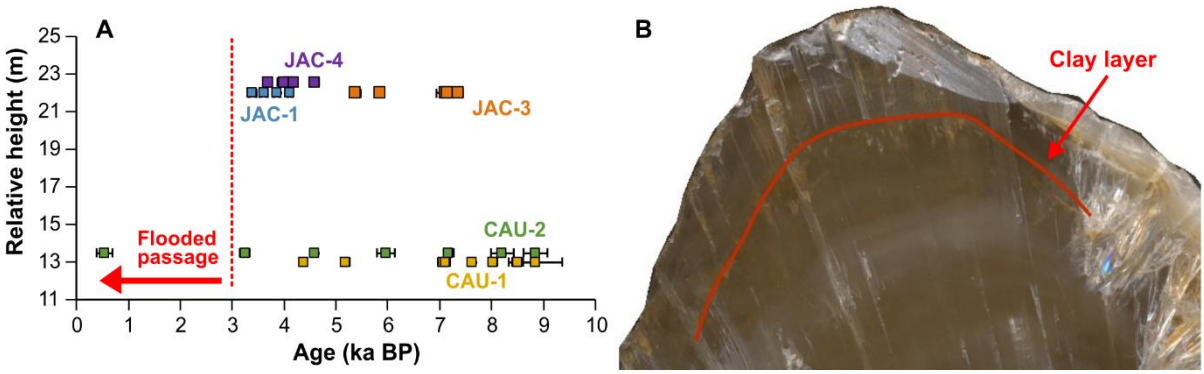

Figure 4. 10. Compilation of Caumont's 5 stalagmites age covering the Holocene, highlighting that all of them stop growing around 3 ka BP (A). The only stalagmite that present regrowth after the hiatus was CAU-2, with calcite layer being deposited after the clay layer (B), indicative of flooding at the Rivière de Robots conduit.

Fairchild and Baker, (2012) stated that since the middle Holocene, the environment of caves in the Northern hemisphere, could result in unstable conditions for stalagmite growth if affected by human impact. In order to assess if the growth stop of all the stalagmites in Caumont (3 ka BP), could be related to human impact on the vegetation cover on the plateau, above the cave, we explored the archaeological records of the Service Regional de l'Archéologie (SRA). The database projected into a Geographic Information System aims to evaluate the presence of human settlements prior to 3 ka BP (late Holocene) and close to Caumont cave. The projected archaeological sites, for the surrounding area of Caumont (Fig. 4.11) show many settlements and vestiges from the Neolithic to the medieval periods. We focused on archaeological sites dated back to the Neolithic (ca. 7100 - 4000 yrs cal BP), Bronze (ca. 4100 - 2800 yrs cal BP), Iron (ca. 2800- 2000 yrs cal BP) and Gallo-Roman periods (ca. 2950 – 1600 yrs BP), (Gonnet t al., 2023; Lemer, 2024).

Above the plateau and in proximity of 5 km radius to Caumont site, we observe vestiges from Neolithic period at Portes de Roumois, Bronze period (purple dot with no name) and Gallo-Roman period in Le Catelier (Fig. 4.11). These vestiges confirm the presence of human settlements near Caumont, prior to the stalagmite growth stop. Even though the type of vestiges are not specified in the records, the site points located close to Caumont coincide with the timing for the general onset of human settlements in Normandy and their effect on the environment

(Frouin et al., 2009; Leroyer et al., 2011; Gonnet et al., 2023). The deforestation caused by human activities (e.g. agriculture and pasturage), could have reduced soil productivity and an increased soil erosion on the plateau (Gonnet et al., 2023).

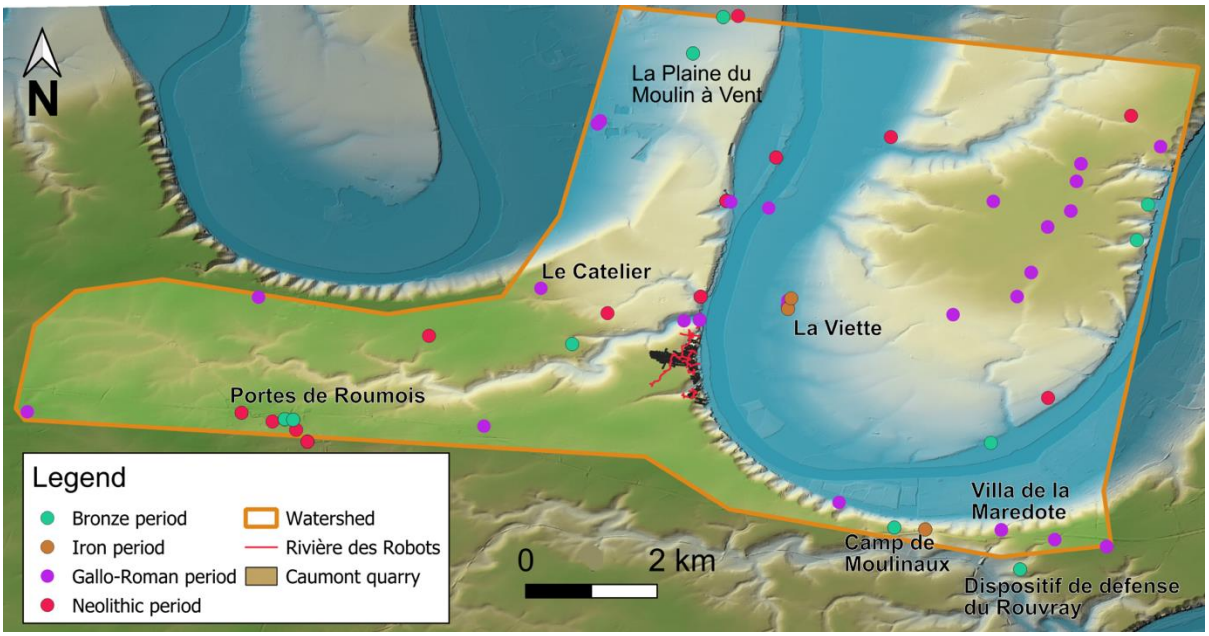

Figure 4. 11. Map of the archaeological vestiges corresponding from the Neolithic to the Gallo-Roman period (from SRA records) along the Seine River and in proximity of Caumont cave (outlined in red). Above the cave and on the plateau two vestiges were found at Portes de Roumois and Le Catelier.

A higher runoff could result from soil degradation and scarcer vegetation, leading to a higher seepage in the cave (Fairchild et al., 2006, 2007), but also a change in the hydrologic system of the surrounding area of Caumont during winter seasons. Such hydrologic change could be the increase of the local water recharge into the cave, as a consequence of higher runoff and fast cave infiltration. Consequently, a higher recharge would contribute to a local water level rise of the Rivière des Robots, eventually flooding the cave system. Repetitive flooding inside the Rivière des Robots conduit could lead to higher sediment infill covering the cave soil and stalagmites, as seen in the clay layers found in CAU-2 stalagmite (Fig. 4.10) and in La Jacqueline.

Another possible factor that could support the origin of flooding in CCS is the sea level rise combined with high water-table level in the karst system. The study on the sea level evolution (Stéphan and Goslin, 2014) along the English channel, gathered data from the North of France, including the Somme, the Seine River estuary and other small coastal rivers. The

reported sea level at the Seine River estuary shows a continuous rise from ca. 8.5 to 3.8 ka BP, leading to a sea level increase of ca.15 m (García-Artola et al., 2018). Moreover, the study of Holocene tufa deposits in the Somme valley (North France), reported a marine transgression that occurred at ca. 3.8 ka BP, which lead to a rise in the fluvial water table and the reactivation of the tufa deposition (Beaumont et al., 2023).

The sea level rise identified in the Somme River (Beaumont et al., 2023)) and the high water-table levels seen in the Plain of Caen (Lemer, 2024), both occurred around ca. 3-4 ka BP. These processes could have also occurred in the lower Seine valley and influence the water-table at the Caumont site with the combination of high fluvial level and high pluvial recharge in the karst during winter-spring seasons. As the Rivières de Robots in Caumont is still active and terminates in a sump linked to the Seine River (Ballesteros et al., 2020), the conditions of cave flooding during exceptional winter seasons (El Janyani et al., 2012), is highly plausible. CCS has a sub-horizontal chalk bedrock (Ballesteros et al., 2021), with a height difference of ca. 8 m, between the two sampling locations (Rivière de Robots and La Jacqueline, Fig. 4.1B). According to the geological context of Caumont, we consider plausible that a rise in the water table of Rivière des Robots during winter seasons combined with higher soil erosion at the plateau could lead to an increase in water infiltration from the surface and water recharge in the karst. Such conditions may lead an increase of flooding events in the cave system. Additionally, at the Plain of Caen, Lemer, (2024) identified a period water table rise from 4.3 - 3.6 cal ka BP (Fig. 4.9). This period of regional flooding observed in the Somme valley as well as in Chicheboville may also coincide along the Seine River with repetitive flooding events at the Rivière des Robots (clay layers in stalagmites). This could lead to infill, clogging of the karst conduits and the growth stop of Caumont stalagmites.

4.5.3 Caumont's records significance in the north-west European context

4.5.3.1 Holocene climate change events vs longer trend climate signal

Several authors have described rapid climate change events during the Holocene period (see section 1.3 for further details). Wanner et al., (2011), defined that these cold events mark the interruption of the relatively stable and warmer climate during the middle Holocene and are attributed to solar forcings. Bond et al., (2001), related the cold events to ice drafted debris into the North Atlantic, impacting the deep-water circulation.

However, not all the Holocene cold events are identifiable and do not show an overall drastic shift in the isotopic signal (~1.3 ‰ $\delta^{18}O$) in the Caumont cave records. As mentioned in section 4.1, these events present a spatial disparity in Europe, yet we also consider that the specificity of the chalk bedrock of Caumont cave and the local parameters of the stalagmite sites could also have an impact. There is an evident difference between the stalagmites from La Jacqueline, which present a faster growth rate and different internal crystalline structure than the stalagmites from Rivière de Robots, with slower growth rates. The difference could be the result of different infiltration pathways and transmissivity dynamics from the epikarst into the stalagmite sites (Fairchild and Baker, 2012). Therefore, the slow growth rate present in CAU-1 and CAU-2 stalagmites (see sections 4.4.1 and 4.5.1.1), could result in slight buffering of the isotopic response to the fast Holocene climate variations.

One of the most relevant events is the 8.2 ka event, described in several studies as being generated by melt water coming from North American continent and adding fresh water to the North Atlantic (Alley et al., 1997; Barber et al., 1999; Alley and Ágústsdóttir, 2005). The quick 8.2 ka event brought cold and dry winter conditions, which in central-northern Europe displayed lower precipitation $\delta^{18}O$ values (Grafenstein et al., 1999). Depleted $\delta^{18}O$ values were identified with a sharp decrease in Père Noël (Verheyden et al., 2014; Allan et al., 2018b), and in a less extent for the Bunker stalagmite records (Fohlmeister et al., 2012) (see below, Fig. 4.12 and 4.13). The fact that this event is not clearly highlighted in the Caumont and Crag cave, shows that not all sites respond similarly to the rapid climate changes. Moreover, the specificity of the other cave sites and possible difference in infiltration parameters with Caumont cave could also explain the dampened isotopic signal response to the climate change/cold events, as the 8.2 ka. Consequently, this shows the variability and complexity of the drivers of climatic changes during the Holocene (Mayewski et al., 2004). For the Caumont records we conclude that, besides the specificity of the cave's parameters, the effects of the 8.2 ka BP events were perhaps not strong enough. Fohlmeister et al., (2020), mentions the possibility that the climatic conditions were likely not remarkably dry to alter drastically the isotopic signal, which could also be the case for Caumont cave.

The comparison done between the Caumont records and the other north-west European proxies, focuses then on the longer trends observed in the isotopic records rather than in

identifying specific cold events. The results of the comparison with the Europe continental and marine proxy records for the Holocene period are described separately in the next sections.

4.5.3.2 Comparison with continental proxies

Holocene climatic studies in Europe have used different type of continental proxies to help disentangle its variability and patterns, as mentioned in section 4.1. Most of the continental archives in Central Europe (e.g. lake sediments and tree rings), record paleoclimate data attributed to spring and summer seasons, meanwhile stalagmites allow to study proxies that record paleoclimate variability during autumn or winter (Wackerbarth et al., 2010). The study of stalagmite records provides insight into different seasons than the other proxies, which allows to have a better understanding of the past climate variability (Fohlmeister et al., 2012).

For this study, we complement the comparison of Caumont stalagmite records with other speleothem records and terrestrial archives such as lake sediments, from which pollen and ostracods records were investigated (Fig. 4.12). One of the nearby lake sediment studies to CCS are from Holzmaar lake, in western Germany, with pollen a record that cover the last 11 ka BP (Litt et al., 2009). Likewise, the ostracod record from Amersee lake, southern Germany, spans over the last 15.5 ka BP (Grafenstein et al., 1999).

Stalagmite-based studies in the north-western Europe are limited. There is no other research on stalagmites in the North of France, except from CCS. In north-western Europe, the closest stalagmite-based records to Caumont are located in Ireland, Belgium and Germany (Fig. 4.12) as well as a study on tufa (calcite precipitation in open air conditions) record, in Luxemburg. The Crag record (Ireland) covers the last 10.1 ka BP (McDermott et al., 2001), the Père Noël record (Belgium) grew from 12.8 to 1.8 ka BP (Verheyden et al., 2014; Allan et al., 2018a), and Bunker record (Germany) spans the last 10.7 ka BP (Fohlmeister et al., 2012). The tufa record, deposited in the Mamer River, Luxemburg, is a discontinuous record and covers from ca. 10.6 ka to 0.8 ka cal. BP (Dabkowski et al., 2015).

Figure 4. 12. North-west European proxy records compilation compared to Caumont stalagmite records (red star), including ostracods (purple triangle), pollen (square), three stalagmite records (dots) and marine proxies, such as planktonic foraminifera (core MD99-2322 green diamond), hematite-stained grains (core VM29-191 blue diamond) and $\delta^{18}O$ ice core records (NGRIP black diamond).

The pollen taxa, from Holzmaar lake, used for the comparison with Caumont is mainly focused on Quercus, given that it is present during most of the Holocene (Fig. 4.13A). Additionally, it does not show a direct influence of human impact, like other species, whose content drastically decreased or increased at ca. 4 ka BP (Litt et al., 2009). Moreover, the ostracod isotopic record from Amersee was interpreted as linked primarily to temperature, showing warmer climate conditions with higher $\delta^{18}O$ values (Grafenstein et al., 1999) (Fig. 4.13B).

The significance and interpretation of the $\delta^{18}O$ signal of stalagmites and tufa isotopic records mentioned in this study, varies between records. The $\delta^{18}O$ signal variations in Crag stalagmite derive from accentuated temperature-driven changes synchronous to water vapor supply and were interpreted as reflecting cold climate conditions with lower $\delta^{18}O$ values and warm climate with higher values (McDermott et al., 2001; McDermott, 2004) (Fig. 4.13C). The Père Noël $\delta^{18}O$ signal interpretation differs from Crag cave, as the $\delta^{18}O$ signal is driven by water availability, with drier (wet) conditions reflected in higher (lower) $\delta^{18}O$ values

(Verheyden et al., 2014; Allan et al., 2018a) (Fig. 4.13D). In Bunker cave, higher $\delta^{18}O$ values reflect drier/colder climatic conditions during the Holocene, as the $\delta^{18}O$ isotopic record is mainly driven by both winter surface temperature and amount of precipitation. (Fohlmeister et al., 2012) (Fig. 4.13E). The tufa $\delta^{18}O$ record is interpreted as being temperature driven, indicating higher temperature with higher $\delta^{18}O$ values (Dabkowski et al., 2015). In Caumont cave, the $\delta^{18}O$ variability in both CAU-1 and CAU-2 (CAUs) records is considered driven by precipitation and drip water amount, with a bias towards winter infiltration (Bejarano-Arias et al., 2024). The lower $\delta^{18}O$ values are interpreted then, as drier conditions and vice-versa (Fig. 4.13F).

The early Holocene (11.7 – 8.2 ka BP), starts with the transition from a cooler, Younger Dryas climate, to a warmer and/or wetter conditions. This transition is visible in the ostracods (Amersee Lake) record with a general warming trend, until ca. 8.5 ka BP, which coincide with the high $\delta^{18}O$ values (warm conditions) from Crag record, until ca. 9 ka. Although Crag cave record presents a big shift to more negative values between 9.41-9.08 ka BP, the trend towards warmer conditions persists, reaching its highest value (-0.82 ‰) at 8.59 ka BP (Fig. 4.13C). The short high $\delta^{18}O$ values interval observed in CAU-1 at ca. 10.3 ka BP, could be related to a quick cooling event also identified in the Père Noël record (Verheyden et al., 2014), reflecting drier conditions (Fig. 4.13D). During the early Holocene, the Caumont records present a general decreasing trend towards lower $\delta^{18}O$ values, from 10.3 to ca. 8.5 ka BP (Fig. 4.13F), and lower $\delta^{13}C$ values from 10.5 - 7.5 ka BP (Fig. 4.9), interpreted as wetter conditions. The shift from drier to wetter climate, seem at first sight in agreement with the Bunker record, presenting an excursion of low $\delta^{18}O$ values, reaching its minimum value (-7.05 ‰) at ca. 10 ka BP (Fig. 4.13E). However, from 10 ka to 8.5 ka BP, the Bunker $\delta^{18}O$ values present a decreasing trend (drier climate), differing from Caumont. However, the decreasing trend was not to ascribed to lower temperature but rather to the reorganisation effect of the atmospheric circulation producing storm tracks, after the deglaciation, carrying higher $\delta^{18}O$ values. This effect, is not observed in Caumont records, which show a steady decrease in $\delta^{18}O$ signal (wet climate). The Quercus record (Holzmaar lake), in proximity to Bunker cave, also shows a general increasing trend (Fig. 4.13A), indicating suitable climatic conditions for forest development. The forest expansion is likely the result of warmer and wetter conditions, identified in other proxies.

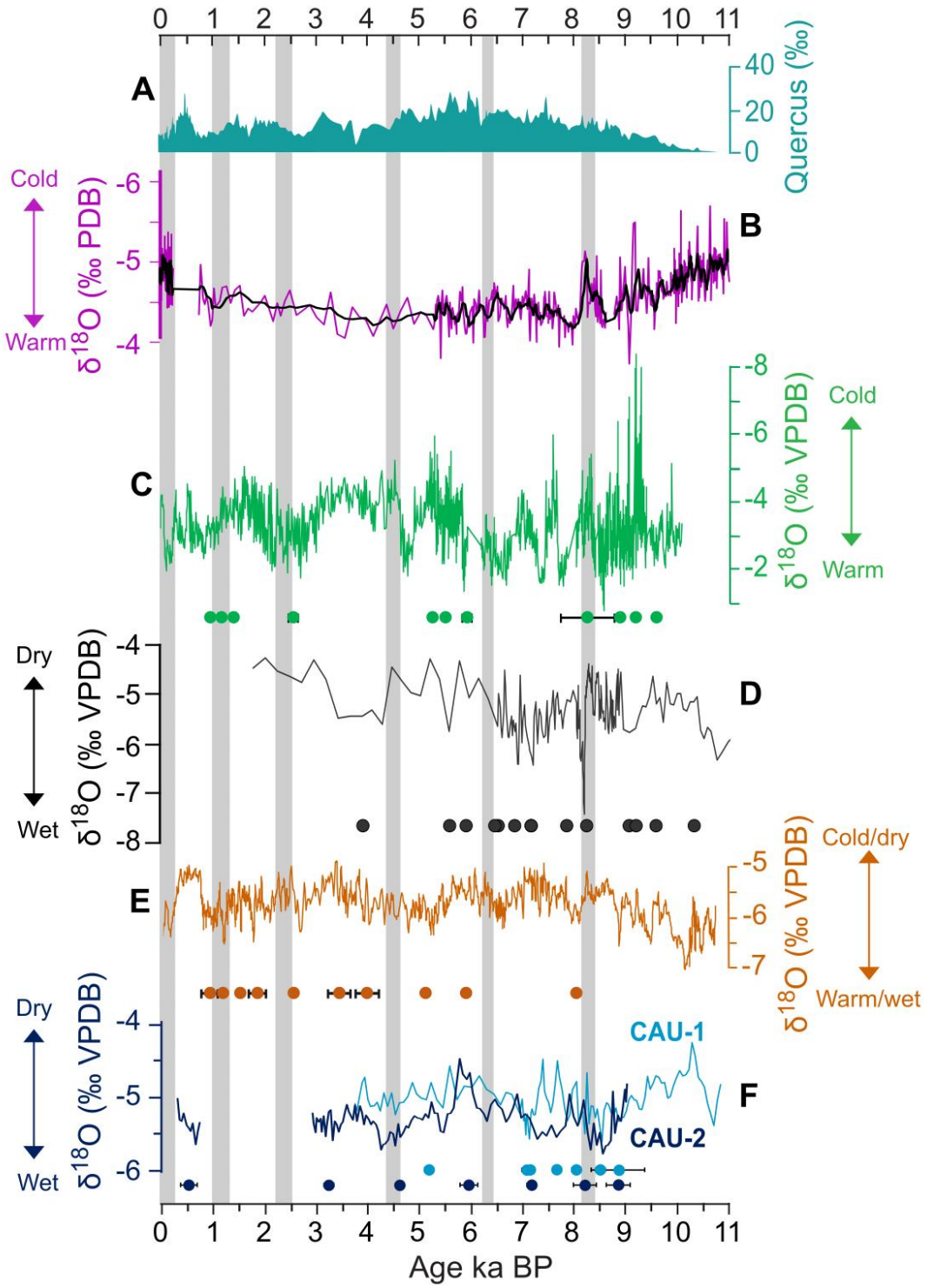

Figure 4. 13. Comparison of Caumont cave stalagmites $\delta^{18}O$ records (F), with pollen data from Holzmaar lake (A) and $\delta^{18}O$ ostracod record from Amersee lake (B), in Germany, stalagmite $\delta^{18}O$ record from Crag cave, in Ireland (C), $\delta^{18}O$ from Pere Noël cave in Belgium (D) and $\delta^{18}O$ records from Bunker cave in Germany (E). Grey panels indicate cold events during the Holocene (Wanner et al., 2011).

During the middle Holocene (8.2 - 4.2 ka BP), the CAUs $\delta^{18}O$ records show a variability of ca. 1.2 ‰, with an average of -5.26 ‰ (CAU-2) and -5.05 ‰ (CAU-1). There are two intervals of high values between 7.7 - 7.4 ka BP and 5.9 - 5.6 ka BP, reflecting drier conditions. The lower $\delta^{18}O$ values, between these intervals reflect wetter climate conditions (Fig. 4.13F). The CAUs record variability however, does not show drastic changes in the $\delta^{18}O$ signal nor in the trace elements records, that correspond to the defined cold events of the middle Holocene, (e.g. 8.2 ka, 6.3 ka, 4.7 ka BP, see section 4.5.3.1).

After 8.2 ka BP, the ostracod record reflects an increase in $\delta^{18}O$ values until ca. 5.4 ka BP (Fig. 4.13B), coinciding with rise in Quercus taxa percentage, (peaks at ca. 6 ka and 5.5 ka BP) indicating wetter and warmer conditions in western Germany. The warmer conditions observed in Père Noël, are in agreement with the declining trend of $\delta^{18}O$ values until ca 7 ka BP. The Crag $\delta^{18}O$ record also shows a decreasing trend until 7.8 ka BP, interpreted as warm climate. The CAU-2 $\delta^{18}O$ record display a similar decreasing trend but until 7.3 ka BP, and slightly later for CAU-1, at 7.1 ka BP.

Between 6.3 and 5.6 ka BP, both CAUs records present a short shift towards drier conditions. The $\delta^{18}O$ values increase is also observed in Père Noël record at ca. 5.8 ka BP, and in Bunker cave between ca. 6 and 5.6 ka BP. The $\delta^{18}O$ shift is seen later, from 5.8 to 5.2 ka BP, in Crag record and in the high peak in ostracods record at ca.5.4 ka BP. This short dry/cold period is followed by a change to wetter conditions in CAUs for the rest of the middle Holocene, except at ca. 4.2 ka BP, where it presents a low $\delta^{18}O$ value peak. The shift to lower $\delta^{18}O$ value in CAUs is in phase with a lower $\delta^{18}O$ peak in Crag record (ca. 4.8 ka BP), and with the Père Noël $\delta^{18}O$ record, but less evident when comparing to Bunker, Amersee lake or Quercus records. Overall, the dominant wet and warm conditions, observed in the different proxies, are in agreement with the Holocene climate optimum period (7 and 4.2 ka BP), characterised by elevated summer temperatures along the Northern Hemisphere (Alverson et al., 2003).

For the Late Holocene (4.2 ka BP to present), both CAUs records show an increase in $\delta^{18}O$ values, indicating a shift towards drier conditions. A similar trend is observed in Bunker until 3.4 ka BP and in Père Noël $\delta^{18}O$ records, which corresponds also with a decrease in Quercus percentages around 3.7 ka BP. The ostracods record has low resolution from 5.2 ka BP onwards and does not show major variability. However, the Mg and Sr records of CAU-2

also present, at ca. 3.4 ka BP, a peak to higher values, confirming drier conditions. Moreover, the period between 3.3 ka and 2.5 ka BP is classified as a cold event (Wanner et al., 2011), caused by the drastic decrease in solar activity. The colder climate conditions were reported in different proxies in Europe and Greenland (Allan et al., 2018a), and match with the last section until the growth stop in both CAUs records, at ca 2.9 ka BP.

The CAU-2 record restarted growing at 0.77 ka BP, showing a general trend towards higher $\delta^{18}O$ values, before the final growth stop, at 0.33 ka BP. The increasing CAU-2 $\delta^{18}O$ signal trend seems in agreement with Bunker and Crag records and a decrease in Quercus percentages, all indicative of drier climate conditions. As mentioned in section 4.5.1.3, this dry period coincides with the LIA, characterized by cold and dry winter conditions, also identified in the North Atlantic (Bond et al., 2001).

4.5.3.3 Comparison with North Atlantic and marine proxies

On a millennial scale, the Holocene climate is described as presenting small variations and its drivers have been mainly related to the solar summer insolation hemispheric trends; especially a decreasing trend in the Northern hemisphere (NH) (Berger and Loutre, 1991) (Fig. 4.14A). However, on a multicentennial to multidecadal scale, the Holocene climate is considered variable between warm/humid and cold/dry phases (Wanner et al., 2011). Stalagmites CAU-1 and CAU-2 present a multidecadal timescale (Fig. 4.14 E), providing a good resolution to disentangle the Holocene climate variability on a regional scale and to be compare to other continental and North Atlantic records. For this purpose, the CAUs $\delta^{18}O$ records are compared to global proxies, such as NH summer insolation, NGRIP $\delta^{18}O$ records (central Greenland ice core) and both hematite-stained grains (HSG) and planktonic foraminifera records (NPS, see Fig. 4.14 legend), from North Atlantic deep-sea cores. The NGRIP record (Fig. 4.14B) is interpreted as showing higher $\delta^{18}O$ values with warmer conditions (Vinther et al., 2006). The HSG variations are related to the advection of cold, ice-bearing surface waters into the North Atlantic, from Nordic and Labrador seas, (Bond et al., 2001; Wanner et al., 2011), where higher percentages are interpreted as cold periods (Fig. 4.14C). The planktonic record (Fig. 4.14D) generally indicates colder conditions with higher $\delta^{18}O$ values (Jennings et al., 2011).

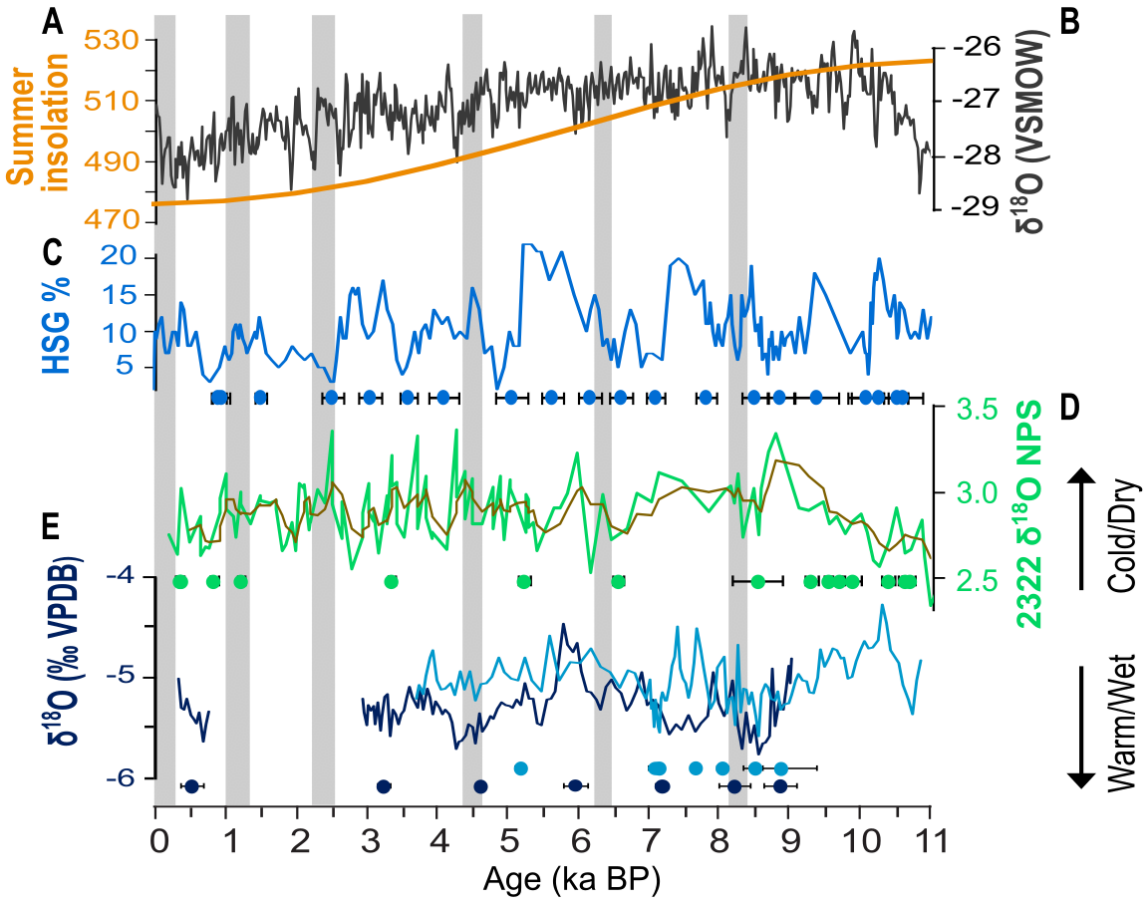

Figure 4. 14. Compilation of marine proxy records, with summer insolation (A), North Greenland Ice Core Project – NGRIP (B), Hematite-stained grains (C) and planktonic foraminifera N. pachyderma sinistral -NPS (D) are compared with $\delta^{18}O$ record from Caumont. The grey panels highlight the cold periods following (Wanner et al., 2011).

Based on the analysis of the solar insolation, volcanic forcings, solar activity and CO_2 concentrations, Wanner et al., (2011) presented a general three period subdivision of the Holocene, from 11.7 ka – 7 ka BP, 7 ka – 4.2 ka BP and Neoglacial (4.2 ka BP to the beginning of the 20th century). The first period is characterized by high summer insolation with cool/temperate conditions, especially in proximity to melting glaciers. During this period, the NGRIP record shows an increasing trend of $\delta^{18}O$ values, indicating warmer climate until 9.9 ka BP, with a short shift to lower values (colder) at ca. 10.3 ka BP. In both CAUs records, we also observe a peak at ca. 10.3 ka BP (less constrained, modelled age). The cold/dry shift is also reflected in the peak of high percentage of HSG record. In the planktonic record, Jennings et al. (2011), mention a meltwater release from Greenland, between 10.5 ka – 10.1 ka BP, reflected in the lower $\delta^{18}O$ values.

After 10.3 ka BP, the CAUs $\delta^{18}O$ records present a warming trend until ca. 8.5 ka BP. This period of lower $\delta^{18}O$ values in Caumont coincides with low HSG percentages and low planktonic $\delta^{18}O$ values, indicating warm/wet conditions. At 7.7 ka and 7.4 ka BP, CAU-1 shows peaks of higher $\delta^{18}O$ values, agreeing with high HSG percentages and reflecting a shift to cold/dry conditions. This dry period in Caumont seems to be in agreement with the 5a cold Bond event, (Bond et al., 2001). However, the high $\delta^{18}O$ values are not clear in CAU-2 record.

The second period (7 ka - 4.2 ka BP) was described as presenting high summer temperatures in the NH (Wanner et al., 2011), related to the "climatic optimum". In Caumont, the onset of this period does not coincide entirely, given that the wettest conditions are observed earlier, since 8.5 ka BP (Fig. 4.14E). In fact, from ca. 7.2 to 5.8 ka BP in CAU-2 record and until 5.6 ka BP for CAU-1 record, the $\delta^{18}O$ values increase, indicating drier conditions. The drying trend in Caumont coincides with higher planktonic $\delta^{18}O$ and corresponds broadly with high HSG percentages (Bond event 4), and with a small shift to lower $\delta^{18}O$ ice core values, all of which also indicate colder climate. Moreover, around 7.5 ka BP, the summer insolation seems to have a decreasing slope, which could result in enhanced colder conditions on the continent. At the end of the middle Holocene (4.2 ka BP), both CAUs $\delta^{18}O$ records show a general trend of wetter conditions from 5.8 ka (CAU-2) and 5.6 ka BP (CAU-1) until 4.2 ka BP. The shift to wet climate is also identifiable in the shift to higher $\delta^{18}O$ values in the Greenland ice core and lower planktonic $\delta^{18}O$ signal, indicating a return to warmer climate.

The third period is referenced as "Neoglaciation" (4.2 ka BP to present), dominated by low summer temperatures in the NH (Wanner et al., 2011). In Caumont, the $\delta^{18}O$ records show a decreasing trend, until the stalagmites stopped growing (CAU-1 at 3.7 ka BP and CAU-2 at 2.9 ka BP), reflecting drier conditions. In the planktonic $\delta^{18}O$ record the period after 3.5 cal ka BP is described as cold, as a result of higher freshwater input coming from the Artic (Jennings et al., 2011). The HSG record presents higher percentages, corresponding to a cold event between 3.4 ka and 2.9 ka BP. While the CAUs $\delta^{18}O$ records do not show a big excursion at this period, the trend to colder conditions is still identifiable.

The last part of the CAU-2 $\delta^{18}O$ record (0.77 ka – 0.33 ka BP), shows a general increasing trend which coincides with the lowest summer insolation, low NGRIP $\delta^{18}O$ values, high HSG percentages and a minor trend towards higher planktonic $\delta^{18}O$ values. All the records

indicate cold conditions, which is reflected as dry climate in Caumont. The cold conditions seen in the marine proxies, after 0.77 ka BP, also coincide with the comparison of Caumont records and the continental proxies, where this cold period is related to the LIA. Overall, the records from Caumont cave seem to agree with the different dry/wet phases identified in the North Atlantic proxies, during the Holocene.

4.6 Conclusions

The study of the Holocene climate variability, based on stalagmite records, has increased in recent decades due to the dating accuracy, with U/Th, and obtained high-resolution proxy records. Although many studies in western Europe focus on the Holocene climate variability, there are some areas that still lack high resolution records like Normandy, northern France. Here, we show that Caumont cave stalagmites (Normandy), provide a precisely dated and highly resolved stable isotope ($\delta^{18}O$ and $\delta^{13}C$) and trace elements records of the Holocene. Stalagmites CAU-1 and CAU-2 present the longest age model that covers from 10.8 to 2.9 ka BP, with an additional short growth after the hiatus, between 0.8 and 0.3 ka BP, for CAU-2. The analysis of the stable isotope records from Caumont indicate that the $\delta^{18}O$ signal reflects regional precipitation dynamics, biased to winter season. The $\delta^{13}C$ signal reflects local seasonal and vegetation variations as well as long-term moisture deficit, enhancing prior calcite precipitation (PCP). For the trace elements, Mg and Sr, records PCP was also found as the main driver for their variability during the Holocene. The study of the multi-proxy records from Caumont showed that they faithfully record multi-millennial to multi-centennial climate variations during the Holocene.

The regional comparison of the existing Normandy proxies, composed mainly by pollen and sedimentary analysis from plateaus, river valleys and peat bogs, with the Caumont records shows similar trends in the environmental evolution and paleoclimate variations. At the onset of the Holocene, the decreasing trend in Caumont $\delta^{13}C$ values, from ca. 10.5 to 8.5 ka BP, indicates a shift to wetter conditions. The shift coincides with the increase of arboreal pollen and the change from detrital sedimentation to pedogenesis and peat accumulation, indicating wetter/warmer climate that allows soil and vegetation development. After 8.5 ka BP there are relatively stable conditions until ca. 5 ka BP, from which the Caumont $\delta^{13}C$ values present an increasing trend at ca. 4 ka BP for CAU-1 and before 3 ka BP for CAU-2. The increase in $\delta^{13}C$

values indicates drier conditions, which coincides with the reduction of arboreal pollen at ca. 3.9 ka BP, a return to detrital sedimentation in the floodplains at ca. 3 ka BP and soil erosion at the plateaus since 3 ka BP. During this period, the environmental changes recorded in the sedimentary proxies are ascribed more to the increasing impact of human settlements on the landscape with the onset of agricultural practices, pastoralism and farming.

We consider that the combination of the human impact above the cave, affecting the soil development and enhancing erosion, along with the water table and sea level rise occurring shortly before 3 ka BP, could influence the Caumont cave environment producing flooding events. We suggest such flooding events as the plausible cause for the growth stop identified in all the studied stalagmites from Caumont. The quarrying activities in Caumont during the medieval period, result in the extraction of sediments and reopening of the Rivière de Robots stream, where the stalagmites CAU-1 and CAU-2 were sampled. We attribute the restart of CAU-2 at 0.8 ka BP to the reopening of the stream, allowing again the stalagmite calcite deposition for ca. 400 years.

We compare the Caumont records with European continental and North Atlantic marine proxies to contextualise the climate dynamics in Normandy within the broader Holocene period in western Europe. The comparison shows that the Caumont records reflect variations in paleoclimate conditions that follow global patterns such as increasing humid conditions during the early Holocene. The middle Holocene presents lower $\delta^{18}O$ values than in the early Holocene, reflecting wetter conditions, with some shifts to higher values, indicating drier periods. The drying trend during the middle Holocene in Caumont (ca. 7.2 to 5.7 ka BP) seems to coincide with the cold phases seen in other proxy records, such as hematite-stained grains. After 5.7 ka BP, wetter conditions return with a decreasing trend in Caumont $\delta^{18}O$ values. For the Late Holocene, the Caumont records presented a drying trend, both before and after the hiatus, towards higher $\delta^{18}O$ values.

Overall, the analysis of the Holocene climate variability seen in Caumont multiproxy record shows sufficient sensitivity to faithfully record the complexity of the Holocene climate variability. Moreover, the comparison with north-west European proxies shows how the Holocene climate changes can present spatial disparities, giving proof of the relevance of having proxy records in the gap areas, such as Caumont site in Normandy.

Chapter 5: General Conclusions

5.1 Conclusions

This thesis project presents the first stalagmite-based paleoclimate studies in Normandy and north-western France.

The multi-proxy records from Caumont cave provide new insight into the paleoclimate and environmental changes over decadal time scales while previous studies in Normandy, based mainly on pedo-sedimentary and palynological proxies lacked such high resolution. The new stalagmite records from Caumont present a highly resolved proxy records with a robust age model, achieved through U/Th dating, oxygen and carbon stable isotope and trace elements analysis. Such highly-resolved reconstruction helped to date more precisely the climate change throughout the Holocene and the last century.

The main results of the three thematic chapters of this thesis are summarised below, followed by a synthetic diagram of the used proxies, the main drivers of calcite deposition and the climatic and anthropogenic impact present in Caumont cave (Table 5.1).

- The monitoring campaign (Nov. 2019 - Jul. 2021) provides insight into the factors influencing calcite deposition in the Caumont cave environment. During this time, the internal climatic conditions at Caumont were stable with temperature variations of less than 1 °C throughout the year, in the natural conduits and deep galleries.

- The $\delta^{18}O$ drip water ($\delta^{18}O_{dw}$) values plot close to the local (Fontainebleau station) and standardized global meteoric water lines. The comparison of the $\delta^{18}O_{dw}$ values and the precipitation values, from Fontainebleau station, reveals that the Caumont $\delta^{18}O_{dw}$ values are biased towards the high infiltration season during winter. The low $\delta^{18}O_{dw}$ variability suggests that the infiltrating water is well mixed in the epikarst.

- The calcite $\delta^{18}O$ variability is mainly influenced by the precipitation amount, with wetter conditions reflecting higher $\delta^{18}O$ values. The drivers of the calcite $\delta^{13}C$ variability reflect the processes occurring in the soil above the cave and in the epikarst, where negative

effective infiltration periods enhance prior calcite precipitation leading to higher $\delta^{13}C$ values.

- The Hendy test done on modern calcite shows that the $\delta^{18}O$ signal presents no discernible kinetic effects. Hence, the calcite $\delta^{18}O$ reflects values close to the original signature of the infiltration water. Moreover, the equilibrium test reveals that the values plot near the equilibrium regression lines suggesting near equilibrium isotope fractionation conditions.

- The recent stalagmite CCB-1 age model covers the 20th century, allowing a comparison with instrumental data and historical records. The resulting high resolution multi-proxy record reliably shows the hydroclimate variability of the 20th century.

- The major fluctuations in $\delta^{18}O$, $\delta^{13}C$, Mg and Sr values are found in agreement with the regional drought index (October SPEI6). The relationship between $\delta^{13}C$, Mg and Sr with PCP is confirmed by their higher values corresponding to infiltration deficits. Additionally, the identified peaks of drier climatic conditions in the CCB-1 geochemical records generally coincide with the mayor historical drought events recorded in western Europe during the 20th and 21st centuries.

- The comparison with the temperature records shows how peaks of the multi-proxy record coincides with higher temperatures, except in the recent decades. The combined analysis of CCB-1 records with the meteorological data and October SPEI6 drought index reveals a change in drought dynamics, from mainly precipitation deficit driven events during the 20th century to a regime that is gradually controlled by rising temperatures in the past two decades.

- The study of the drought events recorded in a recent stalagmite from Caumont cave and quarry system evidences the complexity and irregularity of drought events and how different climatic parameters can shift over time. The use of a stalagmite-based multi-proxy record is a suitable tool to help disentangle the complex mechanisms that influence drought events.

- The stalagmites from two separate natural conduits, Rivière de Robots (RR) and La Jaqueline (LJ), in Caumont cave yield U/Th ages that cover the Holocene period. The stalagmites from RR (CAU-1 and CAU-2), present the longest age model, covering from ca. 10.8 to 2.9 ka BP with a later short regrowth of CAU-2 from 0.8 to 0.3 ka. The stalagmite based multi-proxy record ($\delta^{18}O$, $\delta^{13}C$ and trace elements) with a centennial to decadal resolution allows the evaluation of Holocene climate variability at the regional scale and in the north-west European context.

- The stalagmite-based record from Caumont cave is the first highly resolved record in the Normandy region and north-west France. The Caumont multi-proxy record allows the regional comparison with existing proxy records in Normandy, mainly based on sedimentary archives such as mires, plateau and flood plains deposits. The stalagmite $\delta^{13}C$ variability presents similarities with pollen and sedimentological records during the Holocene. Overall, the fluctuations to wetter (drier) climate conditions present in the Caumont $\delta^{13}C$ record are in agreement with the increase (decrease) of arboreal pollen, pedogenesis and peat deposit development (detrital sedimentation and erosion). From ca. 4 - 3 ka BP, the variability present on the Normandy sedimentary proxies is not only ascribed to climatic fluctuations but to an increasing human impact from agricultural practices, among others.

- The analysis of the growth-stop of the 5 Holocene stalagmites from Caumont cave includes a combination of causes resulting in flooding of the natural conduits and hindering stalagmite growth at ca. 3 ka BP. Amongst the causes we consider plausible are the increase of human impact in the surroundings above the cave, leading to higher soil erosion, along with coeval sea level and water table rise events influencing the level of the Rivière des Robots in Caumont.

- The comparison of the Caumont multi-proxy records with continental and marine north-west European proxy records show a general agreement with the Holocene climate variability. The multi-millennial and multicentennial climate variations, reflecting wetter/drier conditions in the $\delta^{18}O$ records from Caumont generally coincide with the warmer/colder fluctuations observed in other stalagmite-based records as well as pollen, ostracods and foraminifera records.

Table 5. 1. Synthetic description of the factors driving each proxy record and how they are influenced by climate or anthropogenic impact.

Proxies	Main drivers	Climate impact	Anthropogenic impact	
$\delta^{13}C$ (a) $\delta^{18}O$ (b) Mg, Sr (c) Growth rate (d)	Precipitation amount (a,b,c,d) Effective infiltration (a,b,c,d) Water residence time (a,b,c) Vegetation above the cave (c)	Climatic conditions fluctuations wetter/warmer → > Effective infiltration → > vegetation/ soil development → Lower values (a,b,c,d) drier/colder → > residence time → Higher values (a,b,c,d)	**Late Holocene** Vegetation clearing → > Erosion (+ climatic component*) → Flooding → Stalagmite growth stop	**Last 2 decades** >Temperature >Evaporation → <Effective infiltration → > PCP → Higher values (a, b, c)

***Sea level and water table rise.

Overall, the monitoring shows that the environmental and climatic conditions at Caumont cave are suitable for calcite deposition and therefore speleothems could consistently record recent and past climatic signals. The Caumont multi-proxy records, from the quarry and natural cave, evidence that the studied stalagmites present the sensitivity required to record climate variability during the 20th century and spanning the Holocene. Moreover, the Caumont stalagmites have the capacity to record the climate variability at a high resolution, from multi-centennial to sub-decadal time scales. Additionally, having stalagmite records from the last century allows the comparison with meteorological and historical data, adding value for recent climate change studies.

Furthermore, the stalagmite $\delta^{18}O$ records allow for a better comparison with other global proxies such as ice cores and marine records, providing a more global evaluation. The comparison of the Caumont records with other proxy records shows that the recorded climatic fluctuations are consistent with the paleoclimate dynamics on a regional and north-west European scale for the last 10 ka.

5.2 Perspectives

The results from this PhD thesis shows the wealth of information that stalagmite-based studies can provide, including stalagmites from chalk bedrock caves. However, there is still

additional work that could help further understand the drivers of climate variability and its impact in Caumont cave.

A longer monitoring period, covering complete annual cycles could provide further information about the seasonal variations in Caumont. Given that the monitoring of this study stopped in the summer season 2021, it could greatly benefit from having longer records covering other autumn and winter seasons. This information can provide a longer coverage to assess the response of the water and calcite deposition in Caumont to seasonal parameters such as precipitation, temperature and cave internal CO_2 concentrations. Moreover, the obtained results from previous years could be compared to the new data giving further insight into recent and short-term climatic fluctuations.

Considering the near equilibrium conditions of calcite deposition at Caumont (Chapter 2), other methods like clumped isotopes thermometry, could be tested in the studied stalagmites. This method could provide information about the temperature at the moment of carbonate formation and even further knowledge on the oxygen isotopic fractionation at Caumont. Since all the sampled stalagmites from the lower level of Caumont cave either stopped growing around 3 ka or began around the time that quarrying activities started, perhaps a new sampling campaign of the upper level (Trou du Chien), could provide speleothems that continued growing during the hiatus. If such speleothems are found it will help to complete the record gap and further understand the climate variability during the late Holocene and to assess the possible impact human activities had at Caumont and environment above the cave.

The obtained records from the Caumont cave study shows the value of multi-proxy stalagmite records to better understand Holocene paleoclimate variability, especially in an area that presented information gaps. Therefore, doing similar studies in other areas deserve to be tested, both in chalk bedrock caves from Normandy and in other regions in France. More cave monitoring and stalagmite studies would provide further information allowing to reconstruct a more robust paleoclimate and paleoenvironmental conditions as well as present climate changes. Further data will also allow to close the information gaps both in France and Europe.

Reference list

Allan, M., Deliège, A., Verheyden, S., Nicolay, S., Quinif, Y., Fagel, N., 2018a. Evidence for solar influence in a Holocene speleothem record (Père Noël cave, SE Belgium). Quat. Sci. Rev. 192, 249–262. https://doi.org/10.1016/j.quascirev.2018.05.039

Allan, M., Fagel, N., Lubbe, H., Vonhof, H., Cheng, H., Edwards, R., Verheyden, S., 2018b. High-resolution reconstruction of 8.2-ka BP event documented in Père Noël cave, southern Belgium. J. Quat. Sci. 33. https://doi.org/10.1002/jqs.3064

Alley, R.B., Mayewski, P.A., Sowers, T., Stuiver, M., Taylor, K.C., Clark, P.U., 1997. Holocene climatic instability: A prominent, widespread event 8200 yr ago. Geology 25, 483–486. https://doi.org/10.1130/0091-7613(1997)025<0483:HCIAPW>2.3.CO;2

Alley, R.B., Ágústsdóttir, A.M., 2005. The 8k event: cause and consequences of a major Holocene abrupt climate change. Quat. Sci. Rev. 24, 1123–1149. https://doi.org/10.1016/j.quascirev.2004.12.004

Alverson, K.D., Pedersen, T.F., Bradley, R.S. (Eds.), 2003. Paleoclimate, Global Change and the Future, Global Change — The IGBP Series. Springer, Berlin, Heidelberg. https://doi.org/10.1007/978-3-642-55828-3

Atkinson, T.C., 1977. Diffuse flow and conduit flow in limestone terrain in the Mendip Hills, Somerset (Great Britain). J. Hydrol. 35, 93–110. https://doi.org/10.1016/0022-1694(77)90079-8

Ayalon, A., Bar-Matthews, M., Sass, E., 1998. Rainfall-recharge relationships within a karstic terrain in the Eastern Mediterranean semi-arid region, Israel: δ 18O and δD characteristics. J. Hydrol. 207, 18–31. https://doi.org/10.1016/S0022-1694(98)00119-X

Baker, A., Brunsdon, C., 2003. Non-linearities in drip water hydrology: an example from Stump Cross Caverns, Yorkshire. J. Hydrol. 277, 151–163. https://doi.org/10.1016/S0022-1694(03)00063-5

Baker, A., Duan, W., Cuthbert, M., Treble, P., Banner, J., Hankin, S., 2018. Climatic influences on the offset between d18O of cave drip waters and precipitation inferred from global monitoring data. Earth Arxiv. https://doi.org/10.31223/osf.io/h4pr6

Baker, A., Hartmann, A., Duan, W., Hankin, S., Comas-Bru, L., Cuthbert, M.O., Treble, P.C., Banner, J., Genty, D., Baldini, L.M., Bartolomé, M., Moreno, A., Pérez-Mejías, C., Werner, M., 2019. Global analysis reveals climatic controls on the oxygen isotope composition of cave drip water. Nat. Commun. 10, 2984. https://doi.org/10.1038/s41467-019-11027-w

Bakke, S., Ionita, M., Tallaksen, L.M., 2020. The 2018 northern European hydrological drought and its drivers in a historical perspective. https://doi.org/10.5194/hess-2020-239

Bakke, S., Ionita, M., Tallaksen, L.M., 2022. Recent European drying and its link to prevailing large-scale atmospheric patterns. https://doi.org/10.21203/rs.3.rs-2397739/v1

Bakke, S.J., Ionita, M., Tallaksen, L.M., 2023. Recent European drying and its link to prevailing large-scale atmospheric patterns. Sci. Rep. 13, 21921. https://doi.org/10.1038/s41598-023-48861-4

Baldini, J.U.L., McDermott, F., Baker, A., Baldini, L.M., Mattey, D.P., Railsback, L.B., 2005. Biomass effects on stalagmite growth and isotope ratios: A 20th century analogue from Wiltshire, England. Earth Planet. Sci. Lett. 240, 486–494. https://doi.org/10.1016/j.epsl.2005.09.022

Baldini, J.U.L., Lechleitner, F.A., Breitenbach, S.F.M., van Hunen, J., Baldini, L.M., Wynn, P.M., Jamieson, R.A., Ridley, H.E., Baker, A.J., Walczak, I.W., Fohlmeister, J., 2021. Detecting and quantifying palaeoseasonality in stalagmites using geochemical and modelling approaches. Quat. Sci. Rev. 254, 106784. https://doi.org/10.1016/j.quascirev.2020.106784

Ballesteros, D., Farrant, A., Nehme, C., Woods, M., Todisco, D., Mouralis, D., 2020. Stratigraphical influence on chalk cave development in Upper Normandy, France: implications for chalk hydrogeology. Int. J. Speleol. 49, 187–208. https://doi.org/10.5038/1827-806X.49.3.2319

Ballesteros, D., Painchault, A., Nehme, C., Todisco, D., Varano, M., Mouralis, D., 2021. Normandy chalkstone (France): geology and historical uses from quarries to monuments. Episodes J. Int. Geosci. 44, 31–42. https://doi.org/10.18814/epiiugs/2020/0200s03

Ballesteros, D., Nehme, C., Roussel, B., Delisle, F., Pons-Branchu, E., Mouralis, D., 2022. Historical underground quarrying: A multidisciplinary research in the Caumont quarry (c. 13th–19th centuries), France. Archaeometry 64, 849–865. https://doi.org/10.1111/arcm.12758

Ballesteros, D., Farrant, A., Sahy, D., Genuite, K., Bejarano, I., Nehme, C., 2023. Going with the flow: Sedimentary processes along karst conduits within Chalk aquifers, northern France. Sediment. Geol. 452, 106422. https://doi.org/10.1016/j.sedgeo.2023.106422

Barber, D.C., Dyke, A., Hillaire-Marcel, C., Jennings, A.E., Andrews, J.T., Kerwin, M.W., Bilodeau, G., McNeely, R., Southon, J., Morehead, M.D., Gagnon, J.-M., 1999. Forcing

of the cold event of 8,200 years ago by catastrophic drainage of Laurentide lakes. Nature 400, 344–348. https://doi.org/10.1038/22504

Barker, L.J., Hannaford, J., Parry, S., Smith, K.A., Tanguy, M., Prudhomme, C., 2019. Historic hydrological droughts 1891–2015: systematic characterisation for a diverse set of catchments across the UK. Hydrol. Earth Syst. Sci. 23, 4583–4602. https://doi.org/10.5194/hess-23-4583-2019

Beaumont, L., Garcia, C., Antoine, P., Limondin-Lozouet, N., Brasseur, B., Dabkowski, J., 2023. Les tufs calcaires holocènes de la moyenne vallée de la Somme (Nord de la France) : répartition spatiale, chronostratigraphie et implications paléogéographiques. Géomorphologie Relief Process. Environ. 29. https://doi.org/10.4000/11rh0

Bejarano-Arias, I., Nehme, C., Breitenbach, S., Meyer, H., Modestou, S., Mouralis, D., 2024. Climate monitoring in the Caumont cave and quarry system (northern France) reveal near oxygen isotopic equilibrium conditions for carbonate deposition. Int. J. Speleol. 53, 13–23. https://doi.org/10.5038/1827-806X.53.1.2482

Berger, A., Loutre, M.F., 1991. Insolation values for the climate of the last 10 million years. Quat. Sci. Rev. 10, 297–317. https://doi.org/10.1016/0277-3791(91)90033-Q

Berkelhammer, M., Sinha, A., Stott, L., Cheng, H., Pausata, F. s. r., Yoshimura, K., 2012. An Abrupt Shift in the Indian Monsoon 4000 Years Ago, in: Climates, Landscapes, and Civilizations. American Geophysical Union (AGU), pp. 75–88. https://doi.org/10.1029/2012GM001207

Blöschl, G., Kiss, A., Viglione, A., Barriendos, M., Böhm, O., Brázdil, R., Coeur, D., Demarée, G., Llasat, M.C., Macdonald, N., Retsö, D., Roald, L., Schmocker-Fackel, P., Amorim, I., Bělínová, M., Benito, G., Bertolin, C., Camuffo, D., Cornel, D., Doktor, R., Elleder, L., Enzi, S., Garcia, J.C., Glaser, R., Hall, J., Haslinger, K., Hofstätter, M., Komma, J., Limanówka, D., Lun, D., Panin, A., Parajka, J., Petrić, H., Rodrigo, F.S., Rohr, C., Schönbein, J., Schulte, L., Silva, L.P., Toonen, W.H.J., Valent, P., Waser, J., Wetter, O., 2020. Current European flood-rich period exceptional compared with past 500 years. Nature 583, 560–566. https://doi.org/10.1038/s41586-020-2478-3

Blytt, A., 1876. Essay on the Immigration of the Norwegian Flora During Alternating Rainy and Dry Periods. A. Cammermeyer.

Boch, R., Spötl, C., Kramers, J., 2009. High-resolution isotope records of early Holocene rapid climate change from two coeval stalagmites of Katerloch Cave, Austria. Quat. Sci. Rev. 28, 2527–2538. https://doi.org/10.1016/j.quascirev.2009.05.015

Boch, R., Spötl, C., Frisia, S., 2011. Origin and palaeoenvironmental significance of lamination in stalagmites from Katerloch Cave, Austria. Sedimentology 58, 508–531. https://doi.org/10.1111/j.1365-3091.2010.01173.x

Bond, G., Kromer, B., Beer, J., Muscheler, R., Evans, M.N., Showers, W., Hoffmann, S., Lotti-Bond, R., Hajdas, I., Bonani, G., 2001. Persistent Solar Influence on North Atlantic Climate During the Holocene. Science 294, 2130–2136. https://doi.org/10.1126/science.1065680

Bourdon, B., Turner, S., Henderson, G.M., Lundstrom, C.C., 2003. Introduction to U-series Geochemistry. Rev. Mineral. Geochem. 52, 1–21. https://doi.org/10.2113/0520001

Braun, T., Breitenbach, S.F.M., Skiba, V., Lechleitner, F.A., Ray, E.E., Baldini, L.M., Polyak, V.J., Baldini, J.U.L., Kennett, D.J., Prufer, K.M., Marwan, N., 2023. Decline in seasonal predictability potentially destabilized Classic Maya societies. Commun. Earth Environ. 4, 1–12. https://doi.org/10.1038/s43247-023-00717-5

Breitenbach, S.F.M., Adkins, J.F., Meyer, H., Marwan, N., Kumar, K.K., Haug, G.H., 2010. Strong influence of water vapor source dynamics on stable isotopes in precipitation observed in Southern Meghalaya, NE India. Earth Planet. Sci. Lett. 292, 212–220. https://doi.org/10.1016/j.epsl.2010.01.038

Breitenbach, S.F.M., Rehfeld, K., Goswami, B., Baldini, J.U.L., Ridley, H.E., Kennett, D.J., Prufer, K.M., Aquino, V.V., Asmerom, Y., Polyak, V.J., Cheng, H., Kurths, J., Marwan, N., 2012. COnstructing Proxy Records from Age models (COPRA). Clim. Past 8, 1765–1779. https://doi.org/10.5194/cp-8-1765-2012

Breitenbach, S.F.M., Lechleitner, F.A., Meyer, H., Diengdoh, G., Mattey, D., Marwan, N., 2015. Cave ventilation and rainfall signals in dripwater in a monsoonal setting – a monitoring study from NE India. Chem. Geol. 402, 111–124. https://doi.org/10.1016/j.chemgeo.2015.03.011

Breitenbach, S.F., Plessen, B., Waltgenbach, S., Tjallingii, R., Leonhardt, J., Jochum, K.P., Meyer, H., Goswami, B., Marwan, N., Scholz, D., 2019. Holocene interaction of maritime and continental climate in Central Europe: New speleothem evidence from Central Germany. Glob. Planet. Change 176, 144–161.

Breitenbach, S.F.M., Marwan, N., 2023. Acquisition and analysis of greyscale data from stalagmites using ImageJ software. Cave Karst Sci. 50, 69–78.

Büntgen, U., Trouet, V., Frank, D., Leuschner, H.H., Friedrichs, D., Luterbacher, J., Esper, J., 2010. Tree-ring indicators of German summer drought over the last millennium. Quat. Sci. Rev. 29, 1005–1016.

Büntgen, U., Tegel, W., Nicolussi, K., McCormick, M., Frank, D., Trouet, V., Kaplan, J., Herzig, F., Heussner, K.-U., Wanner, H., Luterbacher, J., Esper, J., 2011. 2500 Years of European Climate Variability and Human Susceptibility. Science 331, 578–82. https://doi.org/10.1126/science.1197175

Büntgen, U., Kyncl, T., Ginzler, C., Jacks, D.S., Esper, J., Tegel, W., Heussner, K.-U., Kyncl, J., 2013. Filling the Eastern European gap in millennium-long temperature reconstructions. Proc. Natl. Acad. Sci. 110, 1773–1778. https://doi.org/10.1073/pnas.1211485110

Büntgen, U., Urban, O., Krusic, P.J., Rybníček, M., Kolář, T., Kyncl, T., Ač, A., Koňasová, E., Čáslavský, J., Esper, J., Wagner, S., Saurer, M., Tegel, W., Dobrovolný, P., Cherubini, P., Reinig, F., Trnka, M., 2021. Recent European drought extremes beyond Common Era background variability. Nat. Geosci. 14, 190–196. https://doi.org/10.1038/s41561-021-00698-0

Burke, K.D., Williams, J.W., Chandler, M.A., Haywood, A.M., Lunt, D.J., Otto-Bliesner, B.L., 2018. Pliocene and Eocene provide best analogs for near-future climates. Proc. Natl. Acad. Sci. 115, 13288–13293. https://doi.org/10.1073/pnas.1809600115

Camenisch, C., Salvisberg, M., 2020. Droughts in Bern and Rouen from the 14th to the beginning of the 18th century derived from documentary evidence. Clim. Past 16, 2173–2182. https://doi.org/10.5194/cp-16-2173-2020

Cantat, O., 2004. Analyse critique sur les tendances pluviométriques au 20ème siècle en Basse-Normandie : réflexions sur la fiabilité des données et le changement climatique. Ann. Assoc. Int. Climatol. 1, 11–31. https://doi.org/10.4267/climatologie.963

Carolin, S.A., Walker, R.T., Day, C.C., Ersek, V., Sloan, R.A., Dee, M.W., Talebian, M., Henderson, G.M., 2019. Precise timing of abrupt increase in dust activity in the Middle East coincident with 4.2 ka social change. Proc. Natl. Acad. Sci. 116, 67–72. https://doi.org/10.1073/pnas.1808103115

Chen, Z., Auler, A.S., Bakalowicz, M., Drew, D., Griger, F., Hartmann, J., Jiang, G., Moosdorf, N., Richts, A., Stevanovic, Z., Veni, G., Goldscheider, N., 2017. The World Karst Aquifer Mapping project: concept, mapping procedure and map of Europe. Hydrogeol. J. 25, 771–785. https://doi.org/10.1007/s10040-016-1519-3

Cheng, H., Edwards, R.L., Broecker, W.S., Denton, G.H., Kong, X., Wang, Y., Zhang, R., Wang, X., 2009. Ice Age Terminations. Science 326, 248–252. https://doi.org/10.1126/science.1177840

Cheng, H., Sinha, A., Wang, X., Cruz, F.W., Edwards, R.L., 2012. The Global Paleomonsoon as seen through speleothem records from Asia and the Americas. Clim. Dyn. 39, 1045–1062. https://doi.org/10.1007/s00382-012-1363-7

Cheng, H., Lawrence Edwards, R., Shen, C.-C., Polyak, V.J., Asmerom, Y., Woodhead, J., Hellstrom, J., Wang, Y., Kong, X., Spötl, C., Wang, X., Calvin Alexander, E., 2013. Improvements in 230Th dating, 230Th and 234U half-life values, and U–Th isotopic measurements by multi-collector inductively coupled plasma mass spectrometry. Earth Planet. Sci. Lett. 371–372, 82–91. https://doi.org/10.1016/j.epsl.2013.04.006

Cheng, H., Spötl, C., Breitenbach, S.F.M., Sinha, A., Wassenburg, J.A., Jochum, K.P., Scholz, D., Li, X., Yi, L., Peng, Y., Lv, Y., Zhang, P., Votintseva, A., Loginov, V., Ning, Y., Kathayat, G., Edwards, R.L., 2016. Climate variations of Central Asia on orbital to millennial timescales. Sci. Rep. 6, 36975. https://doi.org/10.1038/srep36975

Chevalier, S., 2022. Apport de la cartographie 2D et 3D dans l'appréhension des aléas géomorphologues du sous-sol : cas d'étude des carrières-grottes de Caumont (Normandie). MSc Université de Rouen Normandie, 152 p.

Chuine, I., Yiou, P., Viovy, N., Seguin, B., Daux, V., Ladurie, E.L.R., 2004. Grape ripening as a past climate indicator. Nature 432, 289–290. https://doi.org/10.1038/432289a

Clark, P.U., Dyke, A.S., Shakun, J.D., Carlson, A.E., Clark, J., Wohlfarth, B., Mitrovica, J.X., Hostetler, S.W., McCabe, A.M., 2009. The Last Glacial Maximum. Science 325, 710–714. https://doi.org/10.1126/science.1172873

Columbu, A., 2016. The potential of carbonate speleothems from Mediterranean gypsum caves for palaeoclimate and palaeoenvironmental reconstructions. PhD thesis University of Melbourne, 371 p.

Cook, B.I., Smerdon, J.E., Cook, E.R., Williams, A.P., Anchukaitis, K.J., Mankin, J.S., Allen, K., Andreu-Hayles, L., Ault, T.R., Belmecheri, S., Coats, S., Coulthard, B., Fosu, B., Grierson, P., Griffin, D., Herrera, D.A., Ionita, M., Lehner, F., Leland, C., Marvel, K., Morales, M.S., Mishra, V., Ngoma, J., Nguyen, H.T.T., O'Donnell, A., Palmer, J., Rao, M.P., Rodriguez-Caton, M., Seager, R., Stahle, D.W., Stevenson, S., Thapa, U.K., Varuolo-Clarke, A.M., Wise, E.K., 2022. Megadroughts in the Common Era and the

Anthropocene. Nat. Rev. Earth Environ. 3, 741–757. https://doi.org/10.1038/s43017-022-00329-1

Coplen, T.B., 1994. Reporting of stable hydrogen, carbon, and oxygen isotopic abundances (Technical Report). Pure Appl. Chem. 66, 273–276. https://doi.org/10.1351/pac199466020273

Coplen, T.B., 2007. Calibration of the calcite–water oxygen-isotope geothermometer at Devils Hole, Nevada, a natural laboratory. Geochim. Cosmochim. Acta 71, 3948–3957. https://doi.org/10.1016/j.gca.2007.05.028

Couchoud, I., 2008. Les spéléothèmes, archives des variations paléoenvironnementales. Quat. Rev. Assoc. Fr. Pour Létude Quat. 19, 255–274.

Cubizolle, H., Haas, J.-N., Bielowski, W., Dietre, B., Argant, J., Latour-Argant, C., Chatelard, S., Porteret, J., Lefèvre, J.-P., 2013. Palaeo-paludification, environmental change and human impact during the Mid- and Late Holocene in Western Europe: the example of the La Prenarde-Pifoy mire in the French Massif Central. Quat. Rev. Assoc. Fr. Pour Létude Quat. 419–442. https://doi.org/10.4000/quaternaire.6797

Czuppon, G., Demény, A., Leél-Őssy, S., Óvari, M., Molnár, M., Stieber, J., Kiss, K., Kármán, K., Surányi, G., Haszpra, L., 2017. Cave monitoring in the Béke and Baradla caves (Northeastern Hungary): implications for the conditions for the formation cave carbonates. Int. J. Speleol. 47, 13–28. https://doi.org/ https://doi.org/10.5038/1827-806X.47.1.2110

Dabkowski, J., 2011. Analyse géochimique des tufs calcaires en domaine fluviatile ouest européen : reconstitution de variations des paléotempératures et des paléoprécipitations au cours des interglaciaires des stades 11 et 5. PhD thesis, Sorbonne University, Paris, 342 p.

Dabkowski, J., Brou, L., Naton, H.-G., 2015. New stratigraphic and geochemical data on the Holocene environment and climate from a tufa deposit at Direndall (Mamer Valley, Luxembourg). The Holocene 25, 1153–1164. https://doi.org/10.1177/0959683615580183

Dai, A., Zhao, T., Chen, J., 2018. Climate Change and Drought: a Precipitation and Evaporation Perspective. Curr. Clim. Change Rep. 4, 301–312. https://doi.org/10.1007/s40641-018-0101-6

Davis, B.A.S., Brewer, S., Stevenson, A.C., Guiot, J., 2003. The temperature of Europe during the Holocene reconstructed from pollen data. Quat. Sci. Rev. 22, 1701–1716. https://doi.org/10.1016/S0277-3791(03)00173-2

Davis, D., Oldroyd, R., 2011. Inventing the Present: Historical Roots of the Anthropocene. Earth Sci. Hist. 30, 63–84. https://doi.org/10.17704/eshi.30.1.p8327x7042g3q989

Deininger, M., Fohlmeister, J., Scholz, D., Mangini, A., 2012. Isotope disequilibrium effects: The influence of evaporation and ventilation effects on the carbon and oxygen isotope composition of speleothems – A model approach. Geochim. Cosmochim. Acta 96, 57–79. https://doi.org/10.1016/j.gca.2012.08.013

Demény, A., Kele, S., Siklósy, Z., 2010. Empirical equations for the temperature dependence of calcite-water oxygen isotope fractionation from 10 to 70°C. Rapid Commun. Mass Spectrom. 24, 3521–3526. https://doi.org/10.1002/rcm.4799

Demény, A., Kern, Z., Hatvani, I.G., Torma, C., Topál, D., Frisia, S., Leél-Őssy, S., Czuppon, G., Surányi, G., 2021. Holocene hydrological changes in Europe and the role of the North Atlantic ocean circulation from a speleothem perspective. Quat. Int. 571, 1–10. https://doi.org/10.1016/j.quaint.2020.10.061

Denton, G.H., Karlén, W., 1973. Holocene Climatic Variations—Their Pattern and Possible Cause. Quat. Res. 3, 155–205. https://doi.org/10.1016/0033-5894(73)90040-9

Descamps, F., Faÿ-Gomord, O., Vandycke, S., Schroeder, C., Swennen, R., Tshibangu, J.-P., 2017. Relationships between geomechanical properties and lithotypes in NW European chalks. Geol. Soc. Lond. Spec. Publ. 458, 227–244. https://doi.org/10.1144/SP458.9

Diomard, I., Chéron, E., 2020. Etat des lieux sur le changement climatique et ses incidences agricoles en région Normandie. Observatoire Régional sur l'Agriculture et le Changement cLimatiquE ORACLE.

Domínguez-Villar, D., Wang, X., Cheng, H., Martin-Chivelet, J., Edwards, R., 2008. A high-resolution late Holocene speleothem record from Kaite Cave, northern Spain: δ18O variability and possible causes.

Dorale, J.A., Edwards, R.L., Ito, E., González, L.A., 1998. Climate and Vegetation History of the Midcontinent from 75 to 25 ka: A Speleothem Record from Crevice Cave, Missouri, USA. Science 282, 1871–1874. https://doi.org/10.1126/science.282.5395.1871

Dorale, J.A., Liu, Z., 2009. Limitations of Hendy test criteria in judging the paleoclimatic suitability of speleothems and the need for replication. J. Cave Karst Stud. 71, 73–80.

Dreybrodt, W., 1981. The kinetics of calcite precipitation from thin films of calcareous solutions and the growth of speleothems: Revisited. Chem. Geol. 32, 237–245. https://doi.org/10.1016/0009-2541(81)90146-7

Dreybrodt, W., Scholz, D., 2011. Climatic dependence of stable carbon and oxygen isotope signals recorded in speleothems: From soil water to speleothem calcite. Geochim. Cosmochim. Acta 75, 734–752. https://doi.org/10.1016/j.gca.2010.11.002

Drysdale, R.N., Zanchetta, G., Hellstrom, J.C., Fallick, A.E., McDonald, J., Cartwright, I., 2007. Stalagmite evidence for the precise timing of North Atlantic cold events during the early last glacial. Geology 35, 77–80. https://doi.org/10.1130/G23161A.1

Drysdale, R.N., Paul, B.T., Hellstrom, J.C., Couchoud, I., Greig, A., Bajo, P., Zanchetta, G., Isola, I., Spötl, C., Baneschi, I., Regattieri, E., Woodhead, J.D., 2012. Precise microsampling of poorly laminated speleothems for U-series dating. Quat. Geochronol. 14, 38–47. https://doi.org/10.1016/j.quageo.2012.06.009

El Janyani, S., Massei, N., Dupont, J.-P., Fournier, M., Dörfliger, N., 2012. Hydrological responses of the chalk aquifer to the regional climatic signal. J. Hydrol. 464–465, 485–493. https://doi.org/10.1016/j.jhydrol.2012.07.040

Fairchild, I.J., Borsato, A., Tooth, A.F., Frisia, S., Hawkesworth, C.J., Huang, Y., McDermott, F., Spiro, B., 2000. Controls on trace element (Sr–Mg) compositions of carbonate cave waters: implications for speleothem climatic records. Chem. Geol. 166, 255–269. https://doi.org/10.1016/S0009-2541(99)00216-8

Fairchild, I.J., Frisia, S., Borsato, A., Tooth, A., 2007. Speleothems, in: Geochemical Sediments and Landscapes. Blackwell, p. 21.

Fairchild, I.J., Smith, C.L., Baker, A., Fuller, L., Spötl, C., Mattey, D., McDermott, F., E.i.m.f., 2006. Modification and preservation of environmental signals in speleothems. Earth-Sci. Rev., ISOtopes in PALaeoenvironmental reconstruction (ISOPAL) 75, 105–153. https://doi.org/10.1016/j.earscirev.2005.08.003

Fairchild, I.J., McMillan, E.A., 2007. Speleothems as indicators of wet and dry periods. Int. J. Speleol. 6.

Fairchild, I.J., Treble, P.C., 2009. Trace elements in speleothems as recorders of environmental change. Quat. Sci. Rev. 28, 449–468. https://doi.org/10.1016/j.quascirev.2008.11.007

Fairchild, I.J., Baker, A., 2012. Speleothem science: from process to past environments. Wiley, Hoboken, N.J.

Farrant, A.R., Maurice, L., Ballesteros, D., Nehme, C., 2023. The genesis and evolution of karstic conduit systems in the Chalk, in: Farrell, R.P., Massei, N., Foley, A.E., Howlett, P.R., West, L.J. (Eds.), The Chalk Aquifers of Northern Europe. Geological Society of London, p. 0. https://doi.org/10.1144/SP517-2020-126

Faure, G., 1998. Principles and applications of geochemistry : a comprehensive textbook for geology students. Upper Saddle River, N.J. : Prentice Hall.

Flipo, N., Gallois, N., Labarthe, B., Baratelli, F., Viennot, P., Schuite, J., Rivière, A., Bonnet, R., Boé, J., 2021. Pluri-annual Water Budget on the Seine Basin: Past, Current and Future Trends, in: Flipo, N., Labadie, P., Lestel, L. (Eds.), The Seine River Basin, The Handbook of Environmental Chemistry. Springer International Publishing, Cham, pp. 59–89. https://doi.org/10.1007/698_2019_392

Fohlmeister, J., Schröder-Ritzrau, A., Scholz, D., Spötl, C., Riechelmann, D.F.C., Mudelsee, M., Wackerbarth, A., Gerdes, A., Riechelmann, S., Immenhauser, A., Richter, D.K., Mangini, A., 2012. Bunker Cave stalagmites: an archive for central European Holocene climate variability. Clim. Past 8, 1751–1764. https://doi.org/10.5194/cp-8-1751-2012

Fohlmeister, J., Voarintsoa, N.R.G., Lechleitner, F.A., Boyd, M., Brandtstätter, S., Jacobson, M.J., L. Oster, J., 2020. Main controls on the stable carbon isotope composition of speleothems. Geochim. Cosmochim. Acta 279, 67–87. https://doi.org/10.1016/j.gca.2020.03.042

Ford, D., Williams, P.D., 2007. Karst Hydrogeology and Geomorphology. John Wiley & Sons.

Fronteau, G., Moreau, C., Thomachot-Schneider, C., Barbin, V., 2010. Variability of some Lutetian building stones from the Paris Basin, from characterisation to conservation. Eng. Geol., Natural stones for historical monuments, testing, durability and provenance 115, 158–166. https://doi.org/10.1016/j.enggeo.2009.08.001

Frouin, M., Sebag, D., Durand, A., Laignel, B., Saliege, J.-F., Mahler, B.J., Fauchard, C., 2007. Influence of paleotopography, base level and sedimentation rate on estuarine system response to the Holocene sea-level rise: The example of the Marais Vernier, Seine estuary, France. Sediment. Geol. 200, 15–29. https://doi.org/10.1016/j.sedgeo.2007.02.007

Frouin, M., Durand, A., Sebag, D., Huault, M.-F., Ogier, S., Verrecchia, E.P., Laignel, B., 2009. Holocene evolution of a wetland in the Lower Seine Valley, Marais Vernier, France. The Holocene 19, 717–727. https://doi.org/10.1177/0959683609105295

Frouin, M., Sebag, D., Durand, A., Laignel, B., 2010. Palaeoenvironmental evolution of the Seine River estuary during the Holocene 13.

Garagnon, J., Perrette, Y., Naffrechoux, E., Pons-Branchu, E., 2023. Polycyclic aromatic hydrocarbon record in an urban secondary carbonate deposit over the last three centuries (Paris, France). Sci. Total Environ. 905, 167429. https://doi.org/10.1016/j.scitotenv.2023.167429

García-Artola, A., Stéphan, P., Cearreta, A., Kopp, R.E., Khan, N.S., Horton, B.P., 2018. Holocene sea-level database from the Atlantic coast of Europe. Quat. Sci. Rev. 196, 177–192. https://doi.org/10.1016/j.quascirev.2018.07.031

Genty, D., Baker, A., Massault, M., Proctor, C., Gilmour, M., Pons-Branchu, E., Hamelin, B., 2001. Dead carbon in stalagmites: carbonate bedrock paleodissolution vs. ageing of soil organic matter. Implications for 13C variations in speleothems. Geochim. Cosmochim. Acta 65, 3443–3457. https://doi.org/10.1016/S0016-7037(01)00697-4

Genty, D., Blamart, D., Ouahdi, R., Gilmour, M., Baker, A., Jouzel, J., Van-Exter, S., 2003. Precise dating of Dansgaard–Oeschger climate oscillations in western Europe from stalagmite data. Nature 421, 833–837. https://doi.org/10.1038/nature01391

Genty, D., 2008. Palaeoclimate research in Villars Cave (Dordogne, SW-France). Int. J. Speleol. 37, 173–191. https://doi.org/10.5038/1827-806X.37.3.3

Genty, D., Labuhn, I., Hoffmann, G., Danis, P.A., Mestre, O., Bourges, F., Wainer, K., Massault, M., Van Exter, S., Régnier, E., Orengo, Ph., Falourd, S., Minster, B., 2014. Rainfall and cave water isotopic relationships in two South-France sites. Geochim. Cosmochim. Acta 131, 323–343. https://doi.org/10.1016/j.gca.2014.01.043

Germain-Vallée, C., Lespez, L., 2011. L'apport des recherches géomorphologiques et micromorphologiques récentes à l'archéologie des paysages de la Plaine de Caen (Calvados, Basse-Normandie). Norois Environ. Aménage. Société 143–178. https://doi.org/10.4000/norois.3699

Gibbard, P.L., Head, M.J., 2020. Chapter 30 - The Quaternary Period, in: Gradstein, F.M., Ogg, J.G., Schmitz, M.D., Ogg, G.M. (Eds.), Geologic Time Scale 2020. Elsevier, pp. 1217–1255. https://doi.org/10.1016/B978-0-12-824360-2.00030-9

GIEC, 2023. Publication du 6e rapport de synthèse du GIEC (No. 6). Group intergouvernamental d'experts sur levolution du climat (GIEC).

Giesche, A., Hodell, D.A., Petrie, C.A., Haug, G.H., Adkins, J.F., Plessen, B., Marwan, N., Bradbury, H.J., Hartland, A., French, A.D., Breitenbach, S.F.M., 2023. Recurring

summer and winter droughts from 4.2-3.97 thousand years ago in north India. Commun. Earth Environ. 4, 1–10. https://doi.org/10.1038/s43247-023-00763-z

Gonnet, A., 2017. Du plateau au fond de vallée : apport de l'étude de trois sites archéologiques à la compréhension des dynamiques géomorphologiques holocènes en Normandie (phdthesis). PhD thesis Normandie Université, 478 p.

Gonnet, A., Todisco, D., Rasse, M., Mouralis, D., Lepert, T., 2023. Soil erosion and anthropogenic impact on landscape evolution over the past 2500 years: A case study of the Villers-Ecalles dry valley (Seine-Maritime, Normandy, France). Geomorphology 427, 108623. https://doi.org/10.1016/j.geomorph.2023.108623

Grafenstein, U. von, Erlenkeuser, H., Brauer, A., Jouzel, J., Johnsen, S.J., 1999. A Mid-European Decadal Isotope-Climate Record from 15,500 to 5000 Years B.P. Science 284, 1654–1657. https://doi.org/10.1126/science.284.5420.1654

Hanel, M., Rakovec, O., Markonis, Y., Máca, P., Samaniego, L., Kyselý, J., Kumar, R., 2018. Revisiting the recent European droughts from a long-term perspective. Sci. Rep. 8, 9499. https://doi.org/10.1038/s41598-018-27464-4

Hänsel, S., Hoy, A., Brendel, C., Maugeri, M., 2022. Record summers in Europe: Variations in drought and heavy precipitation during 1901–2018. Int. J. Climatol. 42, 6235–6257. https://doi.org/10.1002/joc.7587

Harris, I., Osborn, T.J., Jones, P., Lister, D., 2020. Version 4 of the CRU TS monthly high-resolution gridded multivariate climate dataset. Sci. Data 7, 109. https://doi.org/10.1038/s41597-020-0453-3

Hellstrom, J.C., McCulloch, M.T., 2000. Multi-proxy constraints on the climatic significance of trace element records from a New Zealand speleothem. Earth Planet. Sci. Lett. 179, 287–297. https://doi.org/10.1016/S0012-821X(00)00115-1

Hellstrom, J., 2003. Rapid and accurate U/Th dating using parallel ion-counting multi-collector ICP-MS. J. Anal. At. Spectrom. 18, 1346–1351. https://doi.org/10.1039/B308781F

Hendy, C.H., 1971. The isotopic geochemistry of speleothems—I. The calculation of the effects of different modes of formation on the isotopic composition of speleothems and their applicability as palaeoclimatic indicators. Geochim. Cosmochim. Acta 35, 801–824. https://doi.org/10.1016/0016-7037(71)90127-X

Hill, C.A., Forti, P., 1997. Cave Minerals of the World, 2nd ed. National Speleological Society, Huntsville, Alabama.

Holland, H.D., Kirsipu, T.V., Huebner, J.S., Oxburgh, U.M., 1964. On Some Aspects of the Chemical Evolution of Cave Waters. J. Geol. 72, 36–67. https://doi.org/10.1086/626964

Honiat, C., 2022. The Last Interglacial period in the Alps: a speleothem perspective. PhD thesis Leopold-Franzens University Innsbruck, 170 p.

Intergovernmental Panel on Climate Change (IPCC), 2007. Climate Change 2007: The Physical Science Basis. Contribution of Working Group I to the Fourth Assessment Report of the Intergovernmental Panel on Climate Change. In: Solomon, S., Qin, D., Manning, M., Chen, Z., Marquis, M., Averyt, K.B., Tignor, M., Miller, H.L. (Eds.). Cambridge University Press, Cambridge, U.K. and New York, NY, USA.

Ionita, M., Boroneant, C., Chelcea, S.M., 2015. Seasonal modes of dryness and wetness variability over Europe and their connections with large scale atmospheric circulation and global sea surface temperature. Clim. Dyn.

Ionita, M., Tallaksen, L.M., Kingston, D.G., Stagge, J.H., Laaha, G., Van Lanen, H.A.J., Scholz, P., Chelcea, S.M., Haslinger, K., 2017. The European 2015 drought from a climatological perspective. Hydrol. Earth Syst. Sci. 21, 1397–1419. https://doi.org/10.5194/hess-21-1397-2017

Ionita, M., Nagavciuc, V., Kumar, R., Rakovec, O., 2020. On the curious case of the recent decade, mid-spring precipitation deficit in central Europe. Npj Clim. Atmospheric Sci. 3, 1–10. https://doi.org/10.1038/s41612-020-00153-8

Ionita, M., Dima, M., Nagavciuc, V., Scholz, P., Lohmann, G., 2021. Past megadroughts in central Europe were longer, more severe and less warm than modern droughts. Commun. Earth Environ. 2, 1–9. https://doi.org/10.1038/s43247-021-00130-w

Ionita, M., Nagavciuc, V., 2021. Changes in drought features at the European level over the last 120 years. Nat. Hazards Earth Syst. Sci. 21, 1685–1701. https://doi.org/10.5194/nhess-21-1685-2021

Jaffey, A.H., Flynn, K.F., Glendenin, L.E., Bentley, W.C., Essling, A.M., 1971. Precision Measurement of Half-Lives and Specific Activities of 235U and 238U. Phys. Rev. C 4, 1889–1906. https://doi.org/10.1103/PhysRevC.4.1889

Jennings, A., Andrews, J., Wilson, L., 2011. Holocene environmental evolution of the SE Greenland Shelf North and South of the Denmark Strait: Irminger and East Greenland current interactions. Quat. Sci. Rev. 30, 980–998. https://doi.org/10.1016/j.quascirev.2011.01.016

Johnsen, S.J., Dahl-Jensen, D., Gundestrup, N., Steffensen, J.P., Clausen, H.B., Miller, H., Masson-Delmotte, V., Sveinbjörnsdottir, A.E., White, J., 2001. Oxygen isotope and palaeotemperature records from six Greenland ice-core stations: Camp Century, Dye-3, GRIP, GISP2, Renland and NorthGRIP. J. Quat. Sci. 16, 299–307. https://doi.org/10.1002/jqs.622

Johnson, K.R., Hu, C., Belshaw, N.S., Henderson, G.M., 2006. Seasonal trace-element and stable-isotope variations in a Chinese speleothem: The potential for high-resolution paleomonsoon reconstruction. Earth Planet. Sci. Lett. 244, 394–407. https://doi.org/10.1016/j.epsl.2006.01.064

Johnston, V.E., Borsato, A., Spötl, C., Frisia, S., Miorandi, R., 2013. Stable isotopes in caves over altitudinal gradients: fractionation behaviour and inferences for speleothem sensitivity to climate change. Clim. Past 9, 99–118. https://doi.org/10.5194/cp-9-99-2013

Juhls, B., Stedmon, C.A., Morgenstern, A., Meyer, H., Hölemann, J., Heim, B., Povazhnyi, V., Overduin, P.P., 2020. Identifying Drivers of Seasonality in Lena River Biogeochemistry and Dissolved Organic Matter Fluxes. Front. Environ. Sci. 8. https://doi.org/10.3389/fenvs.2020.00053

Kalis, A.J., Merkt, J., Wunderlich, J., 2003. Environmental changes during the Holocene climatic optimum in central Europe - human impact and natural causes. Quat. Sci. Rev. 22, 33–79. https://doi.org/10.1016/S0277-3791(02)00181-6

Kaufman, A., Bar-Matthews, M., Ayalon, A., Carmi, I., 2003. The vadose flow above Soreq Cave, Israel: a tritium study of the cave waters. J. Hydrol. 273, 155–163. https://doi.org/10.1016/S0022-1694(02)00394-3

Kim, S.-T., O'Neil, J.R., 1997. Equilibrium and nonequilibrium oxygen isotope effects in synthetic carbonates. Geochim. Cosmochim. Acta 61, 3461–3475. https://doi.org/10.1016/S0016-7037(97)00169-5

Kingston, D.G., Stagge, J.H., Tallaksen, L.M., Hannah, D.M., 2015. European-Scale Drought: Understanding Connections between Atmospheric Circulation and Meteorological Drought Indices. https://doi.org/10.1175/JCLI-D-14-00001.1

Kühl, N., Litt, T., 2003. Quantitative time series reconstruction of Eemian temperature at three European sites using pollen data. Veg. Hist. Archaeobotany 12, 205–214. https://doi.org/10.1007/s00334-003-0019-2

Labuhn, I., 2014. Climate Variability in Southwest France During the Last 2000 Years : Proxy Calibration and Reconstruction of Drought Periods Based on Stable Isotope Records from Speleothems and Tree Rings. PhD thesis, Université Paris-Sud, 216 p.

Lachniet, M.S., 2009. Climatic and environmental controls on speleothem oxygen-isotope values. Quat. Sci. Rev. 28, 412–432. https://doi.org/10.1016/j.quascirev.2008.10.021

Le Roy Ladurie, E., 1967. Histoire du climat depuis l'an mil. Nouv. Bibl. Sci. Fr. Fre.

Lechleitner, F.A., Amirnezhad-Mozhdehi, S., Columbu, A., Comas-Bru, L., Labuhn, I., Pérez-Mejías, C., Rehfeld, K., 2018. The Potential of Speleothems from Western Europe as Recorders of Regional Climate: A Critical Assessment of the SISAL Database. Quaternary 1, 30. https://doi.org/10.3390/quat1030030

Lemer, L., 2024. Impact anthropique, changements environnementaux et systèmes agraires du Néolithique à l'An mille dans la Plaine de Caen. PhD thesis, Université Paris 1 Panthéon-Sorbonne, 553 p.

Leroyer, C., Coubray, S., Allenet, G., Perrie`re, J., Pernaud, J.-M., 2011. Vegetation dynamics, human impact and exploitation patterns in the Paris Basin through the Holocene: palynology vs. anthracology. Saguntun 11, 81–82.

Lespez, L., Germain, C., 2011. Les paléoenvironnements de l'Âge du fer en Basse-Normandie : état des connaissances et problèmes posés, in: Barral, P., Dedet, B., Delrieu, F., Giraud, P., Le Goff, I., Marion, S., Villard-Le Tiec, A. (Eds.), L'âge du Fer en Basse-Normandie. Gestes funéraires en Gaule au Second-Âge du Fer. Volumes I et II, Annales littéraires. Presses universitaires de Franche-Comté, Besançon, pp. 35–49. https://doi.org/10.4000/books.pufc.6367

Lespez, L., Clet-Pellerin, M., Limondin-Lozouet, N., Pastre, J.-F., Fontugne, M., 2005. Discontinuités longitudinales des dynamiques sédimentaires holocènes dans les petites vallées de l'Ouest du Bassin Parisien, l'exemple de la Mue (Basse Normandie). Quat. Rev. Assoc. Fr. Pour Létude Quat. 273–298. https://doi.org/10.4000/quaternaire.482

Lestienne, C., 2023. La sécheresse de 1921, calamité historique. LEFIGARO.

Limondin-Lozouet, N., Preece, R.C., Antoine, P., 2013. The Holocene tufa at Daours (Somme Valley, northern France): Malacological succession and palaeohydrological implications. Boreas 42, 650–663. https://doi.org/10.1111/j.1502-3885.2012.00306.x

Lin, Y., Clayton, R.N., Gröning, M., 2010. Calibration of δ17O and δ18O of international measurement standards – VSMOW, VSMOW2, SLAP, and SLAP2. Rapid Commun. Mass Spectrom. 24, 773–776. https://doi.org/10.1002/rcm.4449

Litt, T., Schölzel, C., Kühl, N., Brauer, A., 2009. Vegetation and climate history in the Westeifel Volcanic Field (Germany) during the past 11 000 years based on annually laminated lacustrine maar sediments. Boreas 38, 679–690. https://doi.org/10.1111/j.1502-3885.2009.00096.x

Luo, X., Rehkamper, M., Lee, D.-C., Halliday, A.N., 1997. High precision 230Th/232Th and 234U/238U measurements using energyfiltered ICP magnetic sector multiple collector mass spectrometry. Int. J. Mass Spectrom. Ion Process. 171, 105–117. https://doi.org/10.1016/S0168-1176(97)00136-5

Magny, M., 1995. Une histoire du climat, des derniers mammouths au siècle de l'automobile. éd. Errance, Paris.

Magny, M., 2004. Holocene climate variability as reflected by mid-European lake-level fluctuations and its probable impact on prehistoric human settlements. Quat. Int., The record of Human /Climate interaction in Lake Sediments 113, 65–79. https://doi.org/10.1016/S1040-6182(03)00080-6

Mangerud, J., Andersen, S.T., Berglund, B.E., Donner, J.J., 1974. Quaternary stratigraphy of Norden, a proposal for terminology and classification. Boreas 3, 109–126. https://doi.org/10.1111/j.1502-3885.1974.tb00669.x

Markonis, Y., Kumar, R., Hanel, M., Rakovec, O., Máca, P., AghaKouchak, A., 2021. The rise of compound warm-season droughts in Europe. Sci. Adv. 7, eabb9668. https://doi.org/10.1126/sciadv.abb9668

Markowska, M., Baker, A., Treble, P.C., Andersen, M.S., Hankin, S., Jex, C.N., Tadros, C.V., Roach, R., 2015. Unsaturated zone hydrology and cave drip discharge water response: Implications for speleothem paleoclimate record variability. J. Hydrol., Advances in Paleohydrology Research and Applications 529, 662–675. https://doi.org/10.1016/j.jhydrol.2014.12.044

Mattey, D.P., Fairchild, I.J., Atkinson, T.C., Latin, J.-P., Ainsworth, M., Durell, R., 2010. Seasonal microclimate control of calcite fabrics, stable isotopes and trace elements in modern speleothem from St Michaels Cave, Gibraltar. Geol. Soc. Lond. Spec. Publ. 336, 323–344. https://doi.org/10.1144/SP336.17

Mayewski, P.A., Rohling, E.E., Curt Stager, J., Karlén, W., Maasch, K.A., Meeker, L.D., Meyerson, E.A., Gasse, F., van Kreveld, S., Holmgren, K., Lee-Thorp, J., Rosqvist, G., Rack, F., Staubwasser, M., Schneider, R.R., Steig, E.J., 2004. Holocene climate variability. Quat. Res. 62, 243–255. https://doi.org/10.1016/j.yqres.2004.07.001

Mazuir, V., Bibily, C., 2022. Retour sur les sécheresses en France depuis 1976. Echos.

McDermott, F., Frisia, S., Huang, Y., Longinelli, A., Spiro, B., Heaton, T.H.E., Hawkesworth, C.J., Borsato, A., Keppens, E., Fairchild, I.J., van der Borg, K., Verheyden, S., Selmo, E., 1999. Holocene climate variability in Europe: Evidence from δ18O, textural and extension-rate variations in three speleothems. Quat. Sci. Rev. 18, 1021–1038. https://doi.org/10.1016/S0277-3791(98)00107-3

McDermott, F., Mattey, D.P., Hawkesworth, C., 2001. Centennial-Scale Holocene Climate Variability Revealed by a High-Resolution Speleothem δ18O Record from SW Ireland. Science 294, 1328–1331. https://doi.org/10.1126/science.1063678

McDermott, F., 2004. Palaeo-climate reconstruction from stable isotope variations in speleothems: a review. Quat. Sci. Rev., Isotopes in Quaternary Paleoenvironmental reconstruction 23, 901–918. https://doi.org/10.1016/j.quascirev.2003.06.021

McDermott, F., Atkinson, T.C., Fairchild, I.J., Baldini, L.M., Mattey, D.P., 2011. A first evaluation of the spatial gradients in δ18O recorded by European Holocene speleothems. Glob. Planet. Change 79, 275–287. https://doi.org/10.1016/j.gloplacha.2011.01.005

Meyer, H., Schönicke, L., Wand, U., Hubberten, H.W., Friedrichsen, H., 2000. Isotope Studies of Hydrogen and Oxygen in Ground Ice - Experiences with the Equilibration Technique. Isotopes Environ. Health Stud. 36, 133–149. https://doi.org/10.1080/10256010008032939

Milankovitch, M., 1941. Canon of insolation and the iceage problem. Koniglich Serbische Akad. Beogr. Spec. Publ. 132.

Mischel, S.A., Scholz, D., Spötl, C., Jochum, K.P., Schröder-Ritzrau, A., Fiedler, S., 2017. Holocene climate variability in Central Germany and a potential link to the polar North Atlantic: A replicated record from three coeval speleothems. The Holocene 27, 509–525. https://doi.org/10.1177/0959683616670246

Moore, G.W., 1952. Speleothem—a new cave term. Natl. Speleol. Soc. News 10, 2.

Mühlinghaus, C., Scholz, D., Mangini, A., 2007. Modelling stalagmite growth and δ13C as a function of drip interval and temperature. Geochim. Cosmochim. Acta 71, 2780–2790. https://doi.org/10.1016/j.gca.2007.03.018

Mühlinghaus, C., Scholz, D., Mangini, A., 2009. Modelling fractionation of stable isotopes in stalagmites. Geochim. Cosmochim. Acta 73, 7275–7289. https://doi.org/10.1016/j.gca.2009.09.010

Müller, W., Shelley, M., Miller, P., Broude, S., 2009. Initial performance metrics of a new custom-designed ArF excimer LA-ICPMS system coupled to a two-volume laser-ablation cell. J. Anal. At. Spectrom. 24, 209–214. https://doi.org/10.1039/B805995K

Nagavciuc, V., Perșoiu, A., Bădăluță, C.-A., Bogdevich, O., Bănică, S., Bîrsan, M.-V., Boengiu, S., Onaca, A., Ionita, M., 2022. Defining a Precipitation Stable Isotope Framework in the Wider Carpathian Region. Water 14, 2547. https://doi.org/10.3390/w14162547

Nehme, C., Farrant, A., Ballesteros, D., Todisco, D., Rodet, J., Sahy, D., Grappone, J.M., Staigre, J.-C., Mouralis, D., 2020. Reconstructing fluvial incision rates based on palaeo-water tables in chalk karst networks along the Seine valley (Normandy, France). Earth Surf. Process. Landf. 45, 1860–1876. https://doi.org/10.1002/esp.4851

Nehme, C., Verheyden, S., Nader, F.H., Adjizian-Gérard, J., Genty, D., De Bont, K., Minster, B., Salem, G., Verstraten, D., Clayes, P., 2019. Cave dripwater isotopic signals related to the altitudinal gradient of Mount-Lebanon: implication for speleothem studies. Int. J. Speleol. 48, 63–74. https://doi.org/10.5038/1827-806X.48.1.2253

Nicholson, S.L., Jacobson, M.J., Hosfield, R., Fleitmann, D., 2021. The Stalagmite Record of Southern Arabia: Climatic Extremes, Human Evolution and Societal Development. Front. Earth Sci. 9. https://doi.org/10.3389/feart.2021.749488

Nicod, J., 1995. Carte géomorphologique des karsts de France. Notice d'une maquette au 1/3 000 000 environ. https://doi.org/10.3406/karst.1995.2351

Oster, J.L., Montañez, I.P., Guilderson, T.P., Sharp, W.D., Banner, J.L., 2010. Modeling speleothem δ13C variability in a central Sierra Nevada cave using 14C and 87Sr/86Sr. Geochim. Cosmochim. Acta 74, 5228–5242. https://doi.org/10.1016/j.gca.2010.06.030

Paasche, Ø., Bakke, J., 2009. The Holocene Turnover - A global climatic shift at ~4 Ka. Presented at the EGU, Geophysical Research Abstracts.

Palacios, D., Hughes, P.D., Jomelli, V., Tanarro, L.M., 2023. European Glacial Landscapes: The Holocene. Elsevier.

Palmer, W.C., Havens, A.V., 1958. A graphical technique for determining evapotranspiration by the thornthwaite method. Mon. Weather Rev. 86, 123–128. https://doi.org/10.1175/1520-0493(1958)086<0123:AGTFDE>2.0.CO;2

Pons-Branchu, E., Douville, E., Roy-Barman, M., Dumont, E., Branchu, P., Thil, F., Frank, N., Bordier, L., Borst, W., 2014. A geochemical perspective on Parisian urban history based on U–Th dating, laminae counting and yttrium and REE concentrations of recent

carbonates in underground aqueducts. Quat. Geochronol. 24, 44–53. https://doi.org/10.1016/j.quageo.2014.08.001

Pons-Branchu, E., Ayrault, S., Roy-Barman, M., Bordier, L., Borst, W., Branchu, P., Douville, E., Dumont, E., 2015. Three centuries of heavy metal pollution in Paris (France) recorded by urban speleothems. Sci. Total Environ. 518–519, 86–96. https://doi.org/10.1016/j.scitotenv.2015.02.071

Pons-Branchu, E., Barbarand, J., Caffy, I., Dapoigny, A., Drugat, L., Dumoulin, J.P., Medina Alcaide, M.A., Nouet, J., Sanchidrián Torti, J.L., Tisnérat-Laborde, N., Jiménez de Cisneros, C., Valladas, H., 2022. U-series and radiocarbon cross dating of speleothems from Nerja Cave (Spain): Evidence of open system behavior. Implication for the Spanish rock art chronology. Quat. Sci. Rev. 290, 107634. https://doi.org/10.1016/j.quascirev.2022.107634

Rehfeld, K., Münch, T., Ho, S.L., Laepple, T., 2018. Global patterns of declining temperature variability from the Last Glacial Maximum to the Holocene. Nature 554, 356–359. https://doi.org/10.1038/nature25454

Riechelmann, D.F.C., Schröder-Ritzrau, A., Scholz, D., Fohlmeister, J., Spötl, C., Richter, D.K., Mangini, A., 2011. Monitoring Bunker Cave (NW Germany): A prerequisite to interpret geochemical proxy data of speleothems from this site. J. Hydrol. 409, 682–695. https://doi.org/10.1016/j.jhydrol.2011.08.068

Riechelmann, D.F.C., Deininger, M., Scholz, D., Riechelmann, S., Schröder-Ritzrau, A., Spötl, C., Richter, D.K., Mangini, A., Immenhauser, A., 2013. Disequilibrium carbon and oxygen isotope fractionation in recent cave calcite: Comparison of cave precipitates and model data. Geochim. Cosmochim. Acta 103, 232–244. https://doi.org/10.1016/j.gca.2012.11.002

Riechelmann, S., Breitenbach, S., Schroder-Ritzrau, A., Mangini, A., Immenhauser, A., 2019. Ventilation and cave air PCO2 in the Bunker-Emst Cave System (NW Germany): implications for speleothem proxy data. J. Cave Karst Stud. 81, 98–112. https://doi.org/10.4311/2018ES0110

Roberts, M.S., Smart, P.L., Baker, A., 1998. Annual trace element variations in a Holocene speleothem. Earth Planet. Sci. Lett. 154, 237–246. https://doi.org/10.1016/S0012-821X(97)00116-7

Roberts, N., 2013. The Holocene: An Environmental History. John Wiley & Sons.

Rodet, J., 1992. Le karst dans l'évolution quaternaire de la Basse Seine (Normandie, France). pp. 362–382.

Rodet, J., 2013. Karst et évolution géomorphologique de la côte crayeuse à falaises de la manche. l'exemple du massif d'aval (Etretat, Normandie, France). Quat. Rev. Assoc. Fr. Pour Létude Quat. 303–314. https://doi.org/10.4000/quaternaire.6745

Roy-Barman, M., Pons-Branchu, E., 2016. Improved U–Th dating of carbonates with high initial 230Th using stratigraphical and coevality constraints. Quat. Geochronol. 32, 29–39. https://doi.org/10.1016/j.quageo.2015.12.002

Schneider, C.A., Rasband, W.S., Eliceiri, K.W., 2012. NIH Image to ImageJ: 25 years of Image Analysis. Nat. Methods 9, 671–675.

Sebag, D., 2002. Apports de la matière organique pour la reconstitution des paléoenvironnements holocènes de la basse vallée de la Seine : fluctuations des conditions hydrologiques locales et environnements de dépôt. PhD thesis Université de Rouen, 356 p.

Séchet, G., 2003. Les chroniques météo de l'année 1934 [WWW Document]. Meteo-Paris. URL https://www.meteo-paris.com/chronique/annee/1934 (accessed 2.23.24).

Sernander, R., 1908. On the evidences of Postglacial changes of climate furnished by the peat-mosses of Northern Europe. Geol. Fören. Stockh. Förh. https://doi.org/10.1080/11035890809445601

Sharp, Z., 2017. Principles of Stable Isotope Geochemistry, 2nd Edition. Open Textb. https://doi.org/ https://doi.org/10.25844/h9q1-0p82

Sibout, P., 2011. La longue histoire des carrières de Caumont. Études Normandes 60, 27–36. https://doi.org/10.3406/etnor.2011.2875

SIGES, S. d'information pour la gestion des eaux souterraines en S.-N., 1974. Pedologie du bassin Seine-Normandie.

Sinclair, D.J., 2011. Two mathematical models of Mg and Sr partitioning into solution during incongruent calcite dissolution: Implications for dripwater and speleothem studies. Chem. Geol. 283, 119–133. https://doi.org/10.1016/j.chemgeo.2010.05.022

Sinclair, D.J., Banner, J.L., Taylor, F.W., Partin, J., Jenson, J., Mylroie, J., Goddard, E., Quinn, T., Jocson, J., Miklavič, B., 2012. Magnesium and strontium systematics in tropical speleothems from the Western Pacific. Chem. Geol. 294–295, 1–17. https://doi.org/10.1016/j.chemgeo.2011.10.008

Smart, P.L., Friederich, H., 1986. Water movement and storage in the unsaturated zone of a maturely karstified carbonate aquifer, Mendip Hills, England, in: Proceedings of the Environmental Problems in Karst Terranes and Their Solutions Conference. National Water Well Association, Dublin OH. 1986. p 59-87, 11 Fig, 5 Tab, 38 Ref.

Smith, A.B., Matthews, J.L., 2015. Quantifying uncertainty and variable sensitivity within the US billion-dollar weather and climate disaster cost estimates. Nat. Hazards 77, 1829–1851. https://doi.org/10.1007/s11069-015-1678-x

Spinoni, J., Naumann, G., Vogt, J.V., 2017. Pan-European seasonal trends and recent changes of drought frequency and severity. Glob. Planet. Change 148, 113–130. https://doi.org/10.1016/j.gloplacha.2016.11.013

Spötl, C., 2004. A simple method of soil gas stable carbon isotope analysis. Rapid Commun. Mass Spectrom. 18, 1239–1242. https://doi.org/10.1002/rcm.1468

Spötl, C., Fairchild, I.J., Tooth, A.F., 2005. Cave air control on dripwater geochemistry, Obir Caves (Austria): Implications for speleothem deposition in dynamically ventilated caves. Geochim. Cosmochim. Acta 69, 2451–2468. https://doi.org/10.1016/j.gca.2004.12.009

Steenstrup, J. J. S. (1841). Kongelige Danske Videnskabernes Selskabs Afhandlinger. GeognostikGeologisk Undersє‌ogelse av Skomvmosserne Vidnesamog Lillemose i det nordlige Sjelland, ledsaget af sammenlignende Bemærkninger, hentede fra Danmarks Skov-, Kjær og Lyngmoser i Almindelighed, vol. 9, pp. 17-120.

Surić, M., Lončarić, R., Bočić, N., Lončar, N., Buzjak, N., 2018. Monitoring of selected caves as a prerequisite for the speleothem-based reconstruction of the Quaternary environment in Croatia. Quat. Int., Quaternary of Croatia 494, 263–274. https://doi.org/10.1016/j.quaint.2017.06.042

Treble, P.C., Bradley, C., Wood, A., Baker, A., Jex, C.N., Fairchild, I.J., Gagan, M.K., Cowley, J., Azcurra, C., 2013. An isotopic and modelling study of flow paths and storage in Quaternary calcarenite, SW Australia: implications for speleothem paleoclimate records. Quat. Sci. Rev. 64, 90–103. https://doi.org/10.1016/j.quascirev.2012.12.015

Tremaine, D.M., Froelich, P.N., Wang, Y., 2011. Speleothem calcite farmed in situ: Modern calibration of δ18O and δ13C paleoclimate proxies in a continuously-monitored natural cave system. Geochim. Cosmochim. Acta 75, 4929–4950. https://doi.org/10.1016/j.gca.2011.06.005

Trzpit, J.-P., 1978. La sécheresse en Basse-Normandie : calamité accidentelle ou mal récurrent ? Études Normandes 27, 55–74. https://doi.org/10.3406/etnor.1978.2425

Valo, M., 2022. Droughts threaten most of France this summer. Le Monde.fr.

van der Schrier, G., Allan, R.P., Ossó, A., Sousa, P.M., Van de Vyver, H., Van Schaeybroeck, B., Coscarelli, R., Pasqua, A.A., Petrucci, O., Curley, M., Mietus, M., Filipiak, J., Štěpánek, P., Zahradníček, P., Brázdil, R., Řezníčková, L., van den Besselaar, E.J.M., Trigo, R., Aguilar, E., 2021. The 1921 European drought: impacts, reconstruction and drivers. Clim. Past 17, 2201–2221. https://doi.org/10.5194/cp-17-2201-2021

van der Velde, M., Tubiello, F.N., Vrieling, A., Bouraoui, F., 2012. Impacts of extreme weather on wheat and maize in France: evaluating regional crop simulations against observed data. Clim. Change 113, 751–765. https://doi.org/10.1007/s10584-011-0368-2

Van Loon, A.F., Stahl, K., Di Baldassarre, G., Clark, J., Rangecroft, S., Wanders, N., Gleeson, T., Van Dijk, A.I.J.M., Tallaksen, L.M., Hannaford, J., Uijlenhoet, R., Teuling, A.J., Hannah, D.M., Sheffield, J., Svoboda, M., Verbeiren, B., Wagener, T., Van Lanen, H.A.J., 2016. Drought in a human-modified world: reframing drought definitions, understanding, and analysis approaches. Hydrol. Earth Syst. Sci. 20, 3631–3650. https://doi.org/10.5194/hess-20-3631-2016

Van Rampelbergh, M., Verheyden, S., Allan, M., Quinif, Y., Keppens, E., Claeys, P., 2014. Monitoring of a fast-growing speleothem site from the Han-sur-Lesse cave, Belgium, indicates equilibrium deposition of the seasonal δ18O and δ13C signals in the calcite. Clim. Past 10, 1871–1885. https://doi.org/10.5194/cp-10-1871-2014

Vanderlinden, K., Giráldez, J.V., Meirvenne, M.V., 2008. Spatial Estimation of Reference Evapotranspiration in Andalusia, Spain. J. Hydrometeorol. 9, 242–255. https://doi.org/10.1175/2007JHM880.1

Verheyden, S., Keppens, E., Fairchild, I.J., McDermott, F., Weis, D., 2000. Mg, Sr and Sr isotope geochemistry of a Belgian Holocene speleothem: implications for paleoclimate reconstructions. Chem. Geol. 169, 131–144. https://doi.org/10.1016/S0009-2541(00)00299-0

Verheyden, S., 2004. Trace elements in speleothems. A short review of the state of the art. Int. J. Speleol. 33, 95–101. https://doi.org/10.5038/1827-806X.33.1.9

Verheyden, S., Baele, J.-M., Keppens, E., Genty, D., Cattani, O., Hai, C., Edwards, L., Hucai, Z., Strijdonck, M.V., Quinif, Y., 2006. The Proserpine stalagmite (Han-Sur-Lesse Cave,

Belgium): preliminary environmental interpretation of the last 1000 years as recorded in a layered speleothem. Geol. Belg. 12.

Verheyden, S., Genty, D., Deflandre, G., Quinif, Y., Keppens, E., 2008. Monitoring climatological, hydrological and geochemical parameters in the Père Noël cave (Belgium): implication for the interpretation of speleothem isotopic and geochemical time-series. Int. J. Speleol. 37, 221–234. https://doi.org/10.5038/1827-806X.37.3.6

Verheyden, S., Keppens, E., Quinif, Y., J. Cheng, H., R. Edwards, L., 2014. Late-glacial and Holocene climate reconstruction as inferred from a stalagmite - grotte du Père Noël, Han-sur-Lesse, Belgium. Geol. Belg.

Verheyden, S., Nehme, C., Onac, B., 2022. Les spéléothèmes au fil du temps Speleothem science – A short review and state of the art. KARSTOLOGIA 79, 53–60.

Vicente-Serrano, S.M., Beguería, S., López-Moreno, J.I., 2010. A Multiscalar Drought Index Sensitive to Global Warming: The Standardized Precipitation Evapotranspiration Index. J. Clim. 23, 1696–1718. https://doi.org/10.1175/2009JCLI2909.1

Vicente-Serrano, S.M., Domínguez-Castro, F., Murphy, C., Hannaford, J., Reig, F., Peña-Angulo, D., Tramblay, Y., Trigo, R.M., Mac Donald, N., Luna, M.Y., Mc Carthy, M., Van der Schrier, G., Turco, M., Camuffo, D., Noguera, I., García-Herrera, R., Becherini, F., Della Valle, A., Tomas-Burguera, M., El Kenawy, A., 2021. Long-term variability and trends in meteorological droughts in Western Europe (1851–2018). Int. J. Climatol. 41, E690–E717. https://doi.org/10.1002/joc.6719

Vidal, J.-P., Martin, E., Franchistéguy, L., Habets, F., Soubeyroux, J.-M., Blanchard, M., Baillon, M., 2010. Multilevel and multiscale drought reanalysis over France with the Safran-Isba-Modcou hydrometeorological suite. Hydrol. Earth Syst. Sci. 14, 459–478. https://doi.org/10.5194/hess-14-459-2010

Vinther, B.M., Clausen, H.B., Johnsen, S.J., Rasmussen, S.O., Andersen, K.K., Buchardt, S.L., Dahl-Jensen, D., Seierstad, I.K., Siggaard-Andersen, M.-L., Steffensen, J.P., Svensson, A., Olsen, J., Heinemeier, J., 2006. A synchronized dating of three Greenland ice cores throughout the Holocene. J. Geophys. Res. Atmospheres 111. https://doi.org/10.1029/2005JD006921

von Post, L., 1916. On forest tree pollen in South swedish peat bog deposits, (translated from Swedish by K. Faegri and M. B. Davis, 1967). Pollen Spores 9, 375–401.

Wackerbarth, A., Scholz, D., Fohlmeister, J., Mangini, A., 2010. Modelling the δ18O value of cave drip water and speleothem calcite. Earth Planet. Sci. Lett. 299, 387–397. https://doi.org/10.1016/j.epsl.2010.09.019

Walanus, A., Nalepka, D., 2010. Calibration of Mangerud'S Boundaries. Radiocarbon 52, 1639–1644. https://doi.org/10.1017/S0033822200056368

Walker, M., Johnsen, S., Rasmussen, S.O., Steffensen, J.-P., Popp, T., Gibbard, P., Hoek, W., Lowe, J., Andrews, J., Björck, S., Cwynar, L., Hughen, K., Kershaw, P., Kromer, B., Litt, T., Lowe, D.J., Nakagawa, T., Newnham, R., Schwander, J., 2008. The Global Stratotype Section and Point (GSSP) for the base of the Holocene Series/Epoch (Quaternary System/Period) in the NGRIP ice core [WWW Document]. URL https://researchcommons.waikato.ac.nz/items/58a03ad1-488c-4a00-8038-dea92b33c065 (accessed 8.8.24).

Walker, M., Head, M.J., Berkelhammer, M., Björck, S., Cheng, H., Cwynar, L., Fisher, D., Gkinis, V., Long, A., Lowe, J., Newnham, R., Rasmussen, S.O., Weiss, H., 2018. Formal ratification of the subdivision of the Holocene Series/Epoch (Quaternary System/Period): two new Global Boundary Stratotype Sections and Points (GSSPs) and three new stages/subseries. Episodes J. Int. Geosci. 41, 213–223. https://doi.org/10.18814/epiiugs/2018/018016

Wanner, H., Beer, J., Bütikofer, J., Crowley, T.J., Cubasch, U., Flückiger, J., Goosse, H., Grosjean, M., Joos, F., Kaplan, J.O., Küttel, M., Müller, S.A., Prentice, I.C., Solomina, O., Stocker, T.F., Tarasov, P., Wagner, M., Widmann, M., 2008. Mid- to Late Holocene climate change: an overview. Quat. Sci. Rev. 27, 1791–1828. https://doi.org/10.1016/j.quascirev.2008.06.013

Wanner, H., Solomina, O., Grosjean, M., Ritz, S.P., Jetel, M., 2011. Structure and origin of Holocene cold events. Quat. Sci. Rev. 30, 3109–3123. https://doi.org/10.1016/j.quascirev.2011.07.010

Wanner, H., Mercolli, L., Grosjean, M., Ritz, S.P., 2015. Holocene climate variability and change; a data-based review. J. Geol. Soc. 172, 254–263. https://doi.org/10.1144/jgs2013-101

Wassenburg, J.A., Riechelmann, S., Schröder-Ritzrau, A., Riechelmann, D.F.C., Richter, D.K., Immenhauser, A., Terente, M., Constantin, S., Hachenberg, A., Hansen, M., Scholz, D., 2020. Calcite Mg and Sr partition coefficients in cave environments: Implications for

interpreting prior calcite precipitation in speleothems. Geochim. Cosmochim. Acta 269, 581–596. https://doi.org/10.1016/j.gca.2019.11.011

White, W.B., 2004. Paleoclimate Records from Speleothems in Limestone Caves, in: Sasowsky, I.D., Mylroie, J. (Eds.), Studies of Cave Sediments. Springer US, Boston, MA, pp. 135–175. https://doi.org/10.1007/978-1-4419-9118-8_9

Wilhite, D.A., Glantz, M.H., 1985. Understanding: the Drought Phenomenon: The Role of Definitions. Water Int. https://doi.org/10.1080/02508068508686328

Wong, C.I., Breecker, D.O., 2015. Advancements in the use of speleothems as climate archives. Quat. Sci. Rev., Novel approaches to and new insights from speleothem-based climate reconstructions 127, 1–18. https://doi.org/10.1016/j.quascirev.2015.07.019

Woodhead, J., Hellstrom, J., Maas, R., Drysdale, R., Zanchetta, G., Devine, P., Taylor, E., 2006. U–Pb geochronology of speleothems by MC-ICPMS. Quat. Geochronol. 1, 208–221. https://doi.org/10.1016/j.quageo.2006.08.002

Woods, M., 2020. Drought provokes shutdown of nuclear reactors in northeast France. RFI.

World Meteorological Organization (WMO), 2021. WMO Atlas of Mortality and Economic Losses from Weather, Climate and Water Extremes (1970–2019) (Technical No. WMO-No. 1267). Geneva.

Zhao, J., Yu, K., Feng, Y., 2009. High-precision 238U–234U–230Th disequilibrium dating of the recent past: a review. Quat. Geochronol., Dating the Recent Past 4, 423–433. https://doi.org/10.1016/j.quageo.2009.01.012

List of figures

List of Tables

Appendix 1

Climate monitoring in the Caumont cave and quarry system (northern France) reveal near oxygen isotopic equilibrium conditions for carbonate deposition

Ingrid Bejarano-Arias[1*], Carole Nehme[1], Sebastian F. M. Breitenbach[2], Hanno Meyer[3], Sevasti Modestou[2], Damase Mouralis[1]

[1]UMR 6266 IDEES CNRS, University of Rouen Normandy, Mont St-Aignan, 76310, France

[2]Northumbria University, Newcastle upon Tyne, Department of Geography and Environmental Sciences, NE1 8ST, United Kingdom

[3]Alfred Wegener Institute for Polar and Marine Research, Telegrafenberg, Potsdam, 14401, Germany

Table S1. Collected air and water temperature, plus CO_2 data during the 20 months of monitoring for each station in Caumont cave and quarry system.

Date of collection	CAU-1			CAU-2		CAU-3	
	Air T (°C)[1]	Water T (°C)[1]	CO_2 (ppm)[1]	Air T (°C)[2]	CO_2 (ppm)[1]	Air T (°C)[2]	CO_2 (ppm)[2]
02/11/2019	-	-	-	-	-	-	-
18/11/2019	9.5	9.0	-	-	-	-	-
30/11/2019	9.0	-	-	-	-	-	-
15/12/2019	9.7	9.1	-	11.1	-	-	-
11/01/2020	8.5	8.4	-	10.6	-	11.3	-
31/01/2020	9.0	8.6	-	10.2	-	11.3	-
15/02/2020	8.6	9.1	-	10.2	-	11.3	-
03/03/2020	8.1	8.5	-	10.1	-	11.3	-
14/03/2020	8.6	9.3	-	10.1	-	11.3	-
29/05/2020	9.9	9.9	-	10.2	-	11.3	-
13/06/2020	12.5	10.2	-	10.3	-	11.4	-
29/06/2020	10.9	10.4	-	10.4	-	11.3	-
17/07/2020	10.1	10.5	-	10.5	-	11.3	-
01/08/2020	10.8	10.7	-	10.6	-	11.3	-
29/08/2020	11.6	11.1	-	11.0	-	11.3	-
15/09/2020	12.5	11.1	-	11.0	-	11.3	-
08/10/2020	11.7	11.2	-	10.9	-	11.3	-
20/10/2020	-	-	-	-	-	-	-
30/10/2020	11.5	10.7	-	10.8	-	11.3	-
18/11/2020	10.0	10.4	-	10.7	-	11.3	-
18/12/2020	9.3	9.7	-	10.5	-	11.3	-
16/01/2021	4.0	6.5	-	10.2	-	11.3	-
29/01/2021	-	8.5	-	10.3	-	11.4	-
26/02/2021	7.1	8.1	-	-	-	-	-

Table S1. (*continued*)

11/03/2021	7.0	7.9	-	10.1	-	11.4	-
14/04/2021	5.9	7.2	-	10.0	-	11.4	-
18/05/2021	8.6	9.2	-	10.1	-	11.4	-
02/06/2021	9.6	9.6	-	10.1	-	11.4	-
01/07/2021	10.2	10.4	-	10.3	-	11.4	-
15/02/2023	10.7	10.4	540-560	-	560-570	-	550 (entrance) 4940 (inside)

[1]Data measured manually during each visit, except CO_2 which was measured only twice.
[2]Data measured by temperature loggers left during the monitoring period and removed by 01/07/2021

Table S2. Isotopic data collected during 20 months of monitoring in stations CAU-1, CAU-2, and CAU-3. The abbreviations are: sw = stream water, dw = drip water, calc = modern calcite samples, n.a. = not available.

Date of collection	CAU-1					CAU-2									CAU-3				
	$\delta^{18}O_{sw}$ [‰]	1σ	$\delta^{2}H_{sw}$ [‰]	1σ	d-excess	$\delta^{18}O_{dw}$ [‰]	1σ	$\delta^{2}H_{dw}$ [‰]	1σ	d-excess	$\delta^{18}O_{cal}$ [‰]	1σ	$\delta^{13}C_{cal}$ [‰]	1σ	$\delta^{18}O_{dw}$ [‰]	1σ	$\delta^{2}H_{dw}$ [‰]	1σ	d-excess
02/11/2019	-6.92	0.01	-44.87	0.2	10.5	-7.30	0.06	-47.6	0.2	10.9	n.a..	n.a..	n.a..	n.a..	n.a..	n.a..	n.a..	n.a.	n.a.
18/11/2019	-7.09	0.03	-46.57	0.1	10.1	-7.41	0.09	-48.8	0.9	10.4	-4.68	0.06	-8.52	0.04	n.a..	n.a.	n.a.	n.a.	n.a.
30/11/2019	-7.21	0.04	-48.85	0.3	8.9	-7.33	0.00	-48.7	0.3	9.9	n.a..	n.a..	n.a..	n.a..	n.a..	n.a.	n.a.	n.a.	n.a.
15/12/2019	-7.06	0.01	-46.01	0.0	10.4	-7.33	0.02	-47.6	0.2	11.0	-5.05	0.07	-8.92	0.03	n.a.	n.a.	n.a.	n.a.	n.a.
11/01/2020	-6.97	0.03	-45.34	0.2	10.4	-7.26	0.04	-47.3	0.3	10.8	-5.38	0.04	-8.33	0.02	-7.36	0.06	-46.08	0.08	12.79
31/01/2020	-6.95	0.05	-45.32	0.1	10.2	-7.29	0.02	-47.7	0.1	10.7	-5.57	0.06	-10.41	0.03	-7.35	0.02	-46.57	0.14	12.21
15/02/2020	-7.17	0.06	-46.42	0.2	10.9	-7.59	0.05	-48.6	0.1	12.1	-5.10	0.01	-10.23	0.03	-7.69	0.03	-47.53	0.38	13.98
03/03/2020	-6.83	0.04	-45.55	0.1	9.1	-7.31	0.04	-48.0	0.3	10.5	-5.07	0.04	-9.69	0.02	n.a.	n.a.	n.a.	n.a.	n.a.
14/03/2020	-7.33	0.02	-46.62	0.1	12.0	-7.37	0.03	-48.6	0.1	10.3	-5.38	0.03	-10.57	0.02	-7.25	0.04	-46.75	0.29	11.22
29/05/2020	-6.94	0.02	-45.54	0.1	9.9	-7.31	0.02	-48.1	0.1	10.3	-5.04	0.05	-10.47	0.04	-7.34	0.02	-47.40	0.23	11.34
13/06/2020	-6.95	0.02	-46.32	0.40	9.26	-7.36	0.04	-49.45	0.24	9.40	-5.55	0.04	-10.84	0.04	-7.45	0.03	-47.92	0.58	11.67
29/06/2020	-7.13	0.01	-47.11	0.33	9.91	-7.28	0.01	-48.80	0.17	9.47	-5.08	0.05	-10.18	0.03	-7.42	0.01	-48.03	0.41	11.35
17/07/2020	-7.18	0.03	-46.17	0.34	11.25	-7.54	0.02	-48.86	0.26	11.48	-5.41	0.03	-10.38	0.02	-7.60	0.02	-47.51	0.52	13.32
01/08/2020	-7.02	0.04	-46.05	0.34	10.1	-7.48	0.02	-49.19	0.39	10.67	-5.20	0.07	-10.48	0.04	-7.57	0.02	-47.82	0.27	12.77
29/08/2020	-7.13	0.03	-46.07	0.27	10.96	-7.42	0.02	-49.65	0.22	9.70	-4.73	0.03	-7.95	0.03	-7.50	0.02	-47.52	0.39	12.46
15/09/2020	-7.11	0.03	-46.17	0.10	10.71	-7.43	0.04	-47.89	0.10	11.57	-4.92	0.08	-5.68	0.05	-7.52	0.01	-47.42	0.11	12.71
20/10/2020	-7.09	0.03	-45.50	0.1	11.2	-7.36	0.04	-47.34	0.12	11.53	-5.25	0.06	-10.42	0.04	-7.45	0.05	-46.89	0.15	12.72
30/10/2020	-7.06	0.02	-45.33	0.18	11.16	-7.38	0.04	-48.03	0.14	10.97	n.a.	n.a.	n.a.	n.a.	-7.44	0.04	-46.80	0.09	12.76
18/11/2020	-7.07	0.04	-45.66	0.09	10.89	-7.22	0.01	-47.01	0.06	10.75	-4.71	0.06	-7.61	0.02	-7.49	0.02	-47.26	0.04	12.64
18/12/2020	-6.95	0.05	-45.34	0.12	10.24	-7.26	0.09	-47.29	0.18	10.76	-5.34	0.02	-11.13	0.06	-7.37	0.02	-46.86	0.11	12.07
16/01/2021	-6.65	0.18	-44.90	0.4	8.3	-7.32	0.01	-47.4	0.1	11.2	-4.97	0.03	-10.24	0.04	-7.45	0.02	-46.81	0.12	12.82
29/01/2021	-6.77	0.29	-45.19	0.7	8.9	-7.09	0.04	-46.7	0.2	10.0	-5.55	0.05	-10.99	0.04	-6.94	0.31	-45.58	0.76	9.91
26/02/2021	-6.99	0.01	-45.55	0.1	10.4	n.a.	n.a.	n.a.	n.a.	n.a.	n.a.	n.a.	n.a.	n.a.	-7.04	0.01	-45.41	0.12	10.93
11/03/2021	-6.94	0.03	-45.17	0.1	10.3	-7.31	0.01	-47.4	0.1	11.1	-5.93	0.06	-11.04	0.02	-7.12	0.03	-45.92	0.14	11.00
14/04/2021	-6.89	0.08	-44.91	0.2	10.2	-7.26	0.05	-47.4	0.1	10.6	n.a.	n.a.	n.a.	n.a.	-7.39	0.00	-46.70	0.03	12.38

Table S2(*continued*)

18/05/2021	-6.96	0.01	-45.34	0.0	10.3	-7.33	0.02	-47.5	0.1	11.1	n.a.	n.a.	n.a.	n.a.	-7.36	0.03	-46.35	0.18	12.53
02/06/2021	-6.78	0.21	-44.88	0.5	9.3	-7.33	0.01	-47.5	0.1	11.1	-5.36	0.04	-11.03	0.03	-7.27	0.14	-46.53	0.30	11.61
01/07/2021	n.a..	n.a..	n.a..	n.a..	n.a.	n.a.	n.a.	n.a.	n.a.	n.a.	n.a.	n.a.	n.a.	0.03	n.a.	n.a.	n.a.	n.a.	n.a.

Appendix 2

A multi-proxy stalagmite record indicates a shift in forcing of 20th Century drought events in Normandy

Ingrid Bejarano-Arias (*), Carole Nehme, Sebastian F.M. Breitenbach, Monica Ionita, James Baldini, Edwige Pons-Branchu, Sevasti Modestou, Stuart Umbo, Damase Mouralis.

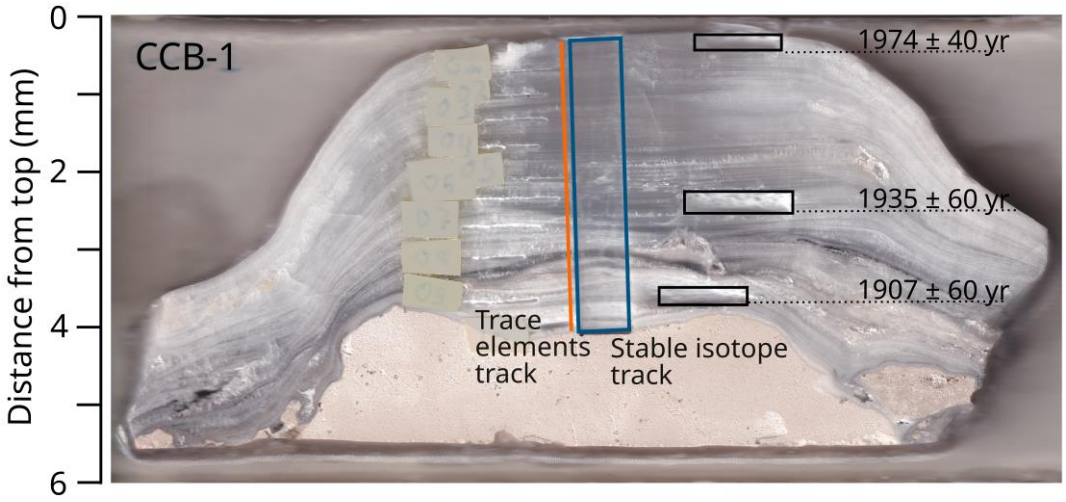

Figure 1. Image of CCB-1 stalagmite with the locations of the U/Th ages (black rectangles, numbers are in calendar years with 2σ errors), stable isotope (blue rectangle) and trace element laser ablation sampling track (orange line).

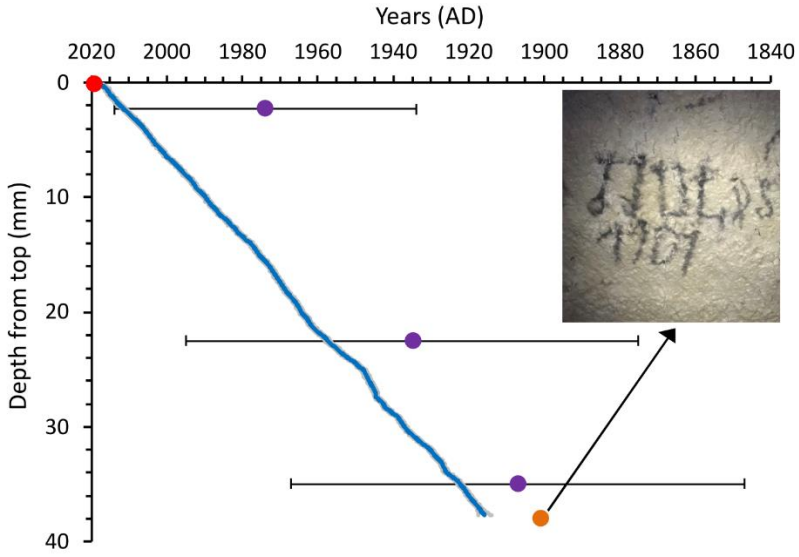

Figure 2. Age-depth model of CCB-1 stalagmite. The blue represents the age-model obtained from COPRA and the grey ones show the 95% confidence intervals. The U-series ages used to build the age model are shown in purple, the stalagmite collection year in red and the year of the historical inscription in orange. Photo of the ceiling indicates the inscription "1901" as the year of opening of the gallery.

Table 1. U and Th content, isotopic activity ratios and U/Th ages from stalagmite CCB-1. $\delta^{234}U_M$ = {[($^{234}U/^{238}U$) $_{sample}$/($^{234}U/^{238}U$) $_{eq}$]-1} x 1000, where ($^{234}U/^{238}U$) $_{sample}$ is the measured atomic ratio and ($^{234}U/^{238}U$)$_{eq}$ is the atomic ratio at secular equilibrium. $\delta^{234}U_{(T)}$ is the initial value and is calculated by the equation: $\delta^{234}U_{(T)}$ = δ^{234}Um exp(λ^{234}t), where t is the corrected age in years and λ^{234} is the decay constant for ^{234}U. Raw ages are given in ka before year of measure (2019). Ages were corrected from detrital fraction using Strutage routine (Roy-Barman and Pons-Branchu, 2016) $^{230}Th/^{232}Th$ initial of the detrital fraction determined using STRUTages routine is 1.24 +/- 0.11. Corrected ages are given as years AD.

Sample ID	Depth (mm from top)	^{238}U (ppm)	Error (2s)	^{232}Th (ppb)	Error (2s)	$\delta^{234}U_M$ (%)	Error (2s)	$^{230}Th/^{238}U$	Error (2s)	$^{230}Th/^{232}Th$	Error (2s)	Age (ka before year of measure*)	Error (2s)	$\delta^{234}U_T$ (%)	Error (2s)	Age (AD) (corrected)
CCB-1-01	1	0.22	0.002	0.32	0.00	101.50	1.20	0.00	0.00	2.93	1.61	0.14	0.07	101.50	1.20	1974 +55 -40
CCB-1-02	16	0.42	0.003	8.92	0.07	99.90	1.20	0.01	0.00	1.71	0.05	1.19	0.04	100.10	1.20	1935 +70 -59
CCB-1-03	34	0.41	0.003	2.82	0.02	107.30	3.20	0.00	0.00	1.90	0.10	0.43	0.03	107.40	3.20	1907 +67 -59

Table 2. Response of the instrumental data and speleothem CCB-1 multi-proxy records to the drought events of the 20th and 21st centuries, in Normandy, France.

Drought events	Drought years	October SPEI6	Effective infiltration (mm)	Annual Temperature (°C)	Annual $\delta^{13}C$ (‰ VPDB)	Annual Mg (ppm)	Annual Sr (ppm)	Annual $\delta^{18}O$ (‰ VPDB)
I	1920	-0.31	460	10.60	-10.28	150.70	16.64	-4.92
	1921	-2.34	397	11.51	-9.11	196.62	15.64	-4.42
	1922	-0.03	731	10.02	-8.20	304.93	23.35	-4.58
	1923*	0.59	862	10.73	-8.32	352.10	22.43	-4.33
II	1934	-1.40	498	11.70	-11.45	102.84	9.97	-5.24
	1937*	-0.48	846	11.35	-8.54	245.67	16.20	-4.64
III	1947	-2.01	600	11.69	-10.22	177.56	15.84	-4.59
	1949	-1.36	524	11.95	-10.96	106.97	9.49	-5.22
	1952*	0.07	816	10.66	-9.69	181.67	21.12	-4.98
IV	1973*	0.04	592	9.79	-10.41	141.52	8.70	-4.78
	1976	-1.87	459	10.45	-10.66	115.81	6.23	-4.87
V	1989	-1.88	504	10.67	-11.52	98.02	7.90	-5.15
	1990	-1.71	611	10.84	-11.54	90.69	9.06	-5.05
	1995*	-1.43	829	11.03	-10.39	139.87	6.59	-5.07
VI	2001*	0.45	1039	10.77	-10.25	147.58	8.61	-4.78
	2003	-1.12	655	11.30	-11.18	104.99	8.60	-5.09
	Mean value	0.00	740	10.60	-10.80	125.39	9.33	-4.94

*Response peaks observed in offset with drought years.

Supplementary methods

Instrumental data for drought index

For this study we used the monthly precipitation amount (P) and monthly mean air temperature (T) from the Rouen-Boos station, covering the period from 1970 - 2017. The precipitation data for 2018 were complemented with the record taken from Royal Netherlands Meteorological Institute (KNMI) Climate Explorer for Rouen. Air temperature data before 1970 was complemented using data from KNMI for the Paris-Le Bourget meteorological station, located ca. 105 km from Caumont. The record at this station dates back to the beginning of the 1900s.